Order Number 9315462

Vibrational circular dichroism of deoxyoligonucleotides

Gulotta, Miriam Susan, Ph.D.

City University of New York, 1993

U·M·I
300 N. Zeeb Rd.
Ann Arbor, MI 48106

VIBRATIONAL CIRCULAR DICHROISM OF DEOXYOLIGONUCLEOTIDES

by

MIRIAM GULOTTA

A dissertation submitted to the Graduate Faculty in Chemistry in partial fulfillment of the requirements for the degree of Doctor of Philosophy, The City University of New York

1993

This manuscript has been read and accepted for the Graduate Faculty in Chemistry in satisfaction of the dissertation requirement for the degree of Doctor of Philosophy.

Date

Chair of Examining Committee

Dec 30, 1992
Date

Executive Officer

Supervisory Committee

The City University of New York

Abstract

Vibrational Circular Dichroism of Deoxyoligonucleotides

by

Miriam Gulotta

Advisers: Professor Dixie J. Goss
Professor Max Diem

In this thesis, infrared (vibrational) circular dichroism (VCD) is shown to be a viable technique for examining the secondary structure of deoxyoligonucleotides. In these studies spectra were taken in the 1550-1750 cm^{-1} carbonyl stretching region. VCD spectra of the low salt conformations of poly(dG)poly(dC), poly(dG-dC)poly(dG-dC), poly(dG-me^5dC)poly(dG-me^5dC), and $pd(CG)_5$ are examined. The B-form VCD spectrum of a CG-deoxyoligonucleotide is characterized by a negative/positive couplet at approximately 1700 cm^{-1} and 1680 cm^{-1} respectively.

High salt Z-form spectra of poly(dG-dC)poly(dG-dC) and poly(dG-me^5dC)poly(me^5dC) are also presented. We have found that the VCD spectra of poly(dG-dC)poly(dG-dC) and poly(dG-me^5dC)poly(dG-me^5dC) in high salt solution varies depending on whether NaCl or $MgCl_2$ is used to induce the B-Z transition. Left-handed conformations are characterized by a positive/negative couplet which is shifted to lower wavenumbers than the B-form couplet.

The Degenerate Extended Coupled Oscillator (DECO) model

is used as a means of interpreting the VCD experimental data. From the cartesian coordinates of the carbonyl groups and applying simple coupled oscillator theory, the model determines the interaction energy between these groups as well as the effect of the interactions on the dipole and rotational strengths. From the output of the model, calculated spectra can be generated. The DECO model is shown to account for the B-form VCD spectra but the model is unable to account for the Z-form spectra. We have attributed the problems with the Z-form calculations to interactions between the oligonucleotide and the salt solution which are not currently taken into account.

Acknowledgements

I would like to thank some of the many people who have made this work possible. To Dixie J. Goss, my mentor, who taught me how to use and fix the spectrometers and taught me how versitile they can be. I thank her also for her confidence and patience and all she has taught me about enjoying life. To Max Diem, my other mentor, who showed me VCD and introduced me to world I did not even know existed in science. To my parents who have always supported me and who did their best to improve the quality of my life during my graduate career. I would also like to thank the present and past members of the Goss and Diem lab groups who I have worked with, laughed with and learned from, especially, Ou Lee, Gull-Maj Roberts, Indira Presad, Arthur Barlow, Winzen Zhong, Susan Carberry, Sheryl Birke, Luisa Balasta and Ting Xiang. I would also like to thank my friends and support groups, Paula Longo, Mercedes Connelly, Suzette Stoler, Bill Bolosky and Patricia Steckler.

VCD OF MODEL DEOXYOLIGONUCLEOTIDES

I. INTRODUCTION:

A. Biological Relevance:

The genetic code of life is contained in the sequence of the bases of DNA. Everything from hair color and eye color to height and susceptibility to certain genetic diseases is coded somewhere in one's DNA. There are copies of the entire genetic code in every cell in the body.

There were essentially four major sets of experiments that led to the conclusion that DNA was necessary for carrying the genetic code from one generation to another. The first of these experiments was done by F. Griffith in 1928 and involved the pneumococci bacteria. Griffith observed that when live mutant non-pathogenic bacteria and heat-killed pathogenic bacteria were simultaneously injected into healthy mice, the mice died. Griffith concluded that the heat-killed pathogenic bacteria were able to transform the live non-pathogenic bacteria into live pathogenic bacteria.[12]

In 1944, O. Avery, C. McLead and M. McCarty determined through further experiments involving bacteria that a nucleic acid was responsible for the transformation observed by Griffith.[2]

In 1951, R. Herriott proposed that when T2 bacteriophage virus attacked a host bacteria cell, only the DNA from the virus was transferred into the host cell.[2]

Herriott's proposal was confirmed by A. Hershey and M. Chase in 1952. Hershey and Chase radioactively labeled phage

DNA and monitored its reaction with host E. coli bacteria. After the reaction, only labeled DNA was found in the host bacteria. Hershey and Chase concluded that only the DNA had a role in progeny formation.[2]

By 1952, it was evident that DNA had a genetic function while proteins did not. However, other than the knowledge of the components of the code, nothing was known about the structure of DNA. The structure of proteins was also unknown.

The first breakthrough came in 1951 when Pauling and Corey presented the α-helix as a geometric structural model of a protein.[3] Pauling's model was largely based on work done with molecular models rather than on experimental results; nevertheless, the model fit all of the known experimental parameters and the experimental evidence supported the model. Pauling's model inspired F. Crick and J. Watson to use a similar approach in determining the structure of DNA. When Watson and Crick started their modeling, little was known about the structure of DNA. X-ray diffraction patterns were not sufficiently resolved to make many clear statements about the structure of DNA. However, while Watson and Crick worked on their model of B-DNA Rosalind Franklin obtained x-ray diffraction photographs which both confirmed and were used to make some small adjustments to Watson and Crick's original model.[4] The model proposed by Watson and Crick had several important features. DNA, composed of purine and pyrimidine bases, has an anti-parallel double stranded helical structure

with the sugar and phosphate groups forming the helical backbone. The bases are aligned almost perpendicular relative to the helix axis. The order of the bases on a single strand does not effect the structure, but every guanine (G) base on one strand is paired with a cytosine (C) base on the other strand and every adenine (A) base is paired with a thymine (T) base. The complementarity of base pairing was deduced from experimental observations made by Chargaff between 1950 and 1953.[3] Chargaff found through a content analysis of DNA that the relative amounts of guanine and cytosine were the same as were the relative amounts of adenine and thymine, but there was no correlation between the amount of guanine and the amount of adenine.[4] The base pairing was particularly important in determining how DNA functioned. The complementary pairing inferred that during cell replication, DNA was unwound and the two strands were separated; the two strands were each used as templates from which an additional complementary strand was regenerated, thereby forming two identical DNAs from the original one. One of the original DNA strands was incorporated into each of the two progeny cells.[2]

Since Watson and Crick's discovery, there has been an explosion of interest in the structure and function of nucleic acids. In addition to the B-form DNA model (see below), Watson and Crick also proposed an A-form DNA model. In addition to these, many more DNA structures have been found. For example, C-DNA resembles B-DNA but is more tightly wound

(9.33 nucleotides/turn versus 10.5 for the B-form[1]). C-DNA is formed when Li^{2+} is used instead of Na^{+} or Mg^{2+} as the stabilizing salt for the nucleic acid. D-form has an even tighter helical structure (8 nucleotides/turn) and is only formed by DNAs with AT sequences. There are even models with other than two strands. For example, V-form is single stranded.[5] There are triple stranded helices with Hoogsteen base pairs in addition to the GC and AT base pairing proposed by Watson and Crick. In Hoogsteen base pairs, hydrogen bonding occurs at the N7 position of the purine base rather than the N1 position as seen with Watson-Crick base pairing. The Hoogsteen geometry is less stable than the Watson-Crick geometry. More recently, tetrastranded synthetic DNA oligonucleotides have been formed. There is no evidence that all of these structures exist in living species.

Watson and Crick had no experimental evidence to suggest that B-DNA was a right-handed helix. It was not until 1980 when the dodecamer 5'CGCGAATTGCGC3' was crystallized that a B-form crystal structure was obtained;[6,7] however, there were left-handed DNA crystal fragments formed as early as 1979.[8] The left-handed or Z-family DNAs were a suggestion of Pohl and Jovin's circular dichroism studies and were confirmed by x-ray diffraction analysis of single crystals of the oligomers $CGCG^{6}$ and $CGCGCG^{9}$.

The ever increasing number and types of DNA structures

---

[1] terminology explained below.

has made it difficult to define a set of general characteristics for the structure of DNA. DNA is composed of a sugar-phosphate backbone and purine and pyrimidine bases. Cytosine bases are usually paired with guanine bases and adenine bases with thymine bases (Watson-Crick base pairing) but GT and AC pairs also exist. The conformation of the sugar varies significantly and attempts to use sugar conformation as an accurate test for a specific form of DNA have not been successful.[10]

In addition, some DNAs have a bent helix axis, some form hairpin loops or cruciforms and some are circular. Mismatches and bulges, kinks and double-stranded DNAs with unequal numbers of bases on each strand have also been found.

It is not yet known whether all of these structures exist in living systems or whether or not a function is associated with these structures. What can be said is that DNA is a highly dynamic structure which is dependent on the base composition and the existing environment.

B. Structural Features of DNA

DNA is composed of a cyclic furanose sugar, purine and pyrimidine bases, and phosphate groups. The sugar is a five membered ring composed of four carbons and an oxygen (Fig. 1a). Attached to the fourth carbon, but not part of the ring is an additional carbon atom.[1] There are two hydroxy groups in DNA attached to the 3′ and 5′ carbons,

Fig. 1a: Furanose Sugar

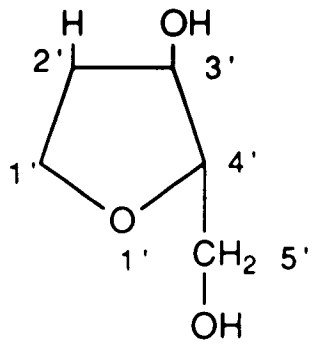

Fig. 1b: The Sugar Phosphate Backbone of DNA

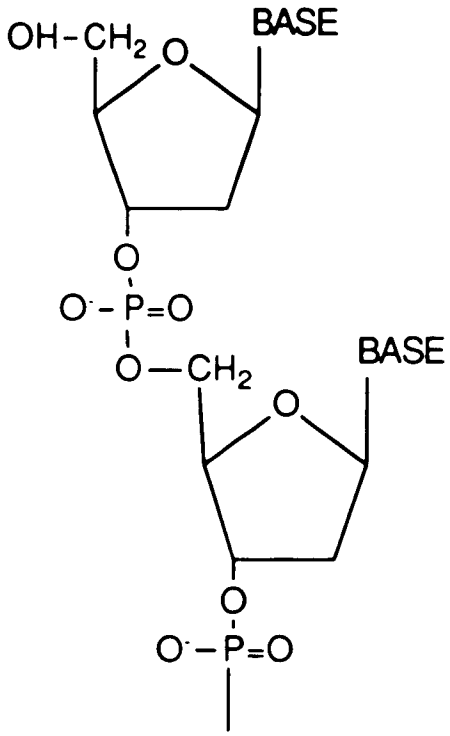

and an additional hydroxy group at the 2′ carbon in RNA. A skeletal diagram of part of a DNA strand is shown in Fig. 1b. The conventional numbering is indicated. When reference is made to the sugar ring of a DNA molecule, the numbers are given primes to distinguish them from the carbons of the bases.

The sugar rings are connected together by phosphodiester linkages to the phosphate groups and constitute the backbone of DNA. A phosphodiester is attached to the sugar at the 3′ position (Fig. 1b).[11] In neutral solution, the phosphomonoester has a double negative charge while the phosphodiester has one negative charge (Fig. 2a,b).[12]

There are two types of bases occurring in DNA, the purines and the pyrimidines (Fig. 3). Pyrimidines are six-membered rings composed of four carbons and two nitrogens. Purines are bicyclic; a pyrimidine ring fused along the C4-C5 edge to a five-membered ring containing two more nitrogens. The bases are attached to the sugar by β-glycosyl C1′-N linkages. Bases are always attached to the 1′ carbon on the sugar ring. The purine bases are attached to the furanose sugar at the N9 position and the pyrimidines are attached at the N1 position. The most commonly found bases are the purines, guanine and adenine, and the pyrimidines, cytosine and thymine (Fig. 4). Thymine, guanine and cytosine have carbonyl- functional groups; adenine, cytosine and guanine also have amino- functional groups. Although the carbonyl

Fig. 2a: Phosphomonoester [Cantor & Schimmel, 1980]

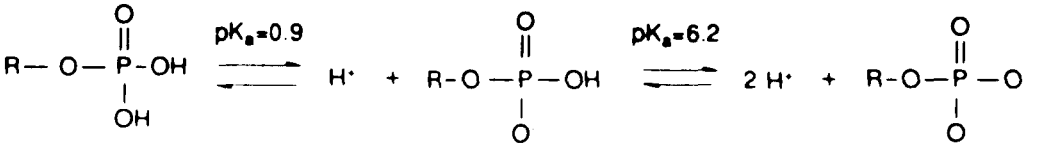

Fig. 2b: 5'GMP

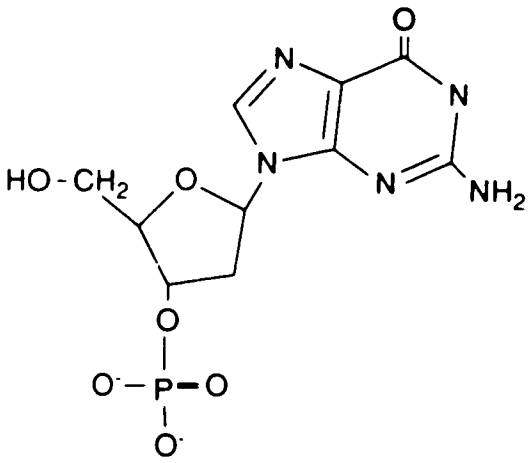

Fig. 3: Skeletal Structures of a Purine and a Pyrimidine Base

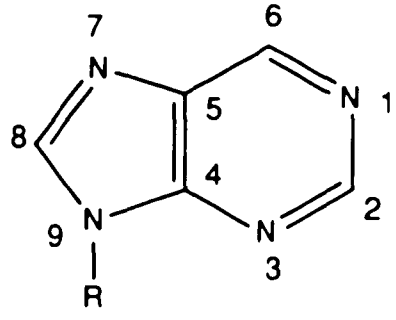

PURINE

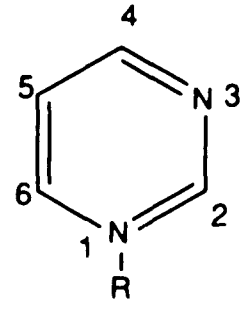

PYRIMIDINE

R designates furanose sugar

Fig. 4: Primary Structures of Cytosine, Guanine Thymine, & Adenine

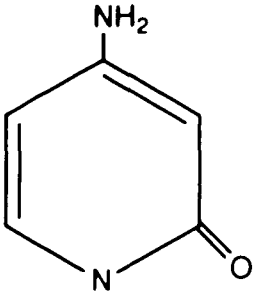

CYTOSINE

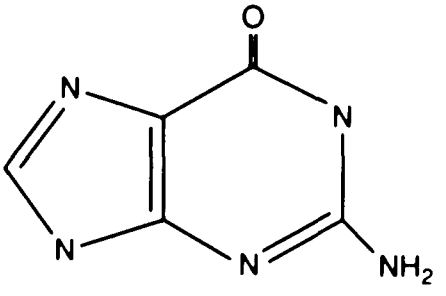

GUANINE

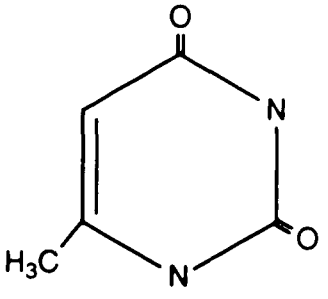

THYMINE

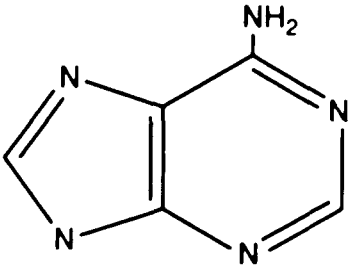

ADENINE

structure (keto-form) is in equilibrium with a hydroxy structure (enol-form), the pK_a is approximately 2 for both bases so the keto-structure is predominant in neutral solution (Fig. 5).[11,13]

The primary structure is usually listed from the 5'- to the 3'- end. Thus, the oligonucleotide seen in Figure 6 would be designated CG, not GC. The phosphate groups are sometimes also included in the name; alternate names for the structure in Figure 6 are: pCpGp or pCGp. When anti-parallel double strands are formed, strand I is paired at the 5' end to the 3' end of strand II and vice versa.

DNA is not a planar molecule as the above discussion suggests and even oligonucleotides as short as a single base have non-planar structures.[6] The sugar conformation forces oligonucleotides as short as two bases to take on a helical structure. Although the sugar is chiral and therefore optically active, it is the helicity that gives rise to most of the observable optical activity.

The definition of DNA secondary structure requires a large number of parameters. Every atom is defined in terms of bond lengths, bond angles and torsion angles with respect to its neighbors (Fig. 7).[*2] In this paper, only terms which are used to differentiate B-form from Z-form oligonucleotides are discussed. A more complete discussion of these parameters

---

[*2] There are many different conventions used in describing the helical parameters. The Cambridge Convention is used here [Dickerson, 1989].

Fig. 5: Keto - Enol Structures for Guanine, Cytosine, & Thymine

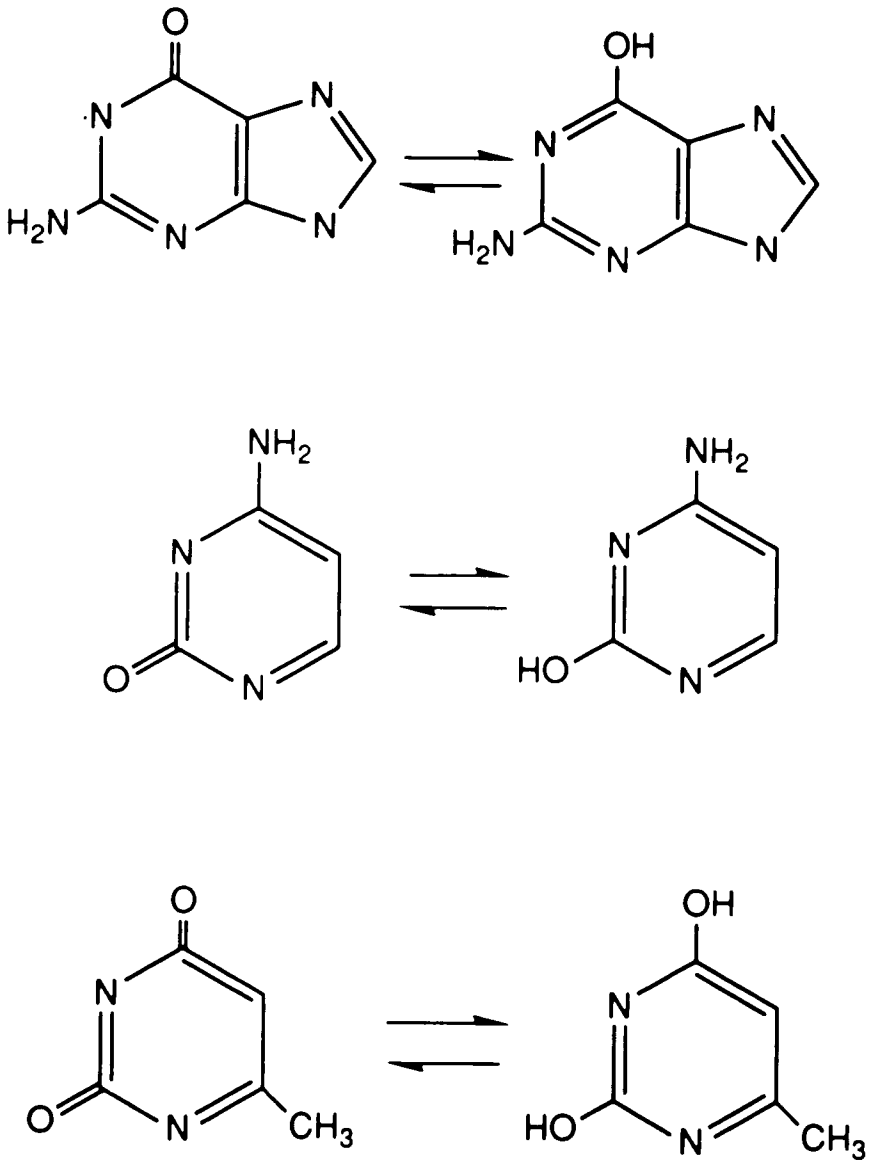

Fig. 6: Structure of 5'pCpGp3'

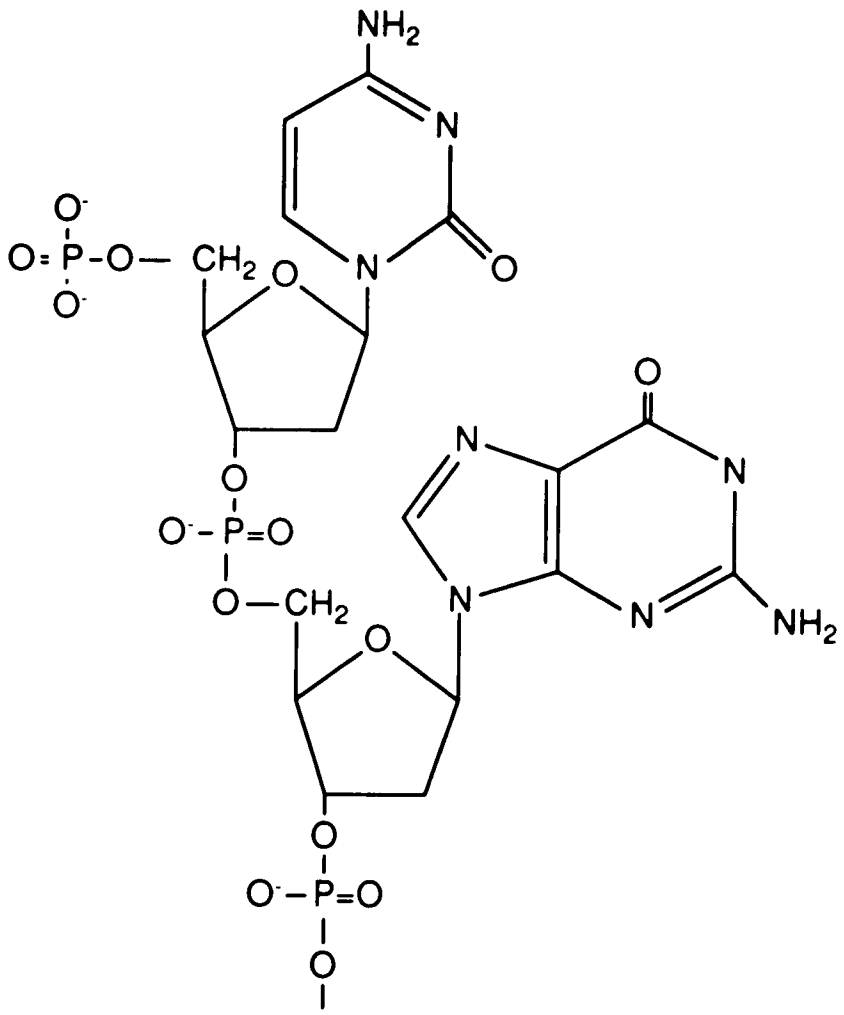

Fig. 7: Torsion Angles Describing DNA Backbone Conformation.

χ designates the angle of the base relative to the sugar and is also shown in Fig. 9.

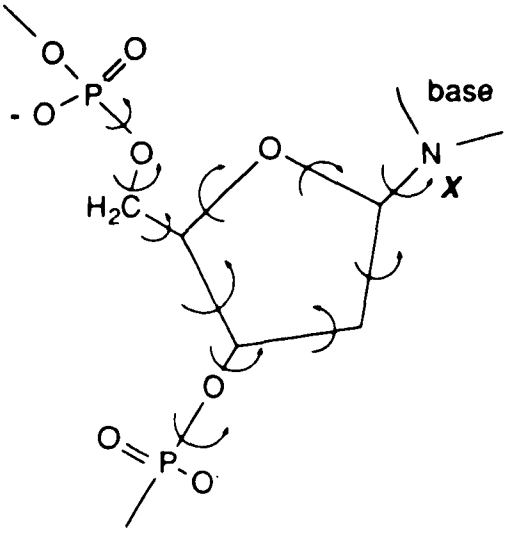

can be found in The Cambridge Convention.[14]

Sugar pucker: The furanose sugar is a nonplanar five-membered ring. The two major classifications for sugar pucker are the envelope (E) and the twist (T) structures. In an envelope structure, four of the atoms are planar or nearly planar while the fifth rises up out of the plane. In the twist conformation, adjacent atoms are on opposite sides of the plane formed by the other three. In both cases, atoms displaced on the same side of the plane as C5', are designated endo while atoms displaced on the opposite side are designated exo (Fig. 8).[11]

Glycosal bond: Orientation about the C1'-N bond between the sugar and the base is important for determining sugar-base interactions as well as determining the distance between bases (Fig. 9). The torsion angle that describes this orientation is χ. χ=0° corresponds to the O1'-C1' bond if it is cis with respect to the N9-C8 bond of a purine base or the N1-C6 bond of a pyrimidine base. The two rotational isomers are designated as "syn" and "anti". Anti conformations have $\chi \approx 0°$, and syn conformations have $\chi \approx 210°$. The orientation of the base to the sugar is most commonly anti.[11]

DNA always forms helical structures. The term helical or spiral refers to "winding round a cylinder or other round body and at the same time rising or advancing forward like a corkscrew" (Fig. 10).[15] Consider an oligonucleotide to be a string where the attachment of a base to the backbone is

Fig. 8: Sugar Puckering Modes.

The **plane** refers to the plane made by 3 or more carbons in the sugar ring envelope structures have one carbon out of the plane made by the rest. Carbons which are **endo** are out of the plane and in the same plane as C5'; carbons which are **exo** lie on the opposite side of the plane from C5'.

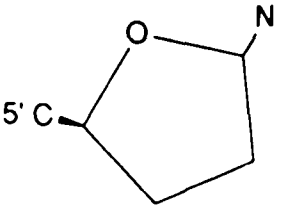

Flat sugar ring
all carbons are in the same plane.

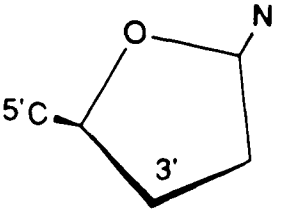

C3'- endo
carbon 3 out of plane in the same plane as carbon 5.

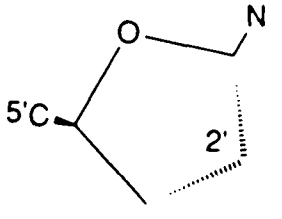

C2'- exo
carbon 2 out of plane

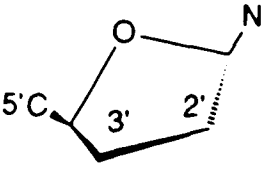

C3'- endo-C2'-exo
symmetrical twist

Fig. 9: Orientation About the C1'-N Bond

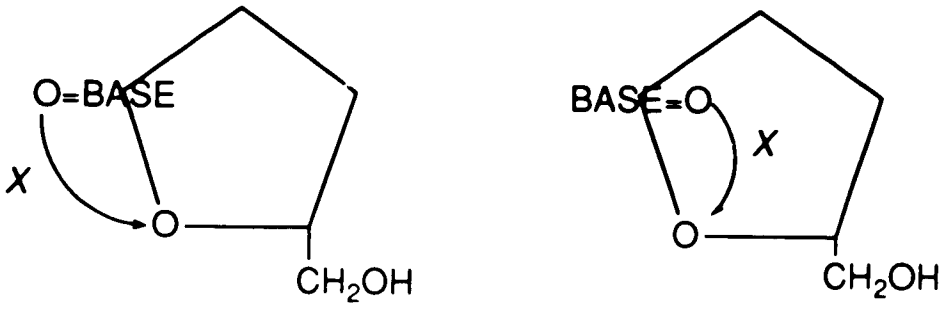

anti

syn

Fig. 10: Helix

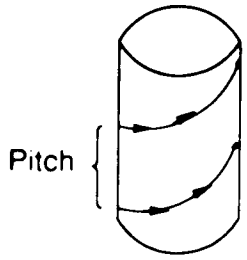

designated as a knots along the string. To generate a helix, the string is wound around a cylinder whose height lies along the z-axis. The mathematical definition states that if this cylinder was unfolded into a plane, the string would unfold into a straight line.[15] The definitions needed to describe the helix are now clear. The vertical distance between knots is called the axial rise/residue. The number of knots required to return to the original horizontal position is the number of residues/repeat (n). The unit twist is simply 360°/n. The vertical movement required to make a turn (the tightness of the coil) is the pitch (P) (Fig. 11).[11,14] These parameters do not give any indication of the direction that the backbone is wrapped around the cylinder. This last parameter refers to the part of the definition "rising or advancing forward like a corkscrew". If the advancement from the 5′ to the 3′ end is clockwise, the helix is right-handed. If this advancement is counterclockwise, the helix is left-handed.

The original model of B-DNA structure described by Watson and Crick in 1953 was a double-stranded helix with anti-parallel strands. "Watson-Crick base pairing" was postulated between opposing bases which are oriented almost perpendicular to the helix axis. In "Watson-Crick base pairing", adenine bases are paired with thymine bases through two hydrogen bonds and cytosine bases are paired with guanine

Fig. 11: Helical Parameters

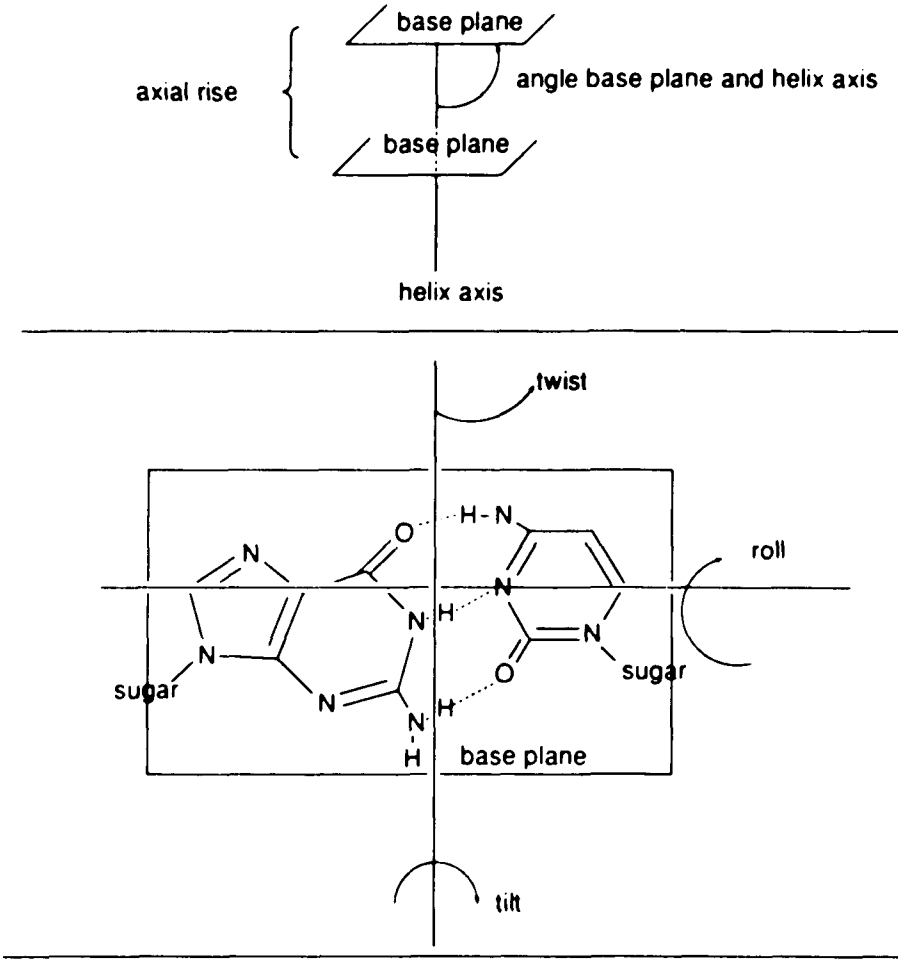

torsion angle

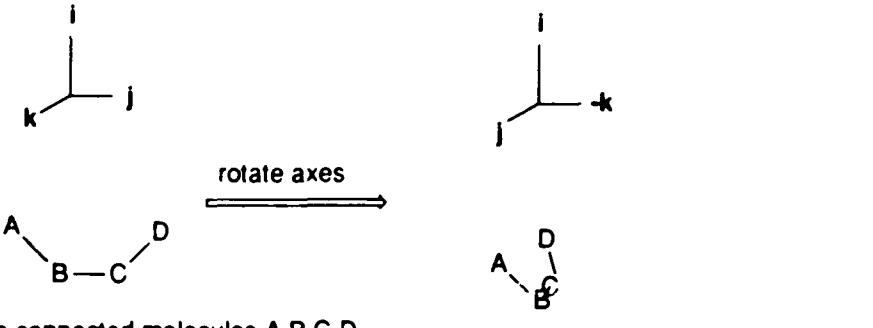

given connected molecules A,B,C,D

angle between projected bonds A-B and C-D is the torsion angle

bases by three hydrogen bonds.*3 The pairing occurs through hydrogen bonds between the carbonyl groups and the amino groups or NH groups in the ring (Fig. 12). Since the model was based solely on fiber diffraction data, there was no information about whether the helix was right- or left-handed.

Most naturally occurring DNAs have been found to conform to this model and have two anti-parallel strands with complementary Watson-Crick base pairs.[5,16] The perpendicular orientation of the bases is characteristic of B-form DNA; refinement of the structure determined that there are 10-11 base pairs/turn, the phosphate groups are 7 Å apart in one strand, and the axial rise/residue is 3.3-3.4 Å. It is known that the sugar pucker is commonly C2'-endo for all sugars in natural B-form DNAs. For synthetic alternating oligonucleotides, the sugar pucker for B-form DNAs is C3'-endo for purines and C2'-endo for pyrimidines.[10,11,16] In the left-handed Z-form conformation, the helix is tighter and there are 12 base pairs/turn. The sugar pucker is syn for purines and anti for pyrimidines.

Fiber diffraction and x-ray crystal analysis has illustrated that most DNAs and synthetic oligonucleotides do not conform exactly to the B-form and Z-form descriptions outlined above and that there is great flexibility in the

---

*3 Watson and Crick's original model showed only two hydrogen bonds between paired guanine and cytosine bases. However, there are actually three hydrogen bonds as shown in Fig. 12.

Fig. 12: Watson-Crick G-C and A-T Base Pairs
dotted lines indicate hydrogen bonds

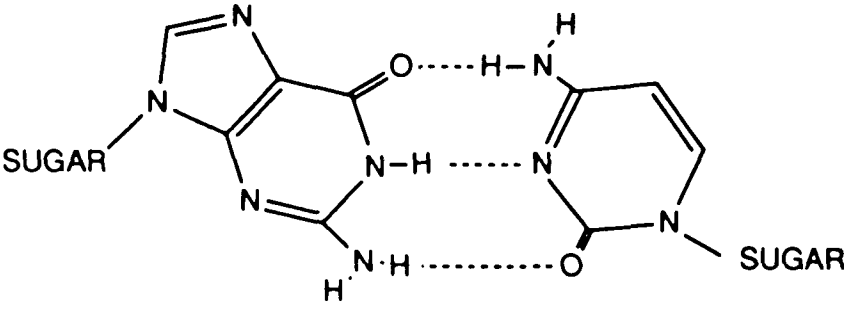

Guanine-Cytosine

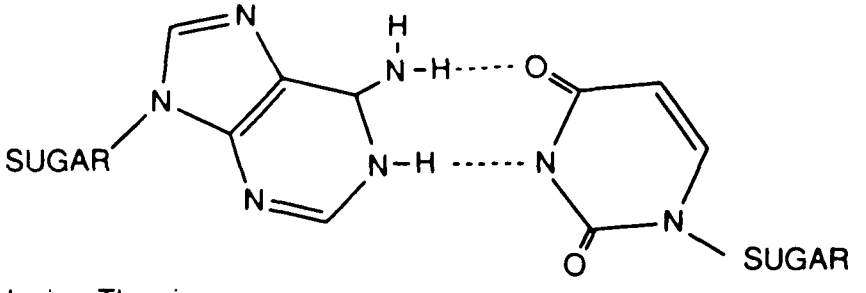

Adenine-Thymine

structure of DNA. In the most general definition, DNAs or oligonucleotides having a right-handed screw sense belong to A- or B-families and those having a left-handed screw sense belong to the Z-family.

All of the oligonucleotides used in this study were double-stranded with the strands anti-parallel to one another and had only Watson-Crick base pairing.

C. Techniques

The interest in DNA structure spawned a growth in the number of techniques used to examine them. Use of elementary chemical analysis, centrifugation, diffusive techniques and electrophoresis were among the early methods used to determine the characteristics of DNA. Enzyme and drug specificity and immunogenesis are a few of the more recently used biological approaches to the study of DNA. Structural information comes mainly from spectroscopy and x-ray diffraction studies. X-ray diffraction analysis of fibers was used to elucidate the original B-DNA model. Fiber diffraction studies can only be used to determine heavy atom position to within approximately 2-3 Å, and cannot be used to obtain information about the handedness of a helical conformation.[11] Single crystals of DNA and DNA complexes diffract x-rays much better, and give the handedness of the helix as well as the atomic coordinates to within 1 Å resolution.[5,10,14] The primary drawback of x-ray crystallography is the difficulty in crystal formation. Crystal formation can take months and even then there is no

guarantee that the crystals will give good diffraction patterns. Not all molecules form single crystals; larger molecules may either not crystalize or become quasi-crystalline and the resulting coordinates are not well resolved.[11]

Nuclear magnetic resonance (NMR) is frequently used for determine nucleic acid structure in solution. From one-dimensional (1-D) NMR spectra changes in hydrogen bonding, in base stacking, in the conformation of the furanose sugar, and in the orientation of the C5′ carbon with respect to the sugar can be determined. The position of the base relative to the sugar can be determined using NOEs. The nuclear Overhauser Effect or NOE measures the change in intensity of a given nuclear spin when a nearby dipole coupled spin is saturated. Protons near the saturated proton are affected by a factor which is proportional to $1/r^6$, where r is the distance between the protons.[5] Two-dimensional (2-D) NMR techniques are also utilized in determining axis bending and secondary and tertiary structure. The drawbacks to using NMR as a structural probe are the amount of sample required and in the case of two-dimensional or higher order NMR spectra, the time required to obtain the data. Milliliter amounts of concentrated sample (ca. 10 mg/ml) are needed.[10,17,19] The concentrations required are similar to those required for Raman spectroscopy, but only microliter amounts are needed to acquire a Raman spectrum. Each 2-D experiment can take

anywhere from 5 hours to several days to run. For nucleic acid structure determination, NMR is also restricted by the size of the helix. In larger helices, interference between the proton signals on one base pair with those of other base pairs makes the spectrum too difficult to assign.

Infrared (ir) techniques provide a wealth of information about DNA structure. Infrared absorbance is considered to be the fingerprinting technique in compound identification. Only identical compounds will have the same ir spectrum. The advantage of infrared techniques over electronic spectroscopic techniques is that there are many more vibrational modes available than there are electronic transitions. Every nonlinear molecule of N atoms has (3N-6) vibrational modes; every linear molecule has (3N-5) vibrational modes. Where 3N represents the movement of each atom along the three Cartesian axes. 3N represents the translational, rotational and vibrational motions of the molecule. To consider only vibrational motion, the three translational motions of the molecule as a whole and the 3 molecular rotational motions of a nonlinear molecule or 2 for a linear molecule are subtracted from 3N. Since the motion of every atom is included in the total number of possible vibrations, the motion of every bond is included somewhere within the complete ir spectrum. However, the center of mass of a molecule is unaffected by vibrational motions and therefore, vibrational motion generally effects sets of bonds rather than individual bonds.

The set of motions that describes a vibrational level is called a normal mode. For every molecule there is a set of normal modes which describes its vibrational motion. Each mode has its own characteristic vibrational frequency.

The task of determining the normal modes gets quadratically much more difficult as the size of the molecule in question increases. For very large molecules like DNA, a common approach is to subdivide the molecule into smaller groups whose normal modes are known. The normal modes of the larger molecule are then defined via a combination of the vibrational motions of the subgroups. It is useful to divide the structure of DNA into the sugar-phosphate backbone, and the bases. The sugar-phosphate backbone can be further divided into the vibrational modes of the sugar and those of the phosphate groups. Table I (last page of this chapter) gives some of the relevant vibrational modes and their characteristic frequencies.

The most intriguing feature of Table I is that there is a set of vibrations of the nucleic acid bases which occur in the double-bond stretching region (1500-1750 cm^{-1}) where no backbone vibrations are seen. In addition, the phosphate stretching region which occurs in the 1050 - 1200 cm^{-1} region is devoid of any signals from the bases. This suggests that the vibrations of the backbone can be separated from those of the bases and can be examined independently which is not possible with the electronic transitions.

Infrared absorbance measures the change in the dipole moment during a normal mode of vibration. Only vibrations which change the vibrational dipole moment can give rise to absorbance peaks and then only if the induced vibration causes alterations in the dipole vector. Symmetric vibrational modes will not absorb ir radiation. However, the symmetrical vibrational modes are detectable through Raman scattering. Raman and infrared absorption are particularly useful for examining base tautomerism. The keto- peaks are far from the enol- peaks.[12] These are also good techniques for looking at the strength of the hydrogen-bonding between bases and at the conformation of the phosphate backbone.[20]

From an experimental standpoint, infrared absorbance and Raman scattering offer some clear advantages over x-ray crystallography and NMR. The drawback of x-ray diffraction techniques are that the technique is only applicable to crystalline samples and that a single experiment can take months to perform. Both NMR spectroscopy and Raman scattering can be performed using solid state samples as well as solution state samples. The concentrations of DNA samples used for ir absorbance and Raman scattering can be as high as 40 mg/ml which is similar to the concentration required for a 2-D NMR or C^{13}NMR experiment; however, sample volumes are in the range of 5 µl for the vibrational techniques, whereas NMR requires a few milliliters of sample. The time required to run an ir absorption or a Raman scattering experiment is only minutes,

not hours like it is for NMR.

The limiting features of infrared techniques are the sample concentration which is still several orders of magnitude higher than that required to perform experiments in the UV-visible region. Neither infrared absorption, Raman scattering, nor NMR can be used to directly determine handedness.

Besides x-ray crystallography there are no other ways to look at DNA handedness per se. For larger DNA molecules, circular dichroism (CD) is the method of choice. CD was the first technique to infer that a left-handed helix existed for DNA.[21] Currently, CD spectroscopy can be used over a greater wavelength range than the 220-400 nm used by Pohl and Jovin. It is possible to acquire CD data on aqueous solutions from 165 nm[22] through the infrared region, 12.5 μm.

Circular dichroism spectroscopy is one of the techniques used to observe the properties of optically active samples. Optical activity is due either to molecular asymmetry or molecular dissymmetry.

The asymmetry of a sample is a function of its structure. For an individual molecule to be optically active it must be chiral. Chirality is both the necessary and the sufficient condition for optical activity in a single molecule. For a molecule to be chiral it cannot posses a mirror plane or a center of symmetry; the molecule is not superimposable on its mirror image.[23] In most cases, chirality is produced by an

asymmetriccally substituted carbon atom as shown in the case of bromochlorofluoromethane (Fig. 13). The other two molecules shown in Figure 13 are not optically active. α-truxillic acid possesses a center of symmetry and 1,1 dibromocyclobutane has a mirror plane in the plane of the cyclobutane ring.

In a molecule with two chiral carbons, the effect of a chiral carbon in one part of a molecule may be "canceled out" by another chiral carbon of opposite orientation somewhere else in the molecule. Isomers of a compound with two chiral carbons but no optical activity are called meso structures (Fig. 14). Even though the individual molecules may themselves be chiral, the solution may still not possess optical activity. If a solution is a mixture of chiral molecules such that both the molecule and its mirror image are present in equal amounts then the solution will not be optically active. The molecule and its mirror image are called enantiomers, and a 50:50 mixture of two enantiomers is called a racemic mixture and is not optically active. Optically pure solutions contain only one of the enantiomers and are optically active.

Dissymmetry which is related to secondary structure is also a source of optical activity and it is for this reason that CD is used heavily in research involving biological molecules. Helices are always chiral. The only symmetry element that a helix inherently possesses is a screw axis.

Fig. 13: Structures of bromochlorofluoromethane, alpha-truxillic acid, and 1,1-dibromocyclobutane.
Only bromochlorofluoromethane is optically active.

alpha-truxillic acid

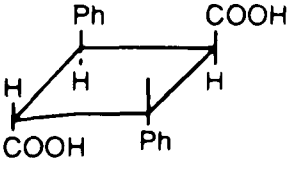

bromochlorofluoromethane

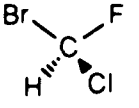

1,1-dibromocyclobutane

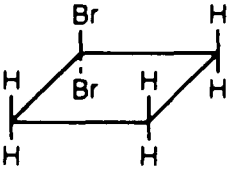

Fig. 14: Molecules with two chiral carbons are not always chiral

There are 3 isomers of 2,3-Butanediol

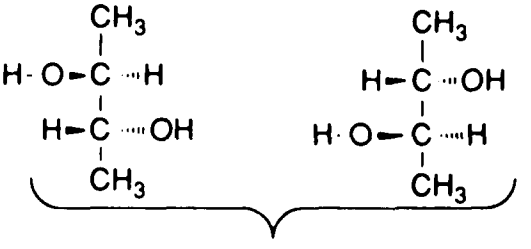

Mirror images nonsuperposable

optically active

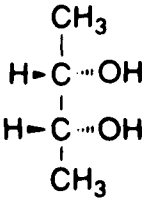

meso

mirror image is superposable

optically inactive

Since proteins form α-helices as well as other disymmetric structures, and DNA molecules also form left- and right-handed helices, there are many applications for CD spectroscopy in biochemistry.

In samples where secondary structure is the source of optical activity, racemates are not generally found. However, it is also rare that a protein will possess only one type of secondary structure and the CD signal observed is then a mixture of signals from each secondary structure present. Unlike absorption techniques, CD signals can be positive or negative and signal overlap can cause peak cancellation. It is extremely difficult to determine the exact nature of the signals which combined to form the CD spectrum observed. This difficulty is responsible for the two major limitations of CD spectroscopy; interpretability and quantitation.

Optical activity can be described by its effect on the light vector transmitted by the sample. Any light wave can be described in mathematical terms by:

$$\underline{E} = \underline{i}E_0\cos(\omega t + \theta) \qquad (1)$$

where E_0 is the maximum amplitude of the electric field, θ describes the phase angle, ω is the angular frequency with $\omega = 2\pi\nu$, ν is the frequency of the light, t is the time, θ is the initial phase, and $\underline{i}$ is the unit vector describing the direction of the electric field. $\underline{i}$ is perpendicular to the

propagation direction. When light is plane polarized, the light is restricted to one plane and $\underline{i}$ is a unit vector in the plane of polarization (Fig. 15).

Optically active samples rotate the plane of polarized light. This effect is known as optical rotation and is one of the oldest definitions of optical activity and certainly the easiest measurement to take. Optical rotary dispersion (ORD) is the ratio of the optical rotation over the wavelength, λ.

Rather than observing ORD, most modern approaches for the observation of optical activity use circular dichroism (CD). In CD, the sample is illuminated with alternating left circularly polarized and right circularly polarized light (CPL), and the difference in absorbance $\Delta A = A_L - A_R$ is observed.[24]

Circularly polarized light can be described by the superposition of two linear polarized components which are at right angles to each other and are $\pm\lambda/4$ (or $\pm\pi/2$) out of phase (Fig. 16).

$$\underline{E} = \underline{E}_L + \underline{E}_R \tag{2}$$

$$\underline{E}_L = \underline{i}E_0\cos(\omega t) + \underline{j}E_0\cos(\omega t + \pi/2) \tag{3}$$

$$\underline{E}_R = \underline{i}E_0\cos(\omega t) + \underline{j}E_0\cos(\omega t - \pi/2) \tag{4}$$

Viewed along the direction of propagation, eqns. 3 and 4 both trace out a circle over time but $\underline{E}_L$ moves in a counterclockwise motion over time while $\underline{E}_R$ moves clockwise. An optically active sample will absorb $\underline{E}_L$ differently from $\underline{E}_R$.

If the right CPL vector is absorbed more than the left

Fig. 15: Light

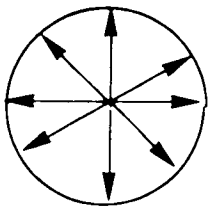

UNPOLARIZED

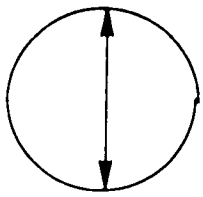

POLARIZED

Fig. 16: Plane Polarized Light may be described as the sum of a right circularly polarized light vector and a left circularly polarized light vector. The two vectors have the same amplitude, angular frequency and initial phase angle.

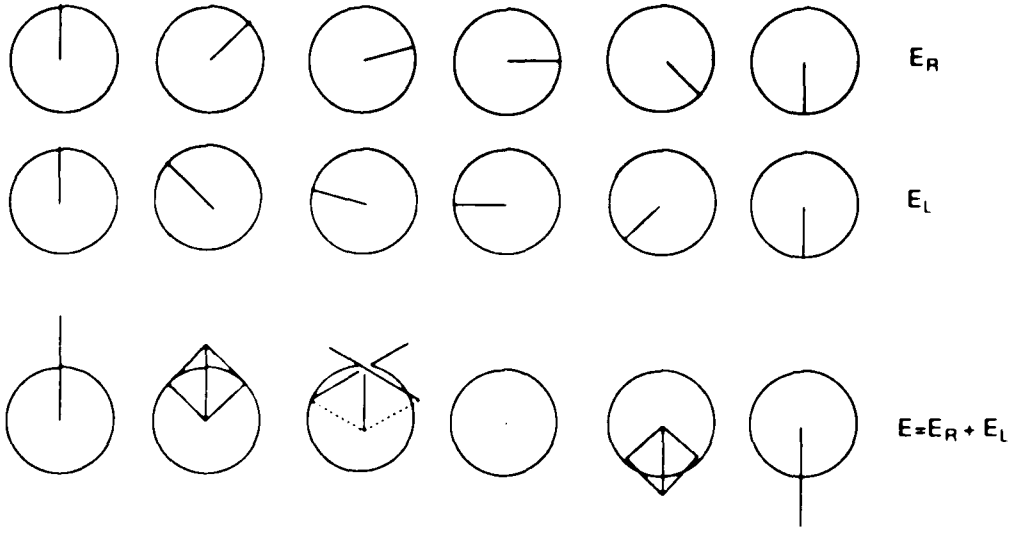

CPL vector then the radius of the circle traced out by $\underline{E}_L$ will be greater than the circle traced out by $\underline{E}_R$ and the combined vector $\underline{E}$ will trace out an ellipse (Fig. 17). Ellipticity is defined as the arctan of the ratio of the minor axis to the major axis of the ellipse (Fig. 18). Ellipticity is usually given as a molar quantity and is designated as $[\theta]$. If $A_L \neq A_R$ at any wavelength then the index of refraction will also be different $n_L \neq n_R$. Therefore the two components will propagate through the sample at different velocities and a phase shift which is proportional to $(n_L - n_R)$ will result. The shift in phase is called circular birefringence and it is responsible for the rotation of the major axis of the ellipse away from the original plane of polarization. Therefore, circular birefringence and optical rotation measure the same phenomenon.[24]

Ellipticity, optical rotation, circular dichroism and circular birefringence are all related mathematically and measurement of any one of them can be used to determine the values for the other three.[24]

At present, most optical activity is measured through circular dichroism. The spectra are plotted as $\Delta\varepsilon$ versus wavelength where

$$[\theta] = 3300\Delta\varepsilon \qquad (5)$$

where $\Delta\varepsilon$ is the difference between left CPL and right CPL.[24] Equation 5 is derived using Beer's law.

Circularly polarized light may be generated from linearly

Fig. 17: An **Elliptical Light Vector** may be described as the sum of two vectors which are circularly polarized in opposite directions and which have different amplitudes. $E_{ellipse} = E_R + E_L$

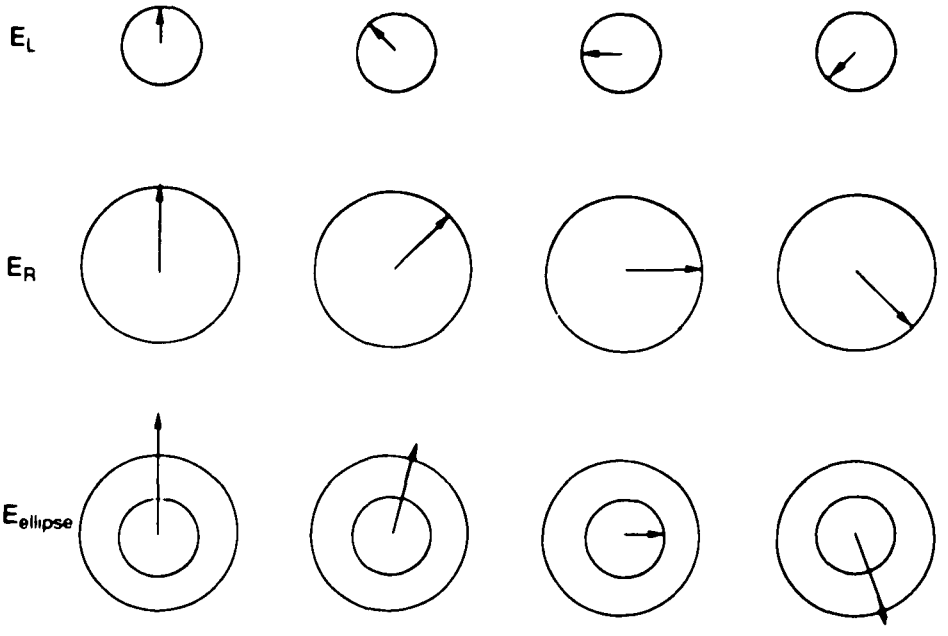

Fig. 18: Ellipticity and Optical Rotation

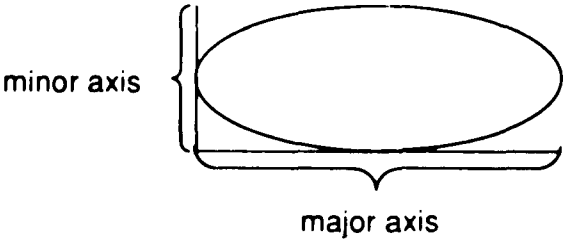

ellipticity: ratio of the minor axis to the major axis

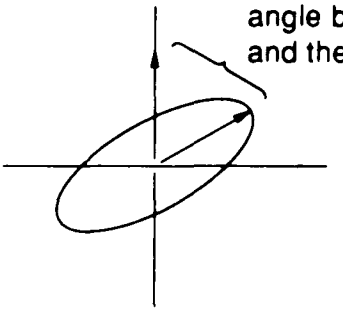

optical rotation: angle between the plane of polarization of the incident light and major axis of the ellipse formed by the resultant light.

polarized light by passing the light through a quarter wavelength retarder. The retarder is a birefringent crystal. Naturally birefringent crystals have a different index of refraction along the crystallographic x- and y-axes (assuming propagation is along the z-axis). The difference in the index of refraction causes the transmitted light along one axis to be retarded relative to that coming from a perpendicular axis. When birefringent crystals are used to generate circularly polarized light, the dimensions of the crystals are such that the retardation is $\pi/2$. In order to be useful for CD measurements, the instrument must be able to produce both left-circularly polarized and right-circularly polarized light. A birefringent crystal could be used if it is rotated by 90° to exchange the x- and y-axes with respect to the direction of CPL. A special type of crystal called a photo-elastic crystal allows both right- and left-circularly polarized light to be produced without altering the position of the crystal. A photo-elastic crystal is isotropic in the absence of a mechanical stress but becomes birefringent when stressed.

The strength of an absorption band (dipole strength, D) and the strength of its optical activity (rotational strength, R) can be described by:

$$D = |\langle\psi_n|\underline{\mu}|\psi_k\rangle|^2 \tag{6}$$

$$R = \mathrm{Im}\ [\langle\psi_n|\underline{\mu}|\psi_k\rangle \cdot \langle\psi_k|\underline{\mathbf{m}}|\psi_n\rangle] \tag{7}$$

where the transition occurs between states n and k; $\underline{\mu}$ and $\underline{\mathbf{m}}$

are the electric and magnetic dipole operators, respectively. These equations are the most general expressions for the observation of absorbance and CD. However, they are not very useful for computations since the exact form of the wavefunctions is not known. Thus, approximate expressions and simplified theories have been developed. One of them is the "coupled oscillator model", which describes the interaction of two identical groups in a molecule and is the simplified model for conformation dependent optical activity (chap. III). For the interaction of two identical monomer transitions, the dipole and rotational strength are given by:

$$D_{12} = D^{+} = \underline{\mu}_1^2 + \underline{\mu}_2^2 \pm \underline{\mu}_1\underline{\mu}_2 \qquad (8)$$

$$R_{12} = R^{+} = +(\pi\nu_0/2c)[\underline{T}_{12}\cdot\underline{\mu}_1 \times \underline{\mu}_2] \qquad (9)$$

where $\underline{\mu}_1$ and $\underline{\mu}_2$ are the dipole transition moments of oscillators 1 and 2 respectively, c is the speed of light; ν_0 is the frequency of the monomer transition; and $\underline{T}_{12}$ is the vector which describes the distance between the monomers. Equation 9 shows a direct correlation between the CD spectrum and the the geometry of the molecule which is governed by $\underline{\mu}_1$ X $\underline{\mu}_2$ and $\underline{T}_{12}$. This correlation makes circular dichroism an invaluable tool in biochemistry for acquiring secondary and tertiary structural information.

Early CD spectroscopy was only carried out in the visible/near UV-CD region (220-700 nm). HgXe and Hg sources produce enough light in this region for CD experiments even at low chromophore concentrations. Samples are typically

micromolar concentrations for DNA when 1 cm pathlengths are used.

The near UV CD region is used for determining the helical conformation of oligonucleotides. The initial data which suggested that a left-handed helix existed for DNA was near UV CD data.[21] However, Tomasz and coworkers found that signals in the near UV CD are not always reliable indications of the existence of a Z-conformation.[25] Near UV CD spectra also show differences in the spectrum of A-form and B-form right-handed DNAs.

Through the use of different light sources and increases in technology of photomultipliers and lock-in amplifiers, the useful range of CD spectroscopy has increased. Now, CD spectra can be taken well into the vacuum UV region, down to approximately 160 nm. The experiments are more difficult in the vacuum UV region than in the near UV region. Water and metal cation solutions both absorb vacuum UV irradiation so the path length must be decreased substantially and the DNA concentration increased in order to acquire a vacuum UV CD spectrum. Path lengths vary from 25 - 75 μm and concentrations are in the millimolar range.

The spectrum of DNA below 200 nm region is also used to determine helix conformation. Although spectra in this region are reliable in determining the handedness of the DNA in the solution, the spectra of B-form and A-form DNAs are indistinguishable. Therefore, in order to determine the

conformation of DNA by UV CD spectroscopy, the spectrum must be taken in both the near UV and vacuum UV regions.

It has long been recognized that a technique which could combine the sensitivity to secondary structure of circular dichroism with the "fingerprinting" ability of the infrared techniques would be very valuable in determining the secondary structure of large biomolecules. The equations used to describe the vibrational optical activity of molecules take the same form as Eqns. 6-9 but $\underline{\mu}$ and $\underline{m}$ now represent vibrational instead of electronic dipole and magnetic transition operators. Theoretical calculations using normal coordinate analysis to determine the transition moments and equations similar to Eqns. 6-9 were used to predict the rotational spectra long before any experiment could be performed. Unfortunately, infrared instrumentation lagged far behind the requirement to measure such small effects since rotational strengths are four to five orders of magnitude weaker than their corresponding dipole strengths.

In the past twenty years, there have been tremendous innovations in infrared instrumentation and two ways of measuring vibrational optical activity have emerged. Vibrational circular dichroism (VCD) measures the difference in absorption of left- and right- circularly polarized infrared light. Raman optical activity (ROA) measures the difference in intensity of scattered right- and left-circularly polarized ultraviolet light by chiral solutions.[26]

Both VCD and ROA spectra of small molecules were performed starting in the 1970s.[27,28,29] The early studies involved examination of the stretching vibrations of the C-H, N-H, O-H and C-D bonds. Studies are still being done today which involve C-H and C-D stretching deformations and have been applied to biological molecules including the L-amino acids.[30]

VCD expanded into examination of the peptide linkages in small di- and tri- peptides and on homopolypeptides.[31] Currently, Keiderling and coworkers are examining the secondary structure of proteins using VCD spectroscopy and have developed a basis set of VCD spectra of proteins with known conformations from which the VCD spectra of proteins with unknown conformations can be derived.[32,33]

Keiderling and coworkers extended the use of VCD spectroscopy to RNA homopolymers and on poly(I-C)poly(I-C).[34] In 1989, Diem and coworkers obtained VCD spectra of the B- and Z-forms of poly(dG-dC).[35] This work has been extended to other DNA oligonucleotides of sizes varying from 4-bases/strand to ca. 1100 bases/strand. A model which relates the VCD spectra of oligonucleotides with their helical conformation has also been developed by Diem's group.[35,36]

This thesis encompasses all of the VCD studies performed on CG-deoxyoligomers of 10 bases or greater as well as interpretation of the results by a simple model, the degenerate extended coupled oscillator (DECO) model. In the

following sections, the use of vibrational circular dichroism as a viable technique for examining the secondary structure of deoxyoligonucleotides is demonstrated. The development and use of the Degenerate Extended Couple Oscillator (DECO) model as an aid in VCD spectral interpretation is also discussed. The DECO model is based solely on the interactions of the carbonyl groups of the purine and pyrimidine (in this case, the guanine and cytosine) bases. Although this is a simple model, the model does well in describing the carbonyl interactions that give rise to the VCD spectra of right-handed oligonucleotides.

Table 1: Assigned Infrared Frequencies for DNA in H_2O and D_2O Solutions. Frequencies are given in wavenumbers (cm^{-1}) (Pilet and Leng 1982)

confor-mation	H_2O	D_2O	assignment
B-form	1711	1686	in plane vibrations of paired bases with strong double bond character
		1650	
	1224	1215	PO^{2-} antisymmetric stretch
	1087	1087	coupling of PO^{2-} with C5'-O5' stretch; includes other backbone vibrations to a lesser extent
	1055	1055	C-O stretch of sugar ring or phosphodiester linkage
	1020	1020	C-O stretch of sugar ring or phosphodiester linkage
	832	832	anisymmetric diester O-P-O stetching character
Z-form	1693	1667	shift of band seen at 1711 (1686) cm^{-1} in B-form spectrum
		1635	shift of band seen at 1650 cm^{-1} in B-form spectrum
	1220	1220	PO^{2-} stretch
	1055	1055	enhancement by 10% of peak seen at 1055 cm^{-1} in B-form spectrum
	1020	1020	PO^{2-} stetch
	1015	1015	enhancement by 70% of peak seen at 1020 cm^{-1} in B-form spectrum

Pilet, J. and M. Leng. (1982). "Comparison of Poly(dG-dC)poly(dG-dC) Conformations in Oriented Films and in Solution." PNAS. 79: 26-30.

II. MATERIALS AND METHODS:

A. Materials:

Poly(dG-dC)poly(dG-dC), pd(CG)$_5$, poly(dG)poly(dC) and poly(dG-me^{5}dC)poly(dG-me^{5}dC) were purchased from Pharmacia Molecular Biologicals. Additional poly(dG-dC)poly(dG-dC), D_2O, NaCl, $NiCl_2$, $CoCl_2$, $MgCl_2$, NaH_2PO_4, Na_2HPO_4 and sodium cacodylate were purchased from Sigma Chemical Co. The $[Co(NH_3)_6]Cl_3$ was a gift from Prof. David Lavallee (Hunter College). Sodium cacodylate was dissolved in D_2O and lyophilized to dryness before use. The metal salts were dissolved in D_2O and dried either on a SpeedVac (Savant Instruments) or on a lyophilizer before use in vibrational CD experiments. pD adjustments were made using DCl and NaOD (Sigma Chemical Co.). Conversion of pD to pH was made by adding 0.4 to the pD values.

B. Methods:

1. UV-Visible Spectral Region

a. Standard Electronic CD and absorbance:

Samples for UV absorbance and near UV CD spectroscopies were prepared in 10 mM sodium phosphate buffer with 10 mM NaCl, pH = 7.1 ± 0.1. The salt concentration of the sample was adjusted by the addition of concentrated buffered salt stock solutions. A delay of thirty minutes to one hour was used to ensure total mixing of the metal salt with the polymer. The same samples were used for both electronic CD and absorbance measurements. Most frequently, sample cells

used were quartz cells with a 1 cm path length although a 0.1 cm path length cell was also employed. Oligomer concentration varied from 6.6×10^{-5} M in base pairs (0.10 mg/ml) to 1.6×10^{-4} M (0.043 mg/ml).

In addition, many of the samples prepared for use in the ir region were also run in the electronic CD instrument. The cell compartment of the CD instrument was modified to accommodate the ir cells (Fig. 1). Preparation of these samples is described in section II.B.2.

Ultraviolet absorbance measurements were performed using a Cary Model 219 spectrophotometer. Electronic circular dichroism (UV CD) measurements were made using a Jobin-Yvon Mark V dichrograph, interfaced to an Apple 2e computer. The light source for the CD instrument is a 250 W xenon (Xe) lamp. The Mark V CD is equipped with a double prism monochromator and circularly polarized light is generated through a photoelastic modulator.

CD spectra of background solutions containing the buffer and the metal salts were subtracted from the spectra of the metal-oligomer complexes. All CD curves except those that include the vacuum UV region were plotted in terms of $\Delta\varepsilon$ where $\Delta\varepsilon$ stands for the differential extinction coefficient between left- and right-circularly polarized light.

$$\Delta\varepsilon = \varepsilon_L - \varepsilon_R \qquad (1)$$

$\Delta\varepsilon$ is calculated from ΔA using a standard Beer's law calculation where pathlength (l) is given in cm and

Fig. 1: Modified Sample Compartment of the Mark V UV CD Instrument 49

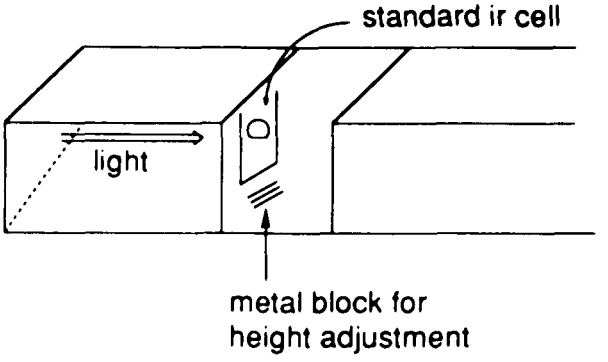

concentration (C) in moles of nucleotide base pair/liter.

$$A = \varepsilon Cl \qquad (2)$$

Plotting the CD spectra in terms of $\Delta\varepsilon$ instead of ΔA eliminates differences between the path length and the concentration of the samples.

b. Vacuum UV-CD using a synchrotron light source:

Some of the vacuum UV-CD measurements were made on the system described above. Most of the samples that were scanned below 200 nm were made using a spectrometer[22] that receives radiation from the VUV electron storage ring of the National Synchrotron Light Source at Brookhaven National Labs.[37] The advantages of using a synchrotron light source over a 250 W Xe lamp are:

1) the synchrotron provides a continuous, almost constant output of light from 3.16 - 1000 nm[22] whereas the 250 W xenon lamp emits a continuous constant amount of light at only 50% of its possible spectral output from 800 - 500 nm but below 500 nm the throughput of the source falls off and reaches a level of 1/1000 of its possible output at approximately 180 nm.

2) the synchrotron source produces linearly polarized light while the light from the xenon arc lamp is unpolarized and must be converted to linear polarization at a loss of more than 50% of the original intensity.

3) synchrotron radiation is produced in vacuum therefore

the light is not effected by the humidity in the air as there is when conventional sources are used.

Samples for vacuum CD were prepared in 10 mM cacodylate buffer, pH 7.0. Oligomer concentrations were on the order of 0.02 M in nucleotide base pairs (20 mg/ml). The path lengths employed varied from 0.1 to 0.0025 cm. For measurements requiring a 0.1 cm path length a quartz cell was employed. At shorter path lengths, a Gray cell was used (Fig. 2).[38] The Gray cell resembles an infrared cell. The sample is placed between two quartz plates and the path length is set by a teflon spacer. The cell holder is comprised of two brass plates which are held together by set screws. Short path lengths were both an asset and a necessity for work in the vacuum UV region. Short path lengths meant that the oligonucleotide concentration in the sample was of the same order of magnitude as the concentration used for the infrared experiments. In addition, short path lengths are a necessity for working below 200 nm because both the water and the salt cations absorb light below 200 nm.

2. Infrared Spectral Region

a. Sample Preparation:

Infrared samples were prepared using 10 mM sodium cacodylate buffers, pH 7.1 ± 0.1. NaCl was added to a final concentration of 10 or 50 mM in all solutions employing multivalent cations. Samples containing $NiCl_2$ were prepared in aqueous solutions without cacodylate buffer, since the

Fig. 2: Gray Cell

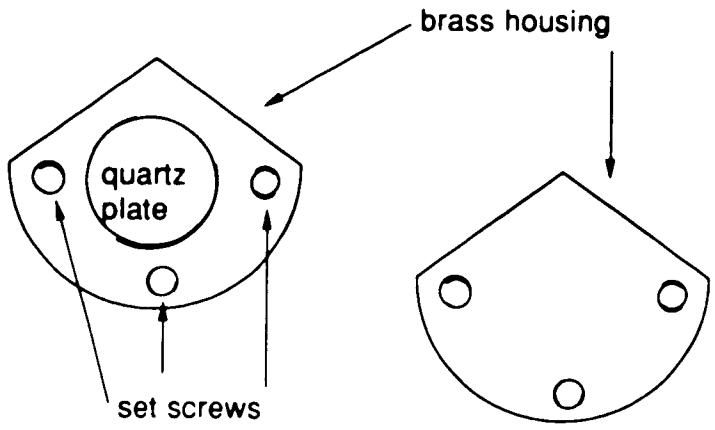

buffer caused the metal to precipitate. The salts were all titrated gradually into the samples, allowing at least 30 minutes between additions so that there was enough time for a conformational change to occur in the oligomer; this prevented aggregation problems which arise at high salt and oligomer concentrations. Salts were either added as concentrated stock solutions or as solids, and the sample incubated in the high salt solution overnight. $MgCl_2$ will induce DNA precipitation over time. Therefore, rather than waiting overnight, these samples were incubated at 60° C for 10 minutes with constant mixing. The samples were allowed to cool in the open air, but the mixing was continued until the sample reached room temperature. The samples were subsequently transferred to 19 mm CaF_2 ir windows separated by teflon spacers of appropriate thickness as indicated above.

b. Instruments:

Infrared absorption and VCD measurements were performed using one of two dispersive infrared dichrographs, designed and constructed in our laboratory[39,40,41]. In both of these instruments, the ir absorbance spectrum is taken as a prescan before the VCD scan. The first VCD instrument (VCI) was originally designed for use in determining the structure of peptides in solution. The instrument was optimized at 1200 cm^{-1} for the amide III region. However, the instrument can be used for measurements in the amide I and amide II regions as well (900 - 1800 cm^{-1}).

The light source is a ceramic Nernst glower. At temperatures between 2200 and 2400 K, the Nernst glower acts as a blackbody.

The light source is modulated by a chopper at 79.5 Hz. There are two optical arrangements used to collect the light. The light is either collected at F/4 and imaged 1:1 on an F/4 monochromator or collected at F/2 and imaged 1:2. F/4 collection is used for work in the amide I carbonyl stretching region.

The monochromator has a ruled grating (120 grooves/mm). For work in the 1200 - 1800 cm^{-1} region the exit and entrance slits are 10 mm high and 2.0 mm wide and the bandpass is 5.5 - 14.2 cm^{-1}. The light from the monochromator is directed through a gold-wire grid polarizer which is positioned directly in front of the photoelastic modulator.

The main component of the photoelastic modulator (PEM) is a broadband antireflection-coated zinc selenide (ZeSe) crystal which has greater than 90% transmission between 12 and 5 μm. The stress axis of the crystal is at a 45° angle with the polarization direction. The crystal is modulated at its resonance frequency (31.2 Hz) at which frequency left- and right-circularly polarized light are produced alternatingly.

The sample is mounted directly to the PEM and a barium fluoride lens focuses the light onto the detector.

The detector is one of the newest innovations of infrared technology. The active element of the detector is

photoconductive mercury cadmium teluride (HgCdTe) which operates at liquid nitrogen temperature. The active area of the detector is 1.01 X 5.08 mm^2. The range is 800 - 1800 cm^{-1}.

The electronics of VCI consist of three lock-in amplifiers controlled by an AT&T personal computer (model 6300). The output current from the detector is amplified and then split into two components. The first component is measured by a digital lock-in amplifier (LIA) which demodulates the signal at 79.5 Hz. This produces the I_{DC} and the absorbance signal. The second component goes to a another lock-in amplifier (Princeton Applied Research, model 124A) to be demodulated at 31.2 Hz (PEM frequency) and then to a second LIA (Princeton Applied Research, model 5207) lock-in amplifier to be demodulated at 79.5 Hz which is the I_{AC} speed. The AT&T computer controls the gain and the sensitivity of the PAR 5207 lock-in amplifier.[41]

ΔA is computed from I_{DC} and I_{AC} as the scan progresses. On the computer monitor, a plot of ΔA versus wavenumber is updated in real time so the scan may be monitored as it progresses. The absorbance spectrum is also displayed on the computer monitor during the VCD acquisition. The computer saves each individual scan automatically. At the end of the allotted number of scans, the computer produces a final VCD spectrum which is a normalized sum of the individual scans. The final VCD spectrum and the absorbance spectrum are also saved on the computer's hard disk.

In addition to controlling the retardation level of the PEM, and the 5207 lock-in amplifier, the computer controls the monochromator and has routines for data display and data manipulation. All of the software as well as the design and assembly of the hardware were done in our laboratory.[39,41,42]

The second VCD instrument, VCII, was designed specifically for work in the carbonyl stretching region (1600-1750 cm^{-1}). This instrument cannot be used at all in the amide II and amide III regions.

VCII uses the same type of source as VCI. VCII is designed with F/3 collection optics and the light is then manipulated to match the F/5.7 optics of the monochromator.

The monochromator (Instruments, SA, HR640) has a ruled grating with 150 grooves/mm. The monochromator allows a faster scan rate than that of the monochromator used in VCI which makes a considerable difference in the data acquisition time. For work in the 1500-1800 cm^{-1} region, 3.0 mm slits are adequate.

After the monochromator, the light passes through a polarizer and then through a photoelastic modulator (Hinds International, Inc., model PEM-80 system II/CF). This PEM uses a CaF_2 crystal which is smaller in size than the ZnSe crystal used in the PEM of VCI. CaF_2 is harder than ZnSe and this feature combined with the smaller size of the crystal means that the modulation frequency is higher (57.6 KHz).

The light is focused onto the detector through a CaF_2

focusing lens. The detector is a HgCdTe detector which was designed for use in this instrument (Infrared Associates, Inc., model HCT-80 6-7 dual element). The detector has an active element which is composed of two 1.01 x 1.01 mm HgCdTe pieces placed vertically together. The responsivity of this detector drops off drastically below 1600 cm^{-1} and the low end cut off of VCII is therefore 1600 cm^{-1}.

A unique feature of this instrument is that the sample chamber is completely isolated from the rest of the system and can be purged separately from the rest of the system. Therefore, any humidity that enters the instrument when the sample chamber is opened affects only the humidity in the sample chamber and does not affect the humidity levels in the rest of the instrument. Therefore, only the sample chamber needs to be purged after the sample cell is placed into the chamber. This cuts down the amount of purge time required between different sample scans.

The electronics of VCII are similar to the electronics of VCI and will not be discussed further here except to mention that both lock-in amplifiers used to measure V_{AC} are computer controlled.[41]

The reasons for using both instruments are:

1) VCI covers a broader range of wavenumbers than VCII does and although the work reported here was done primarily in the 1600-1750 cm^{-1} region covered by VCII, the 1550-1600 cm^{-1} region as well as the 1050-1250 cm^{-1} phosphate region[43] also

provided some interesting results;

2) VCII has a signal-to-noise ratio in the 1600-1750 cm^{-1} region which is three times better than that of VCI in this region.[41]

c. Plotted Spectra:

All VCD spectra shown are averages of 10-60 scans, each scan lasting about 10 minutes on VCII and 15 minutes on VCI. The response time was 1 second for both VCII and VCI instruments.

When the spectra taken on different instruments are compared, the frequency scale of the VCI spectra is altered by 7 cm^{-1} to account for a difference in calibration between the two instruments.

All infrared plots are scaled such that the area under the ir absorbance curves between 1600 and 1750 cm^{-1} are equal.

III. Chiroptical Properties of Right Handed DNA Conformations:

In an aqueous solution at neutral pH and low ionic strength, the conformation of most deoxyoligonucleotides is that of a right-handed helix.

In order to fully use the information available through VCD spectroscopy, both the experimental spectra and a model which correlates the geometry of the oligonucleotide with its spectral characteristics are employed. In this chapter, a quantum mechanical description of the effects that give rise to the rotational strengths measured through VCD spectroscopy are explained. Then the Degenerate Extended Coupled Oscillator (DECO) model, a model which attempts to correlate the observed spectra with the helical geometry, is proposed. In the subsequent sections, the model is applied to small oligonucleotide fragments including single base pairs, two base strands, and trimers. Finally, calculated spectra of double stranded 5'$(CG)_{10}$ and $(G)_{10}(C)_{10}$ are generated and compared with the experimental VCD spectra of poly(dG)poly(dC), poly(dG-dC)poly(dG-dC), and the decamer $pd(CG)_5$. This knowledge is also extended to the interpretation of experimental spectra of poly(dG-me^{5}dC)poly(dG-me^{5}dC).

A. Theory:

The Degenerate Extended Coupled Oscillator (DECO) model is based on a model known as exciton theory first proposed by

solid state physicists,[44] and applied to optical activity by Moffit in the 1950s.[45] Exciton theory applies to the situation wherein identical or nearly identical transitions within a molecule or unit cell couple because of their relative geometries. The carbonyl stretching transitions of the bases of a DNA molecule, for example, couple because of their polar nature and because of the helical geometry of DNA.

Exciton theory states that if one vibrational quantum of energy is absorbed by a group of degenerate oscillators, the resulting excited state may be best described as the sum of all possible one-quantum excitations. The implication of this statement is that the one-quantum excitation is not simply localized on one oscillator but rather it is delocalized over the entire array of degenerate or nearly degenerate oscillators. The delocalized excitation is referred to as an "exciton". The effect of the delocalization is that the degeneracy of the individual one-quantum states is lifted and a group of discrete exciton energy levels are observed. The number of discrete states is equal to the number of original degenerate states which is equal to the number of interacting oscillators.

The quantum mechanical treatment of this phenomenon is described in detail in Figs. 1-9 (which are shown together at the end of this section); the results and a discussion of the results are explained in the text. For a monomer, a, with a one electron polar transition from the ground state to the

first excited state and no magnetic moment, the frequency of the transition, υ^a, and the dipole strength of the transition, $D_{01}{}^a$, are described in Fig. 1. There is no rotational strength because there is no magnetic moment present to generate it.

When a dimer is created from two identical monomers, a and b, where the monomers do not interact with one another, there is no change in the frequency of the transition but the dipole strength of the transition is twice that of the monomeric transition (Fig. 2). The rotational strength is still zero since the two monomers do not interact. If the monomers in the dimer interact, then an interaction term, V^{ab}, must be added to the Hamiltonian (Fig. 3, eqn. 21). The interaction splits the degeneracy of the two one-electron excited states. The difference in the energies of the two newly formed excited states is the exciton splitting and is equal to $2V^{ab}{}_{11}$ where $V^{ab}{}_{11}$ is the interaction energy between the first excited states of monomer a and monomer b. The exciton splitting results in there being two transition frequencies observed in the absorbance spectrum (Fig. 3). The integrated intensity of these peaks is the same as that seen in the non-interacting dimer case. However, the relative intensities of the absorbance peaks is a function of their geometry. There is also a rotational strength due to the geometry of the two oscillators (Fig. 4). The coordinates of the two oscillators in a spherical coordinate system are described in Fig. 5. The effect the oscillator geometry has on the

absorbance and rotational spectra of the dimer is illustrated in Figs. 6,7 and in Table I.[46]

Exciton theory is easily extended to the case of an infinite polymer by denoting the one electron excited state for the polymer as a sum of all possible one electron monomer states (Fig. 8).

To apply the above discussion to a real case, the form of the interaction between the two monomers must be defined explicitly. The perturbation used in the calculations reported here is strictly of the dipole-dipole type and is proportional to the dot product of the dipole vectors for the individual monomers and inversely proportional to the cube of the distance between the center of mass of the two oscillators. The explicit form of V^{ab} is given in Fig. 9.

The discussion outlined above is strictly quantum mechanical and in order to obtain values for the energy splitting, the dipole strength and the rotational strengths, the wavefunctions must be known. Since explicit forms of the wavefunctions are not known to sufficient accuracy, approximate expressions and simplified theories have been developed. The degenerate extended coupled oscillator (DECO) model examines the interaction of identical groups along the helix. The dipole moment vector for each identical group (oscillator) is determined by the distance between the regions of positive and negative charge and the vector direction is taken to be from the positive region to the negative one. The

DECO model uses experimentally determined values of $|\mu|$ and ν_o of the monomers (GMP and CMP) as the starting point of the calculation. The exciton contribution to the optical rotation of infinite helices has been applied to both electronic transitions[44] and to vibrational transitions.[35,36,44] This thesis is concerned only with the exciton contribution to the rotational strength of infrared transitions and more specifically, the interactions between the base carbonyls are explored.

Fig. 1: Monomer

For a monomer with no inherint magnetic moment:

Let $\varphi_0^\bullet$ represent the ground state wavefunction , $\varphi_1^\bullet$ the wavefunction for the first excited state, $H^\bullet$ the Hamiltonian operator, $\bar{\mu}^\bullet \equiv$ dipole moment operator and $\bar{m}^\bullet \equiv$ the magnetic moment operator. Then:

$$\langle \varphi_0^\bullet | H^\bullet | \varphi_0^\bullet \rangle = E_0 \quad \text{the ground state energy;} \tag{1}$$

$$\langle \varphi_1^\bullet | H^\bullet | \varphi_1^\bullet \rangle = E_1 \quad \text{the energy of the first excited state.} \tag{2}$$

For a one-electron transition from the ground state to the first excited state $(0 \rightarrow 1)$:

$$\Delta E = E_1 - E_0 \tag{3}$$

$$\nu^\bullet = \Delta E / h \quad \text{the frequency of the transition} \tag{4}$$

where h is Planck's constant

$$D_{01}^\bullet = \left| \langle \varphi_0^\bullet | \bar{\mu}^\bullet | \varphi_1^\bullet \rangle \right|^2 \quad \text{the dipole strength of the transition} \tag{5}$$

$$R_{01}^\bullet = 0 \quad \text{the rotational strength of the transition} \tag{6}$$

The rotational strength is zero because the magnetic moment of the transition has been defined above.

Fig. 2: Dimer of noninteracting monomers

$$H = H^a + H^b \tag{7}$$

$$\Phi_0 = \varphi_0^a \varphi_0^b \tag{8}$$

$$\Phi_1^A = \varphi_1^a \varphi_0^b \tag{9}$$

$$\Phi_1^B = \varphi_0^a \varphi_1^b$$

$$\bar{\mu} = \bar{\mu}^a + \bar{\mu}^b \tag{10}$$

Φ_1^A and Φ_1^B both satisfy the four conditions of proper wavefunctions[1] . For the dimer:

$$\langle \Phi_0 | H | \Phi_0 \rangle = \langle \varphi_0^a | H | \varphi_0^a \rangle + \langle \varphi_0^b | H | \varphi_0^b \rangle = 2E_0 \tag{11}$$

$$\langle \Phi_1^A | H | \Phi_1^A \rangle = \langle \varphi_1^a | H | \varphi_1^a \rangle + \langle \varphi_0^b | H | \varphi_0^b \rangle = E_0 + E_1 \tag{12}$$

$$\langle \Phi_1^B | H | \Phi_1^B \rangle = \langle \varphi_0^a | H | \varphi_0^a \rangle + \langle \varphi_1^b | H | \varphi_1^b \rangle = E_0 + E_1 \tag{13}$$

Notice, the two one-electron excited states are degenerate.

For the $0 \rightarrow 1$ transition:

$$\Delta E = (E_1 + E_0) - (2E_0) = (E_1 - E_0) \tag{14}$$

$$\nu^{dimer} = (E_1 - E_0)h^{-1} \tag{15}$$

The dimer frequency is the same as that of the monomers.

$$D_{01} = D_{01}^A + D_{01}^B \tag{16}$$

$$D_{01}^A = \left| \langle \varphi_0^a | \bar{\mu}^a | \varphi_1^a \rangle + \langle \varphi_0^b | \bar{\mu}^b | \varphi_0^b \rangle \right|^2 = D_{01}^a + 0 \tag{17}$$

$$D_{01}^B = \left| \langle \varphi_0^a | \bar{\mu}^a | \varphi_0^a \rangle + \langle \varphi_0^b | \bar{\mu}^b | \varphi_1^b \rangle \right|^2 = 0 + D_{01}^b; \text{ where} \tag{18}$$

$$D_{01} = D_{01}^a + D_{01}^b = 2D_{01}^a \text{ since } D_{01}^a = D_{01}^b \tag{19}$$

The dipole strength of the dimer is twice that of the monomer.

$$R_{01} = 0 \tag{20}$$

since the two monomers do not interact

---

[1] The four conditions of proper wavefunctions are described in Appendix 1.

Fig. 3: Dimer of Interacting Monomers:

For a dimer of two identical monomers which do interact, Φ_0, Φ_1^A, and Φ_1^B are defined the same way as they were in the non-interacting dimer case. However, another term must be added to the Hamiltonian to account for the interaction of the monomers.

$$H = H^a + H^b + V^{ab} \qquad (21)$$

The addition of V^{ab} to the Hamiltonian makes Φ_1^A and Φ_1^B improper wavefunctions since

$$\langle \Phi_1^A | H | \Phi_1^B \rangle = \langle \Phi_1^A | V^{ab} | \Phi_1^B \rangle = 2\langle \varphi_1^a | V^{ab} | \varphi_1^b \rangle \neq 0 \qquad (22)$$

and therefore Φ_1^A and Φ_1^B are no longer stationary. Using the four boundary conditions for proper wavefunctions described in Fig. 3, two proper wavefunctions which are linear combinations of Φ_1^A and Φ_1^B are determined to be:

$$\Phi^+ = \sqrt{\frac{1}{2}}(\Phi_1^A + \Phi_1^B) \qquad (23)$$

$$\Phi^- = \sqrt{\frac{1}{2}}(\Phi_1^A - \Phi_1^B) \qquad (24)$$

The energies for these two excited states are:

$$\langle \Phi^+ | H | \Phi^+ \rangle = E_1 + E_0 + V_{11}^{ab} \qquad (25)$$

where

$$V_{11}^{ab} = \langle \varphi_1^a | V | \varphi_1^b \rangle = \langle \varphi_1^b | V | \varphi_1^a \rangle \qquad (26)$$

and

$$\langle \Phi^- | H | \Phi^- \rangle = E_1 + E_0 - V_{11}^{ab} \qquad (27)$$

The degeneracy of the two 1 e^- excited states has been split by $2V_{11}^{ab}$. This splitting is called the **exciton splitting**.

The $0 \rightarrow 1$ transition now has two parts.

$$\nu^+ = (E_1 + E_0 + V_{11}^{ab} - 2E_0)h^{-1} = (E_1 - E_0 + V_{11}^{ab})h^{-1} \qquad (28)$$

$$\nu^- = (E_1 + E_0 - V_{11}^{ab} - 2E_0)h^{-1} = (E_1 - E_0 - V_{11}^{ab})h^{-1} \qquad (29)$$

Therefore, the absorbance spectrum will have two peaks which are centered about the monomer frequency ν^a and which are split in frequency by $2V_{11}^{ab}h^{-1}$.

Fig. 4: Effect of Exciton Splitting on Dipole and Rotational Strength. The dipole strengths and rotational strengths of the transition are as follows:

$$\mathbf{D}^{\pm}_{01} = \left|\langle \Phi_0 | \bar{\mu}^a + \bar{\mu}^b | \Phi^{\pm} \rangle\right|^2 = \left|\langle \varphi^a_0 | \bar{\mu}^a | \varphi^a_1 \rangle \pm \langle \varphi^b_0 | \bar{\mu}^b | \varphi^b_1 \rangle\right|^2 \qquad (30)$$

Since

$$\mathbf{D}^{a}_{01} = \left|\langle \varphi^a_0 | \bar{\mu}^a | \varphi^a_1 \rangle\right|^2 = \left|\langle \varphi^b_0 | \bar{\mu}^b | \varphi^b_1 \rangle\right|^2 \qquad (31)$$

and

$\langle \varphi^a_0 | \bar{\mu}^a | \varphi^a_1 \rangle \langle \varphi^b_0 | \bar{\mu}^b | \varphi^b_1 \rangle$ is the dot product of the two transition dipoles

then

$$\mathbf{D}^{\pm}_{01} = \bar{\mu}^2 \pm \bar{\mu}^a_{01} \bullet \bar{\mu}^b_{01} \qquad (32)$$

where

$\bar{\mu}^a_{01} \equiv \langle \varphi^a_0 | \bar{\mu}^a | \varphi^a_1 \rangle$ and $\bar{\mu}^b_{01} \equiv \langle \varphi^b_0 | \bar{\mu}^b | \varphi^b_1 \rangle$

This result indicates that the relative intensities of the two absorption bands is a function of their relative geometries. However,

$$\mathbf{D}_{01} = \mathbf{D}^{+}_{01} + \mathbf{D}^{-}_{01} = \mathbf{2D}^{a}_{01} \qquad (33)$$

which indicates that the total spectral intensity is twice the monomer intensity as it is in the non-interacting dimer case.

For the rotational strength:

$$\mathbf{R}^{\pm}_{01} = Im[\bar{\mu} \bullet \bar{\mathbf{m}}] = \pm(\pi\nu^a/\mathbf{2c})(\mathbf{T}^{ab} \bullet \bar{\mu}^a_{01} \times \bar{\mu}^b_{01}) \qquad (34)$$

where

$\mathbf{T}^{ab}$ is the vector connecting the center of mass of oscillator a with the center of mass of oscillator b.

Fig. 5: Spherical polar coordinate system for the dimer.

μ^a and μ^b represent dipole vectors for the monomes a and b.

T^{ab} is the vector connecting the center of mass of μ^a with the center of mass of μ^b.

T^{ab} is defined to lie along the X-axis.

Note: only half of each dipole is shown in the diagram.

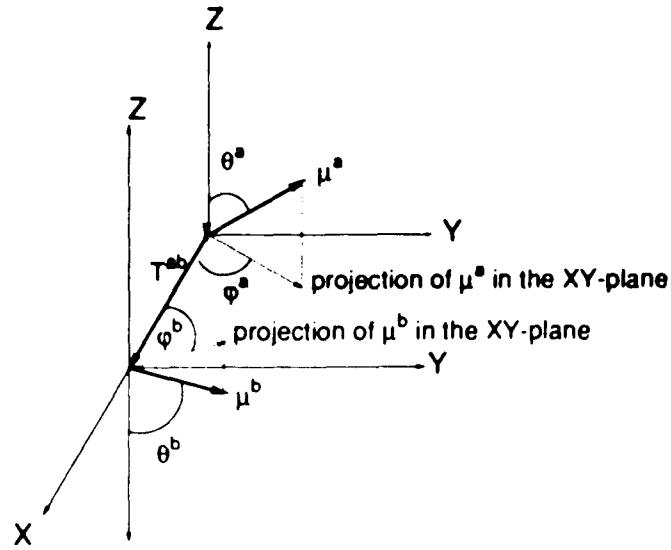

Fig. 6: Relationship Between Geometry and Dipole and Rotational Strength:
Define vectors μ^a and μ^b such that both vectors are perpendicular to vector T^{ab} and such that μ^a lies along the Y-axis. The effects of rotating μ^b in the YZ-plane are described below.

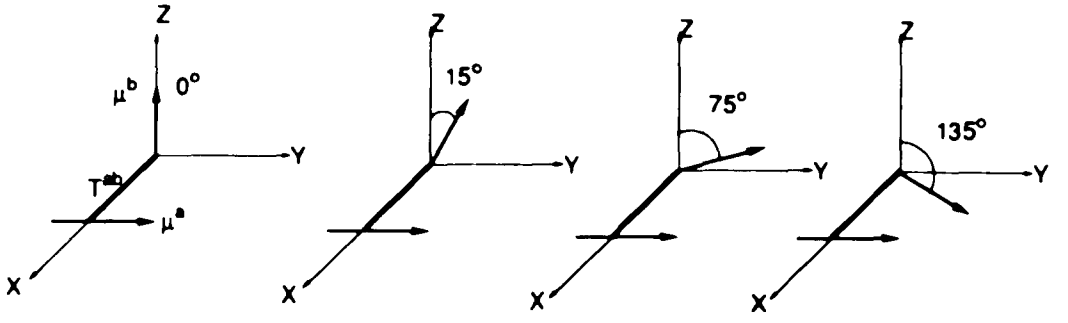

Rotate μ^a in the XY-plane and rotate μ^b as above.

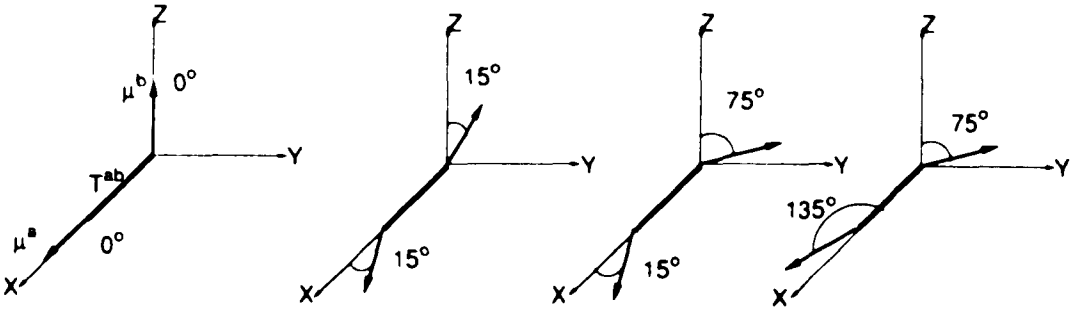

Allow μ^b to rotate in both the XY- and the YZ-planes. Rotate μ^a as above.

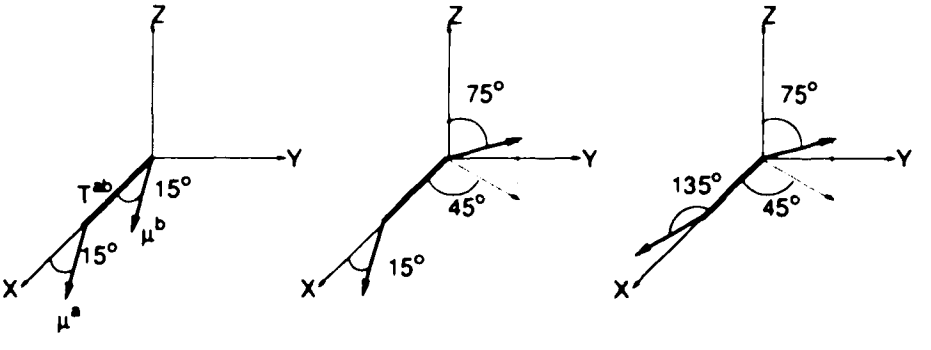

Fig. 7: Calculated ir absorbance (bottom) and VCD (top) spectra for the first 8 dimer configurations shown in Fig. 6. LHS: Spectra of first four dimers from left-to-right in the first row of figure 6. 1) solid line, 2) dashed line, 3) dash-dot-dash line, 4) long dashed line. RHS: Spectra of four dimers in the second row of figure 6. 5) solid line, 6) dashed line, 7) dash-dot-dash line, 8) long dashed line

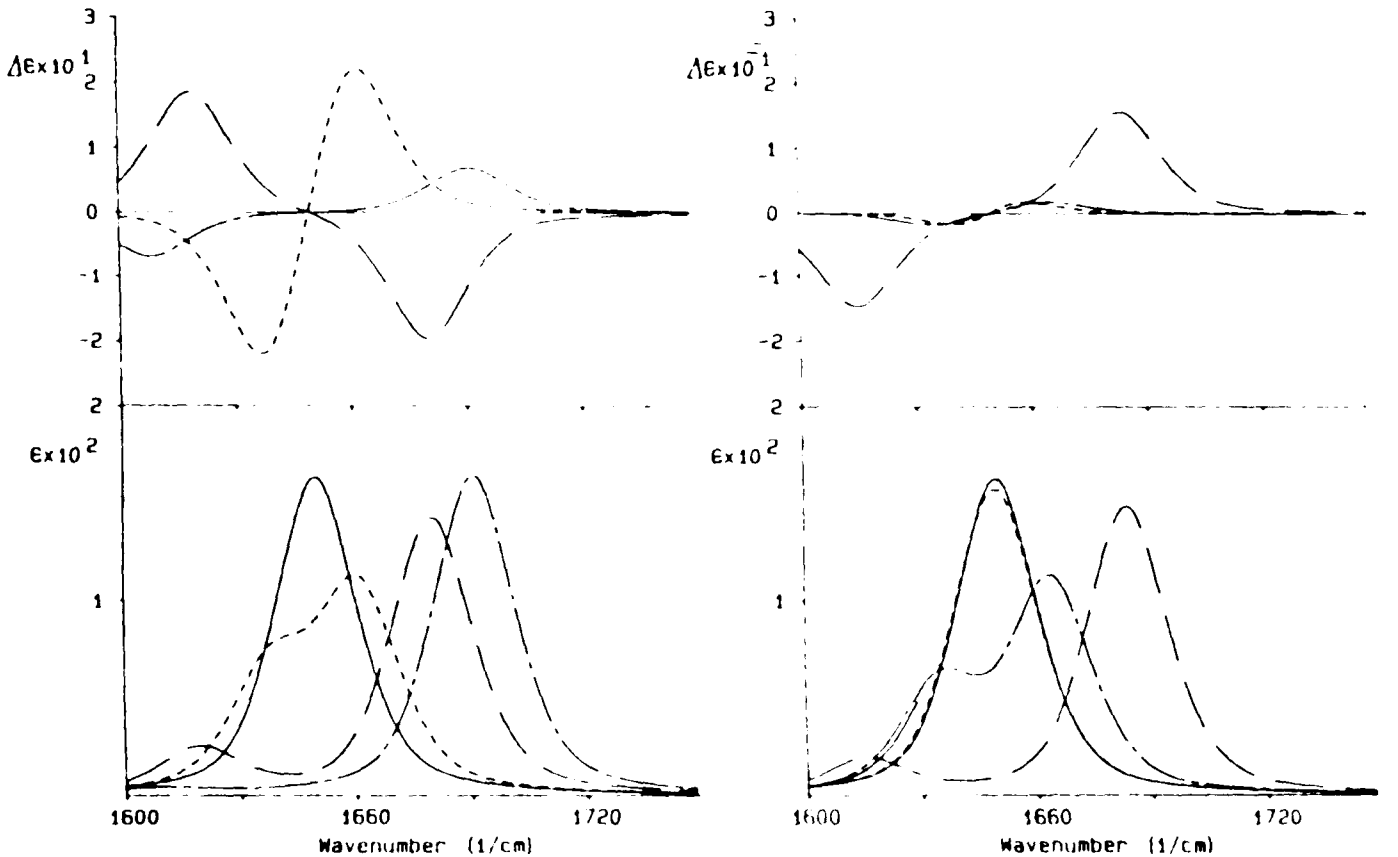

Fig. 8: Exciton Theory Extended to an Infinite Polymer.
For a polymer of identical monomers:

The zero-order wavefunction for the one-electron excited state is written as the sum of monomer one-electron excited states.

$$\Phi_k = \sum_{j=1}^{N} C_{jk}\varphi_j \qquad (35)$$

where Φ_k is the correct zero-order wavefunction for the k^{th} exciton level of a polymer which contains N identical or nearly identical monomers. φ_j is the wavefunction for the 1 e- excited state of monomer j and C_{jk} are the eigenvectors of the perturbation matrix; **V**.
The frequencies of the N-exciton states may be described by:

$$\nu_k = \nu_0 + \sum_{i=1}^{N}\sum_{j=1}^{N} C_{ik}C_{jk}^{*}V_{ij}h^{-1} \qquad (36)$$

where V_{ij} is the interaction energy between the i^{th} and j^{th} monomers and **h** is Plank's constant. C_{ik} and C_{jk}^{*} are the eigenfunction and the complex conjugate of the eigenfunction of the perturbation matrix.
The dipole strength and the rotational strength are described respectively by:

$$D_k = \bar{\mu}_k \bullet \bar{\mu}_k = \left(\sum_{j=1}^{N} C_{jk}\bar{\mu}_j\right)\bullet\left(\sum_{j=1}^{N} C_{jk}^{*}\bar{\mu}_j\right) \qquad (37)$$

$$R_k = Im\ \bar{\mu}_k \bullet \bar{m} = -\ Im\,(\pi\nu_0 i / c)\sum_{i=1}^{N}\sum_{j>i}^{N} C_{ik}C_{jk}^{*}\left[\bar{T}_{ij} \bullet \bar{\mu}_i x \bar{\mu}_j\right] \qquad (38)$$

where $\bar{T}_{ij}$ is the vector between the center of mass of i and the center of mass of j and ν_0 is the frequency of the monomer transition; $i \equiv \sqrt{-1}$.

Fig. 9: The form of the perturbation matrix; V^{ab}.

For calculations using the ECO method, the perturbation matrix is a simple dipole-dipole interaction of the form:

$$V^{ab} = \frac{\bar{\mu}^a \cdot \bar{\mu}^b}{\left\|\bar{T}^{ab}\right\|^3} - \frac{3\left(\bar{T}^{ab} \cdot \bar{\mu}^a\right)\left(\bar{T}^{ab} \cdot \bar{\mu}^b\right)}{\left\|\bar{T}^{ab}\right\|^5}$$

Transformed into spherical polar coordinates:

$$V^{ab} = \frac{\left(\mu^a_{01}\right)^2}{\left\|\bar{T}^{ab}\right\|^3}\left[\sin\theta^b \cos\left(\phi^a - \phi^b\right) - 3\sin\theta^a \sin\theta^b \cos\phi^a \cos\phi^b\right]$$

B. Application to B-form Oligonucleotides:

To apply the DECO model to B-form calculations, the geometry of the helix must be defined. Since only the interactions of the base carbonyls are to be considered, it is only necessary to develop a model which defines the relative positions of the base carbonyls. The simplest test model of a single-stranded helix of carbonyls is the "spiral staircase" model developed by Diem and coworkers in 1989.[35] In this model, the sugar phosphate backbone is considered to be arranged in a vertical line; the helix axis, and the carbonyls are vectors which point away from the helix axis but are attached to it. The carbonyl vectors wind around the axis like a right-handed spiral staircase (Fig. 10). In Diem's calculations, the dipole moment is taken to be that of a C=O stretching vibration of guanosine (dipole strength is 2.8 x 10^{-37} esu^2cm^2). The vertical distance between the dipoles is 0.32 nm and there are 10 dipole vectors/turn. The monomer frequency of the transitions is taken to be 1640 cm^{-1}.[35, 36].

Although the "spiral staircase" geometry led to fairly accurate calculations of the VCD spectra of $pd(CG)_{10}$, it was soon replaced by a more accurate model. In the later model, the desired helical coordinates were generated through a molecular modeling program, Macromodel[47], and the carbonyl vectors then derived from the coordinates generated by another modeling program, DOCK[48]. Macromodel derives its B-form coordinates from the fiber diffraction data of Arnott.[49] The

Fig. 10: Spiral Staircase model of a oligonucleotide.

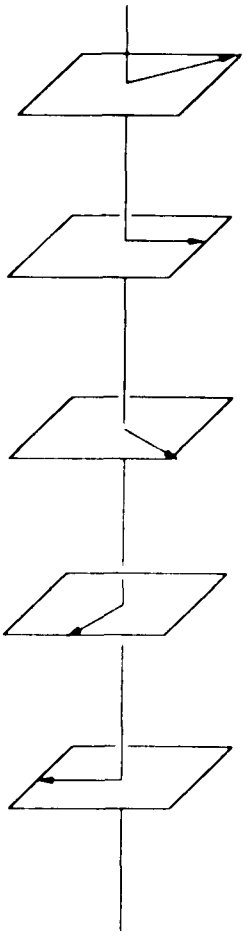

calculations made using this refined geometry are more accurate than the original calculations.[36] All of the calculations made in this thesis use carbonyl coordinates from x-ray diffraction studies.

The VCD signals of a GC-oligonucleotide arise mainly from interactions between a carbonyl on one base and the carbonyls on the bases closest to it, the complementary base, the base directly above or below it on the same strand, and the bases diagonally across from it (Fig. 11).

The interactions between the two carbonyls of a GC base pair are nearly identical to those of a CG pair. The carbonyl oxygens are 5.4 ± 0.05 Å apart and the carbonyls are nearly planar and in a nearly antiparallel alignment. The calculated ir absorbance spectrum shows one peak at 1660 cm^{-1} and the VCD spectrum shows a very weak couplet with a positive peak at 1660 and a negative peak at 1639 cm^{-1} (positive/negative couplet) (Fig. 12). The absorbance spectrum is consistent with the spectrum of a 1:1 5'CMP/5'GMP solution (data not shown). Fig. 13 shows the calculated ir absorbance and VCD spectra for two-base single strands of 5'GC and 5'CG, respectively. The calculated ir absorbance spectrum for 5'CG shows a single symmetric peak at 1660 cm^{-1}. The absence of a VCD spectrum implies a parallel alignment of the carbonyls. As shown in Fig. 6 and Table I, parallel alignment of dipoles will give rise to a strong dipole strength and a negligible rotational strength. Examination of the coordinates of the

Fig. 11: Base carbonyl nearest neighbor interactions:
Interactions of the cytosine carbonyl (°).

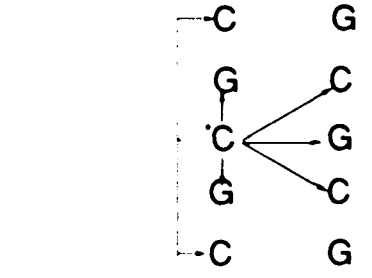

Fig. 12: **Calculated ir absorbance (bottom) and VCD (top) spectra of a CG (dashed line) and a GC (solid line) base pair.**

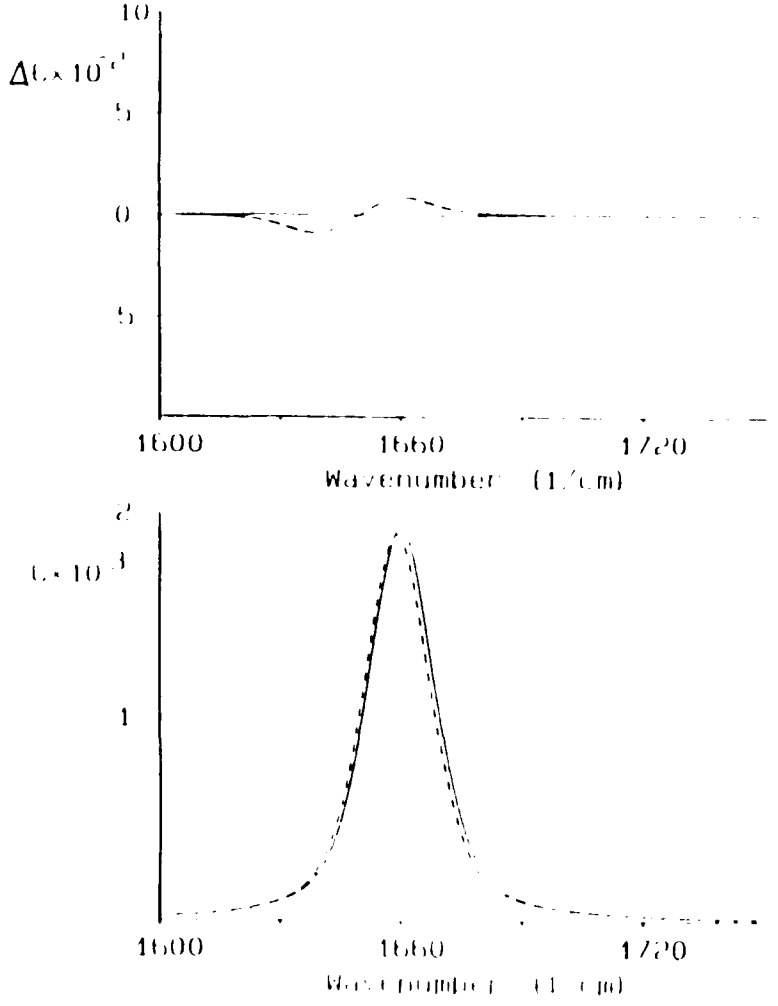

Fig. 13: Calculated ir absorbance (bottom) and VCD (top) spectra of single-stranded 5'CG (dashed line) and 5'GC (solid line) single strands.

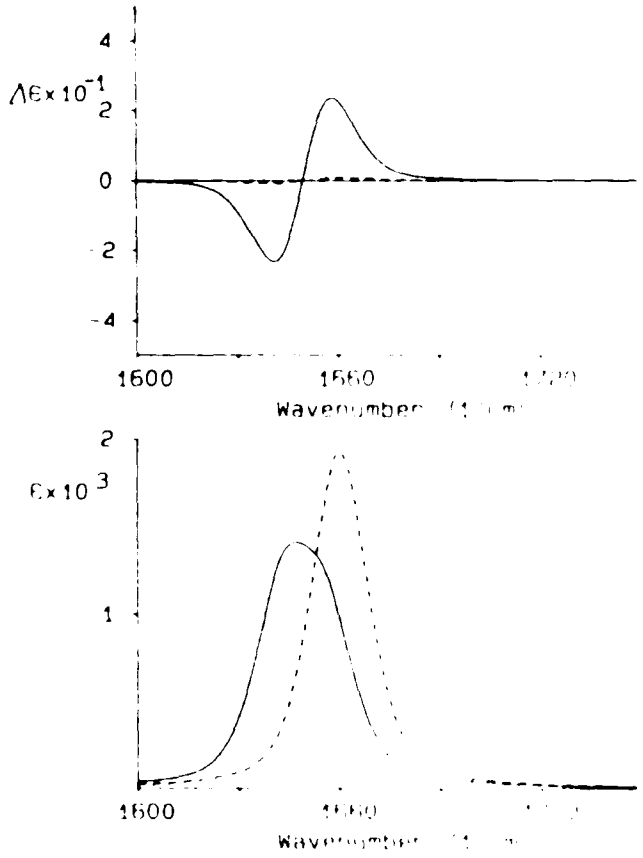

5'CG dimer confirm that the carbonyl group on the cytosine base is aligned nearly parallel to the carbonyl on the guanine base. The calculated ir absorbance spectrum of 5'GC is a combination of two peaks of nearly equal dipole strength, one at 1656 cm^{-1} and the other at 1643 cm^{-1}. The corresponding VCD spectrum shows a strong positive/negative couplet which has a zero-crossing point at 1650 cm^{-1} (Fig. 13). Examination of the coordinates of the carbonyls in the 5'GC alignment indicates that the guanine carbonyl is in a nearly perpendicular alignment to the cytosine carbonyl. The addition of a complementary strand to the 5'CG strand has little effect on the shape of the ir absorbance spectrum; the calculated ir absorbance spectrum is still primarily composed of a single peak; however, the frequency of this peak is 1680 cm^{-1} which is 20 cm^{-1} higher than the single stranded absorbance peak. In addition, there is a weak peak at 1640 cm^{-1} seen in the absorbance spectrum of the double stranded oligomer which is not seen in the absorbance spectrum of single stranded 5'CG. The calculated VCD spectrum shows a positive peak at 1680 cm^{-1} and a negative peak at 1633 cm^{-1}, an exciton splitting of greater than 40 cm^{-1} (Fig. 14). For the double stranded 5'GC oligonucleotide, the calculated ir absorbance peak shows a single broad peak at 1662 cm^{-1}. The calculated VCD spectrum is comprised of a strong negative/positive couplet at 1672 and 1654 cm^{-1} respectively followed by a shallow broad negative peak at ca. 1617 cm^{-1}. The negative/positive sign of the

Fig. 14: Calculated ir absorbance (bottom) and VCD (top) spectra of double stranded 5'CG (dashed line) and 5'GC (solid line).

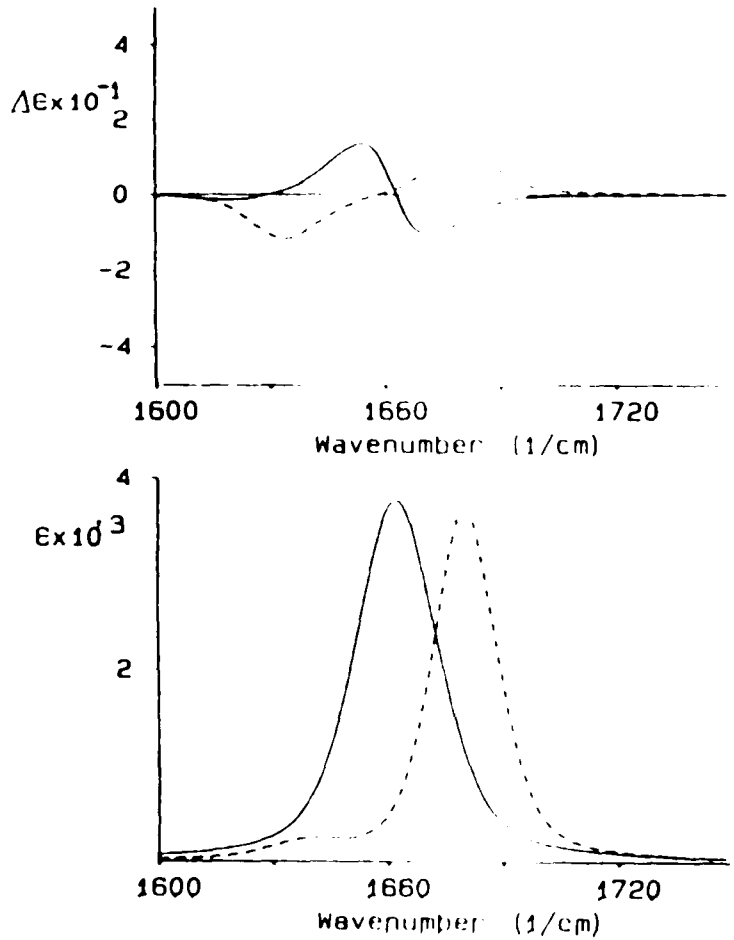

couplet is opposite of the sign of the couplet in the calculated VCD spectra of single stranded 5'GC (Fig. 14). The geometries of the carbonyl groups in the double stranded 5'CG and 5'GC oligomers are plotted in Fig. 15. From this figure it is clear that there are two ways that CG and GC base pairs are stacked in a B-form helix. They can be stacked such that the carbonyl groups on the second pair are parallel to those of the first pair or the stacking may cause the carbonyl groups of the second pair to be perpendicular to those of the first pair. The perpendicular alignment causes moderate exciton splitting (20 cm^{-1}) and the zero-crossing point of the VCD spectrum is at the same frequency as the absorbance maximum. The parallel alignment causes the VCD peaks to be split much further apart and the zero-crossing frequency of the VCD spectrum (1658 cm^{-1}) is not close to the absorbance maximum (1680 cm^{-1}). This result is consistent with the effect of geometric alignment shown in Figures 6, 7 and in Table I.

The calculated ir absorbance and VCD spectra for single stranded 5'CGC and 5'GCG are very similar to one another. The ir absorbance spectrum shows a broad peak between ca. 1630-1690 cm^{-1} and the VCD spectrum is a positive/negative couplet (Fig. 16). The sign of the couplet is opposite to what is observed and is indicative of a change in the handedness of the helix. Although the peaks for both the ir absorbance and the VCD spectra of the single-stranded trimers have similar shapes to the ir absorbance and VCD calculated spectra for

Fig. 15: XY-plot of the carbonyl groups of double stranded 5'GC and 5'CG

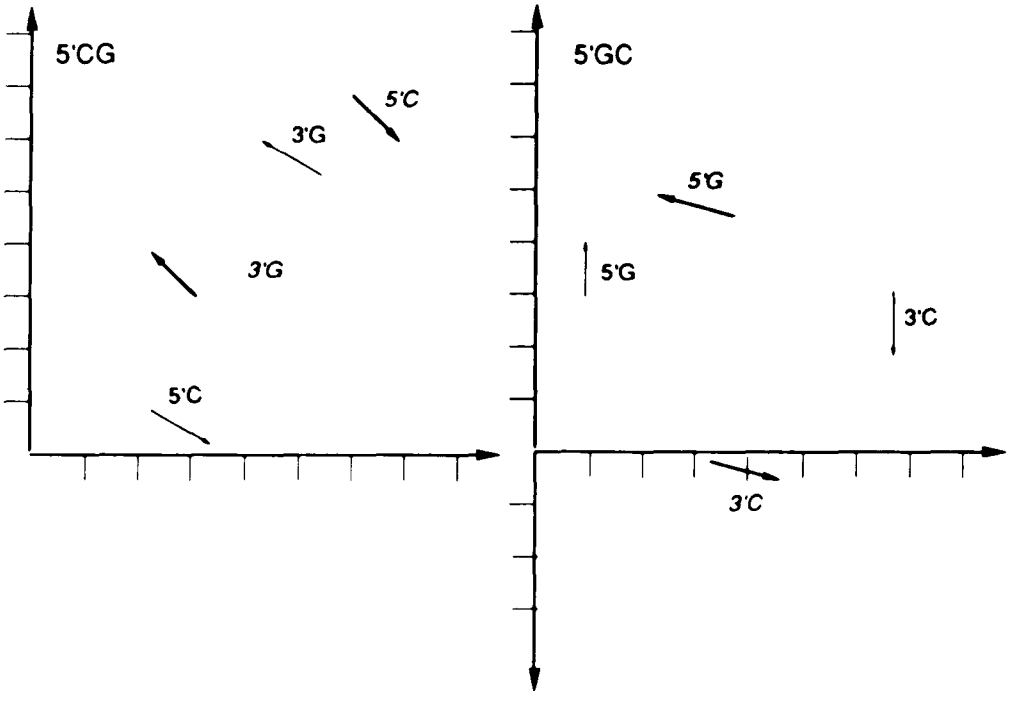

Helix moves out of the plane of the paper. Plain arrows lie in the plane of the paper while bold arrows indicate that the base lies above the plane of the paper.

Fig. 16: Calculated ir absorbance (bottom) and VCD (top) spectra of single stranded 5'CGC (dashed line) and 5'GCG (solid line).

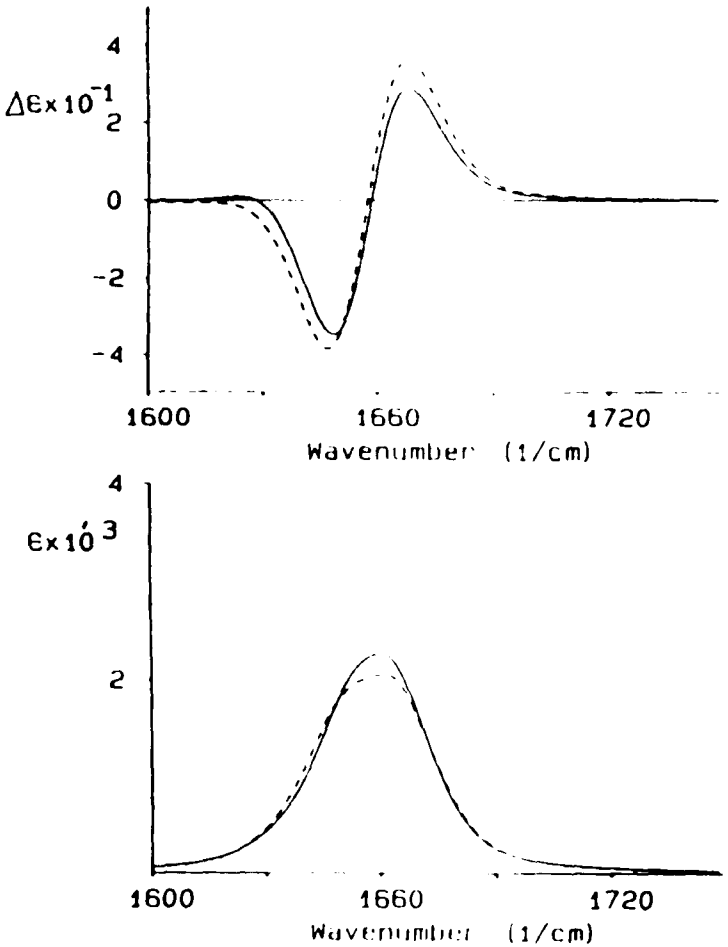

single stranded 5'GC, the trimer spectra are both shifted toward higher wavenumbers by approximately 10 cm^{-1}. In the geometry of the 5'CGC helix, the guanine carbonyl is nearly parallel to the carbonyl on the 5'cytosine and nearly perpendicular to the carbonyl of the terminal cytosine. For 5'GCG, the relative geometries are reversed. The carbonyl of the cytosine base is perpendicular to the carbonyl on the 5'guanine and parallel to the carbonyl group of the terminal guanine. The double-stranded oligomer is a combination of a 5'CGC and a 5'GCG strand (Fig. not shown). The calculated ir absorbance spectrum shows a dominant peak at 1690 cm^{-1} and a smaller peak at 1665 cm^{-1}. The corresponding VCD spectrum has three peaks; a negative peak at 1678 cm^{-1}, a positive peak at 1643 cm^{-1} and another negative peak at 1600 cm^{-1}. The magnitude of the interaction energies between the base pairs (V^{ab}=-11.4 ergs for the two outside pairs and V^{ab}=-12.4 for the GC pair in the middle) are similar to the interaction energies between the bases on the same strand (V^{ab}=-12.0 or 8.3). However, the interaction energy between diagonal positioned bases varies a lot; V^{ab}=3.6 for the interaction between the 5'cytosine and the cytosine carbonyl in the 5'GCG strand and V^{ab}=20.9 for the interaction between the 5'guanine and the guanine carbonyl in the 5'CGC strand. However, the interaction energy for the remaining diagonal CC and GG interactions is similar to the interaction energies for bases in the same strand. Thus interactions between bases in a

single strand or in a base pair affect the dipole and rotational strength of the carbonyl transitions equally and diagonal cross strand interactions can have an even greater effect.

Homopolymers most closely resemble the situation described by the "spiral staircase" geometry. For the single stranded trimer 5'GGG, the distance between the respective base carbonyls is ca. 3.5 Å and the carbonlys are aligned such that for every "step" taken, the helix makes a 36.8° turn. In the 5'CCC single stranded trimer, the axial rise/residue is ca. 4 Å and there is a 42.3° angle between the carbonyl group on the n^{th} residue and the carbonyl on the $(n+1)^{th}$ residue. The interaction energy between the guanine carbonyls in 5'GGG is much greater than the interaction between the cytosine carbonyls in 5'CCC (V^{ab}=26.2 for the interaction between guanine carbonyls and V^{ab}=0.76 for the cytosine carbonyls). The calculated ir absorbance spectra for single stranded 5'CCC and 5'GGG are shown in Figure 17. The calculated VCD spectrum for single stranded 5'CCC is very weak and is negligible compared with the calculated spectra of single stranded 5'GGG.

For oligonucleotides having a large number of bases/strand, the addition of another base or base pair does not effect the calculated ir absorbance or VCD spectra indicating that long range interactions between distant carbonyls have no effect on the calculated spectra. In 1989, Diem and coworkers used the "spiral staircase" geometric model

Fig. 17: Calculated ir absorbance (bottom) and VCD (top) spectra of single stranded 5'CCC (dashed line) and 5'GGG (solid line).

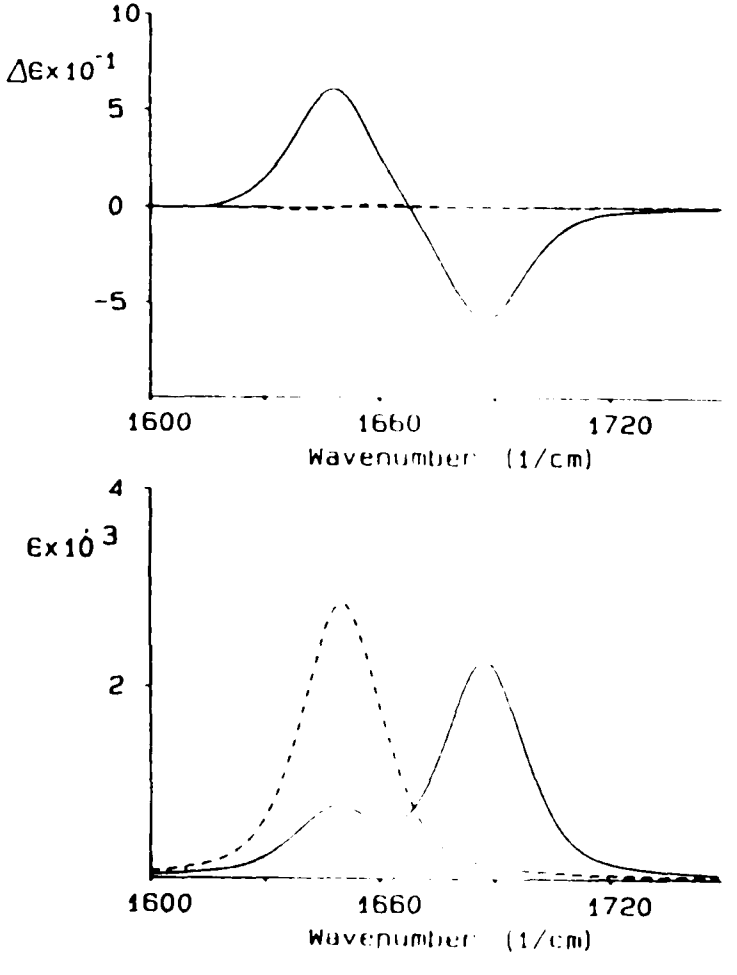

to determine that beyond 10 bases, the calculated spectra for CG-oligonucleotides remained the same. This result was confirmed using helices created through Macromodel (data not shown). The calculated ir absorbance and VCD spectra for double stranded 5'$(CG)_{10}$ and for double stranded $(G)_{10}(C)_{10}$ are shown in Fig. 18. The calculated ir absorbance spectrum for $(G)_{10}(C)_{10}$ has a broad peak at 1706 cm^{-1} and another much smaller peak at 1640 cm^{-1}. The corresponding VCD spectrum shows a negative/positive couplet at 1714 and 1693 cm^{-1} respectively and an additional much weaker positive/negative couplet at 1653 and 1633 cm^{-1}. The second couplet creates a shoulder at 1653 cm^{-1} on the 1693 cm^{-1} positive peak. The calculated ir absorbance spectrum of the alternating oligomer has a large peak at 1693 cm^{-1} and a smaller peak (over an order of magnitude smaller) at 1642 cm^{-1}. The VCD spectrum shows a major negative/positive couplet at 1702 and 1683 cm^{-1} respectively. There is an additional broad negative peak between 1600 and 1656 cm^{-1}. At least part of the intensity of the additional negative peak arises from a positive/negative couplet which is centered at 1656 cm^{-1}. The positive peak of the couplet cannot be resolved from the much larger positive peak at 1683 cm^{-1}. These calculated spectra will be used for comparison with the experimental spectra shown below. When comparing the calculated to the observed spectra, the area under the calculated ir absorbance spectrum (the dipole strength) is scaled to be the same as the area under the

Fig. 18: Calculated ir absorbance (bottom) and VCD (top) spectra of double stranded pd(CG)$_{10}$ (solid line) & pd(G)$_{10}$(C)$_{10}$.

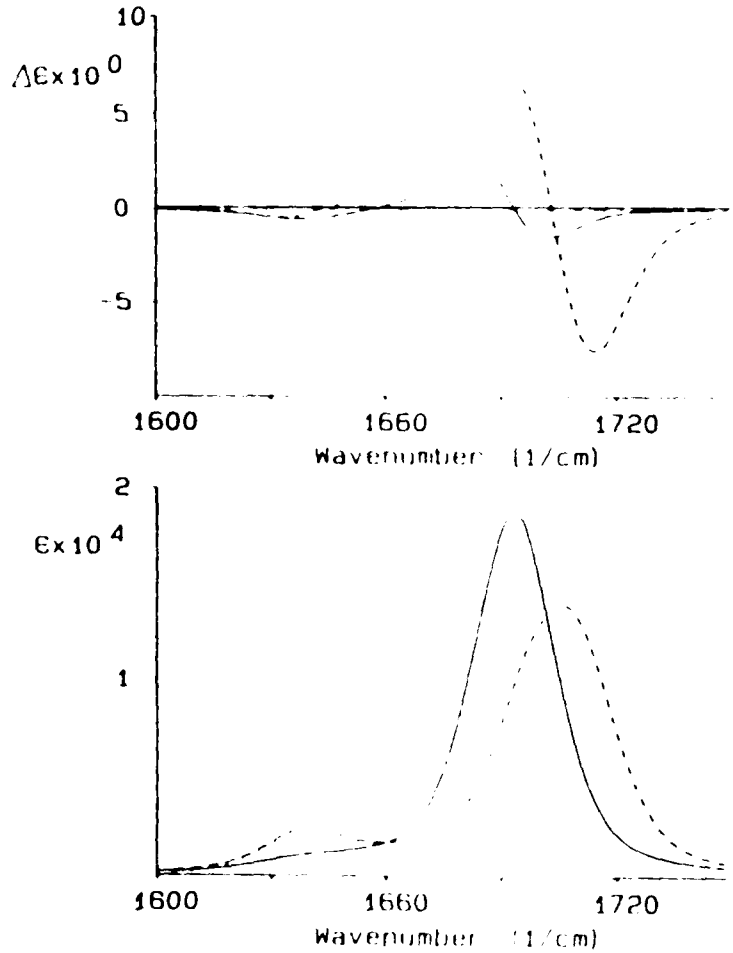

experimental ir absorbance spectrum. The VCD spectra are scaled by the same factor as the ir absorbance spectrum was. This adjustment eliminates the effect of strand length on the intensity of the VCD peaks.

C. Experimental and Calculated Results and Discussion:

In low salt conditions, poly(dG-dC), $pd(CG)_5$, poly(dG)poly(dC) and poly(dG-me^{5}dC)[*4] all form right-handed helices which are members of the A- or B-families. For all four oligonucleotides, the VCD spectra are characterized by a negative peak with frequency above 1690 cm^{-1} followed by a positive peak at approximately 1680 cm^{-1}. This is consistent with the calculated spectra discussed above although the negative/positive couplet is calculated to be at a 10 cm^{-1} higher frequency for the homopolymer. The VCD spectrum of poly(dG)poly(dC) has a shoulder at 1652 cm^{-1}; this shoulder is seen at approximately 1667 cm^{-1} for the alternating oligonucleotides although it is not always seen in the VCD spectrum of poly(dG-dC) and is not seen in the spectrum of $pd(CG)_5$. Remarkably, this result is also predicted by the simple calculations discussed previously therefore the position of this peak is a function of the relative positions of the carbonyls. The calculational results indicate that the appearance of the 1667 cm^{-1} shoulder in the VCD spectrum of poly(dG-dC) is dependent on the height of this peak relative

---

[*4] The polymers poly(dG-dC)poly(dG-dC) and poly(dG-me^{5}dC)poly(dG-me^{5}dC) are abbreviated poly(dG-dC) and poly(dG-me^{5}dC).

to the larger positive peak seen at approximately 1680 cm^{-1} and the frequency difference between the two peaks. However, the effect of the 1667 cm^{-1} peak on the rotational strength is always evident since in both the experimental and in the calculated spectra, the area under the positive VCD peak (including both 1680 and 1667 cm^{-1} components) is always larger than the area under the negative peak centered at approximately 1700 cm^{-1} (ref. Fig. 4 eqn. 34). There is only positive/negative conservation if the broad negative peak below 1655 cm^{-1} is included. Positive/negative conservation occurs when the area under the positive peaks is equal to the area under the negative peaks and indicates that the optical activity observed is generated through a single transition or type of transition and is not due to a coupling of different transitions. The experimental ir absorbance and VCD spectra for poly(dG-dC) and poly(dG)poly(dC) are shown in Figure 19.

The experimental ir absorbance spectra for poly(dG)poly(dC) and for poly(dG-dC) are similar to one another but neither are modeled well by the calculated spectra. The experimental ir absorbance spectrum of poly(dG)poly(dC) is characterized by two peaks of nearly equal intensity at 1690 and 1651 cm^{-1} followed by a small shoulder at approximately 1620 cm^{-1}. The ir absorbance spectrum of poly(dG-dC) has three peaks at 1686, 1658 or 1650 and 1624 cm^{-1} respectively. The frequency peaks in the ir absorbance spectrum of poly(dG)poly(dC) correspond within 4 cm^{-1} to those

Fig. 19: Comparison of the experimental Ir absorbance (bottom) and VCD spectra (top) of poly(dG)poly(dC) & poly(dG-dC): Solid line - poly(dG dC) 17.1 mg/ml, 10mM sodium cacodylate pH6.1, 0.0025 cm path; dashed line - poly(dG)poly(dC) 38 mg/ml, 10mM sodium cacodylate,0.0025 cm path.

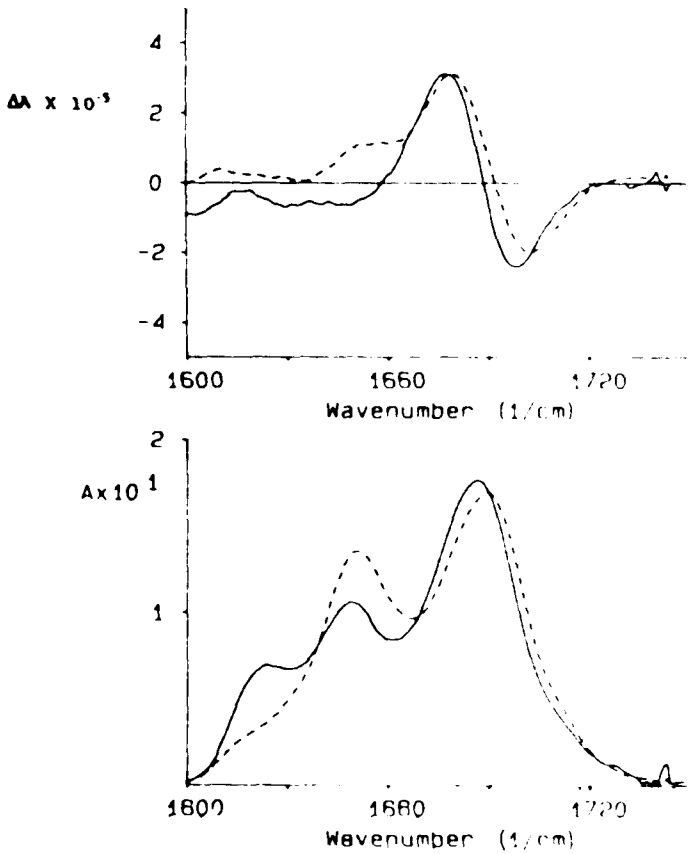

in the spectrum of poly(dG-dC) however, the relative intensities are very different. The high frequency peak seen at 1687 cm^{-1} in the poly(dG-dC) spectrum has nearly the same intensity as the corresponding peak seen at 1690 cm^{-1} in the spectrum of poly(dG)poly(dC). The 1651 cm^{-1} peak of the poly(dG)poly(dC) spectrum has 1.3 times the intensity of the corresponding poly(dG-dC) peak while the 1620 cm^{-1} peak has almost no intensity and the corresponding poly(dG-dC) peak seen at 1624 cm^{-1} is much larger. The calculated ir absorbance spectra for $5'(CG)_{10}$ and $(C)_{10}(G)_{10}$ both show a single strong peak and one much weaker peak at a lower wavenumber. The high frequency peak seen in the calculated ir absorbance spectrum of $5'(CG)_{10}$ corresponds with the 1686 cm^{-1} peak seen in the experimental ir absorbance spectrum. For both the experimental and the calculated spectra, the zero-crossing point of the major negative/positive couplet occurs at the high wavenumber absorbance maximum. In the calculated spectra of $(C)_{10}(G)_{10}$, the high frequency absorbance peak at 1706 cm^{-1} is almost at the same frequency as the zero-crossing point of the major negative/positive couplet of the VCD spectrum. The experimental spectra show the zero-crossing point of the major couplet in the VCD spectrum to be at the same frequency as the highest wavenumber absorbance maximum (1690 cm^{-1}). Although the absorbance maximum of the calculated spectrum is 20 cm^{-1} from the 1690 cm^{-1} absorbance peak seen in the experimental spectrum, the correlation between the ir absorbance

frequencies and their corresponding VCD spectral frequencies imply that two peaks can be given the same vibrational assignment. The calculated spectra are based solely on the coupling of the C=O stretching frequency seen at 1650 cm^{-1} for a 1:1 5'GMP/5'CMP solution. Therefore, the 1690 cm^{-1} peak seen in the experimental ir absorbance spectrum of poly(dG)poly(dC) and the 1686 cm^{-1} in the poly(dG-dC) spectrum are both assigned to the C=O stretch. This is consistent with the assignment made by Tsuboi in 1973.[50] In addition, Tsuboi also indicated that C=C and C=N also have vibrational transitions in the 1550-1750 cm^{-1} region. Tsuboi uses normal coordinate analysis to suggest that C=O stretching vibrations occur above 1650 cm^{-1} and C=C and N=C stretching vibrations occur below 1640 cm^{-1}. It is likely that it is these vibrations and the coupling of these vibrations with the carbonyl stretching vibrations that accounts for the additional ir absorbance peaks seen in the experimental spectra.

There are three arguments for why the C=C and C=N vibrations do not affect the VCD spectra. The first is that the major contribution to the VCD spectra of CG-oligonucleotides occurs above 1650 cm^{-1} the region which Tsuboi assigns primarily to C=O stretching vibrations. The second is that exciton coupling of the carbonyls covers a broad range of frequencies (Fig. 18) and it is therefore possible that the entire VCD spectrum can be attributed to these interactions. The third argument involves the VCD

spectrum of Keiderling and coworkers of the homopolymer poly(rA) which has no carbonyl groups.[34] Keiderling found that the VCD spectrum of poly(rA) in the 1550-1750 cm^{-1} region has a negative VCD maximum just above 1635 cm^{-1} which is presumed to be due to the interactions of the C=N and C=C on neighboring bases. Diem found that the VCD spectrum of poly(dA)poly(dT) showed a positive peak in this region indicating that the positive contribution to the VCD spectrum from the coupling of the carbonyls completely overshadows the negative contribution from C=C and C=N coupled transitions.[36]

It is uncertain whether the conformation of poly(dG)poly(dC) belongs to the A-family or the B-family. GG runs in oligomers facilitate the formation of A-conformations. Tsuboi and coworkers found that in concentrated (0.2 M) aqueous solutions of poly(dG)poly(dC), the oligonucleotide favored the A-conformation and in low concentrations (0.01 M) the B-form was favored but the Raman spectrum still showed some A-form character.[51] In this study the concentration of poly(dG)poly(dC) was 0.12 M in nucleotide base (0.06 M in base pairs) so the conformation of the oligomer was almost certainly a mixture of A- and B-forms. Under the conditions used, poly(dG-dC)poly(dG-dC) is known to take on a B-conformation. However, several different ir absorbance and VCD spectra have been found under similar poly(dG-dC)poly(dG-dC) concentrations and conditions. These differences have been attributed to differences in the source

of the polymer and to end effects.[52] Alternatively, the differences may be due to the existence of several different B-family conformations. Arguments against the feasibility of there being A-forms present as well is presented below. Fig. 20 shows several types of B-form spectra seen for poly(dG-dC). The type I B-form VCD spectrum is nearly identical to the type II VCD spectrum. The difference between the type I and II B-forms (Fig. 20, solid line & dashed line) is in the ir absorbance spectrum. The type III B-form spectrum (Fig. 19, solid line; Fig. 20, dash-dot-dash line) has a very similar ir absorbance spectrum to that of the type II B-form spectrum but the VCD spectrum lacks the positive shoulder seen at 1667 cm^{-1} in the VCD spectra of types I and II. However, the negative peak and the zero-crossing points are nearly identical to those seen in the VCD spectra of the other two forms. All three ir absorbance spectra show three peaks in the 1600-1750 cm^{-1} region. The most intense ir absorbance peak occurs at 1686 ± 1 cm^{-1}, a lower less intense peak is seen at 1650 cm^{-1} (types II & III) or 1658 cm^{-1} (type I), and a third even weaker peak occurs at 1624 ± 2 cm^{-1}. The VCD spectra are all primarily negative/positive couplets with a zero crossing at 1687 ± 2 cm^{-1}. The negative peak is centered at 1697 cm^{-1}; the positive peak is seen at 1678 ± 1 cm^{-1}. The differences occur mostly in the lower frequency (below the negative/positive couplet) region and are probably due to the coupling of N=C and C=C vibrations with each other and with the low frequency

Fig. 20: Experimental Ir absorbance (bottom) and VCD (top) spectra of poly(dG-dC): solid line - type I - poly(dG-dC) 7 mg/ml, 50 mM NaCl, 10 mM sodium cacodylate pH 7, 0.01 cm path; dashed line - type II - poly(dG-dC) 15 mg/ml, 2 2 M NaCl, 10 mM sodium cacodylate pH 7, 0 005 cm path; dash-dot-dash line - type III - poly(dG dC) 17.1 mg/ml, 10 mM NaCl, 10 mM sodium cacodylate pH 6.1, 0.0025 cm path.

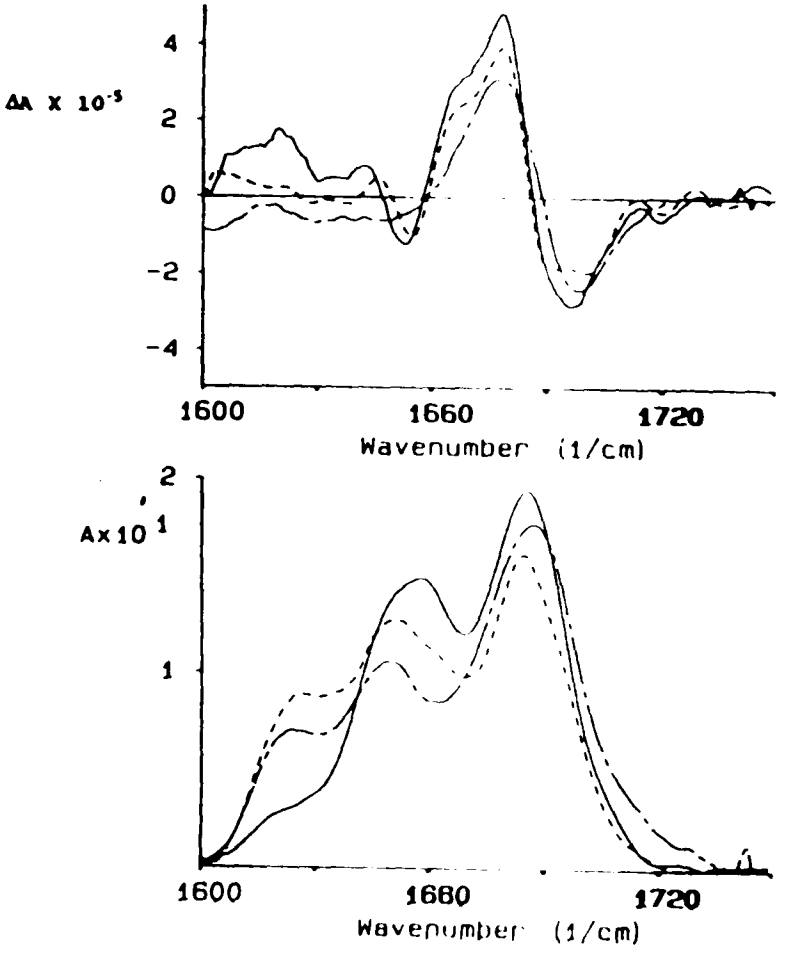

C=O exciton vibrations. In the type II spectrum, the peak below 1630 cm^{-1} is approximately 2.5 times more intense than the corresponding peak seen in the type I ir absorbance spectrum. The higher frequency peak seen at 1658 cm^{-1} in the ir absorbance spectrum of the type I B-form is seen at 1650 cm^{-1} in the spectra of the type II and III B-forms. The difference between the type I and II B-forms is much less pronounced in the VCD spectrum. Neither the 5 cm^{-1} shift in the 1650 cm^{-1} peak nor the loss of intensity of the peak below 1630 cm^{-1} ir absorbance peaks seems to affect the VCD spectra in the carbonyl stretching region and thereby has little effect on the handedness of the conformation. In the VCD spectrum of the type III B-form the small negative peak at 1655 cm^{-1} seen in the other two forms is replaced by a broad negative peak that runs from 1655 to 1600 cm^{-1}. The asymmetry of the positive peak at 1677 cm^{-1} indicates that the peak which causes the positive shoulder seen at 1667 cm^{-1} in the type I & II B-form spectra is again present but is too weak to be distinguishable.

The 1624 cm^{-1} peak in the ir absorbance spectrum of the type I B-form has the same intensity as the corresponding peak in the ir spectrum of poly(dG)poly(dC) (Fig. 20, solid line; Fig. 19, dashed line). However, the higher frequency ir absorption peaks in the ir absorbance spectrum of poly(dG-dC) are closer in frequency and not as close in intensity than the corresponding peaks are in the spectrum of poly(dG)poly(dC).

The VCD spectrum of the type I B-form of poly(dG-dC) is not similar to the VCD spectrum of poly(dG)poly(dC) and the two display the same differences discussed above. The absence of any GG segments in poly(dG-dC) indicates that this oligomer does not go into an A-conformation as easily as poly(dG)poly(dC) and Raman studies have demonstrated that even at 0.2 M poly(dG-dC), there is no evidence of an A-form present.[51]

The spectrum of $pd(CG)_5$ greatly resembles that of the polymer, poly(dG-dC) (Fig. 21, dashed line). The type III spectra of poly(dG-dC) are used for comparison with the $pd(CG)_5$ spectra since the type III spectrum most closely matches the $pd(CG)_5$ data. The absorbance spectrum of $pd(CG)_5$, shows two prominent peaks at 1682 and 1648 cm^{-1} respectively and a small shoulder at approximately 1626 cm^{-1}. The VCD spectrum shows a negative/positive couplet with a zero-crossing at 1685 cm^{-1}, a negative peak at 1695 and a positive peak at 1675 cm^{-1}. In addition, there is a broad negative region below 1658 cm^{-1}. These features are all also present in the type III B-form spectrum of poly(dG-dC). The high frequency negative peak of the $pd(CG)_5$ VCD spectrum also has a shoulder at 1705 cm^{-1} which is not seen in the poly(dG-dC) type III VCD spectrum but is seen in the type II spectrum. The similarity between the ir absorbance spectra of $pd(CG)_5$ and poly(dG-dC) as well as the similarity in their VCD spectra confirms the calculated result that oligomers which

Fig. 21: Experimental Ir absorbance (bottom) and VCD (top) spectra of poly(dG-dC) & pd(CG)5: solid line - type III B-form spectra of poly(dG-dC) - poly(dG-dC) 17.1 mg/ml, NaCl 10 mM, sodium cacodylate 10 mM pH 6.1, 0.0025 cm path; dashed line - pd(CG)5 ca. 20 mg/ml, sodium cacodylate 10 mM, 0.0025 cm path

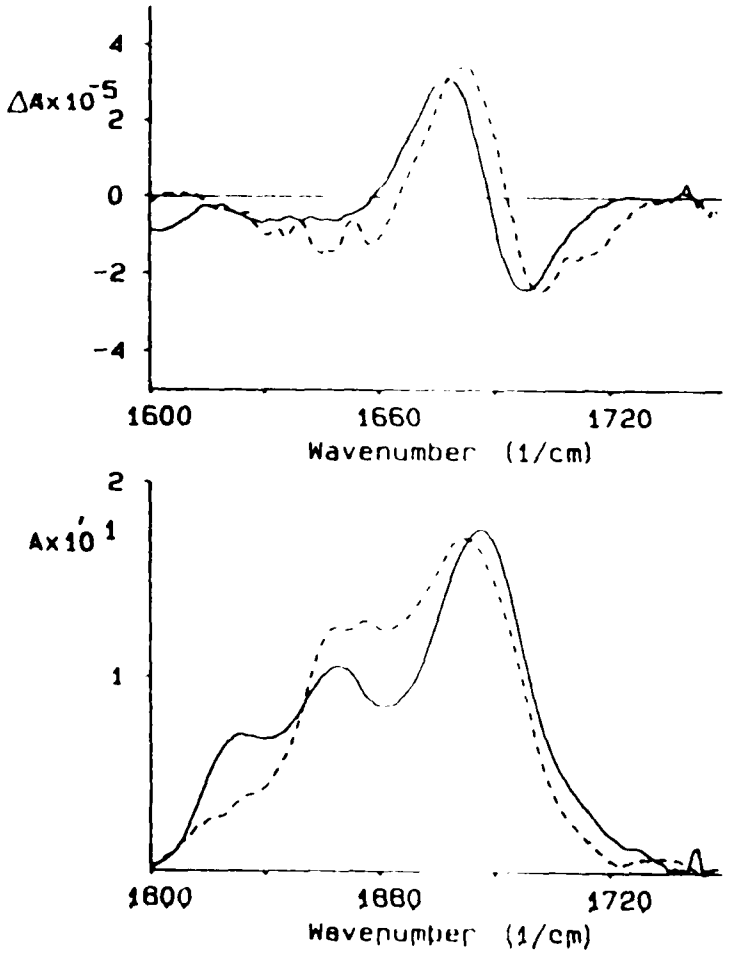

are one full turn or larger have the same conformation in low salt solution.

In Figure 22, the ir absorption and VCD spectra of the B-forms of poly(dG-dC) and poly(dG-me^{5}dC) are compared. Like the ir absorbance spectra of both poly(dG)poly(dC) and poly(dG-dC), the ir absorbance spectrum of poly(dG-me^{5}dC) in the 1600-1750 cm^{-1} region is comprised of three peaks. The ir absorbance peaks of poly(dG-me^{5}dC) are seen at 1689, 1658 and 1626 cm^{-1} respectively which is also the order of decreasing intensity. The VCD spectrum has a positively biased negative/positive couplet; the negative peak at 1697 and the positive peak at 1683 cm^{-1} with a shoulder at 1666 cm^{-1}. In addition, there is a small negative peak at 1655 ± 1 cm^{-1}. This is consistent with the characteristics of the spectra of poly(dG-dC) with the exception of a shift to higher frequency of the 1686 cm^{-1} peak of the ir absorbance spectrum (peak seen at 1689 cm^{-1} in the spectrum of poly(dG-me^{5}dC)) and in the frequencies of the zero-crossing and the higher frequency positive peak of the VCD spectrum; for poly(dG-dC) the zero-crossing point of the VCD spectrum is seen at 1686 cm^{-1} and the positive peak at 1679 cm^{-1} while in the VCD spectrum of poly(dG-me^{5}dC) these frequencies are 1690 cm^{-1} and 1683 cm^{-1} respectively. The 4 cm^{-1} shift in frequency may indicate a slight shift in the frequency of the carbonyl stretching frequency but the tremendous similarities in the spectra of poly(dG-dC) and poly(dG-me^{5}dC) indicate that their helical

Fig. 22: Experimental ir absorbance (bottom) and VCD (top) spectra of poly(dG-dC) & poly(dG-me^{5}dC): solid line - type I B-form spectra of poly(dG-dC) - poly(dG-dC) 7 mg/ml, NaCl 50 mM; dashed line - poly(dG-me^{5}dC) 12 5 mg/ml, NaCl 52 mM. Both samples were dissolved in sodium cacodylate buffer 10 mM pH 7 and both spectra were taken in a 0 005 cm path length cell

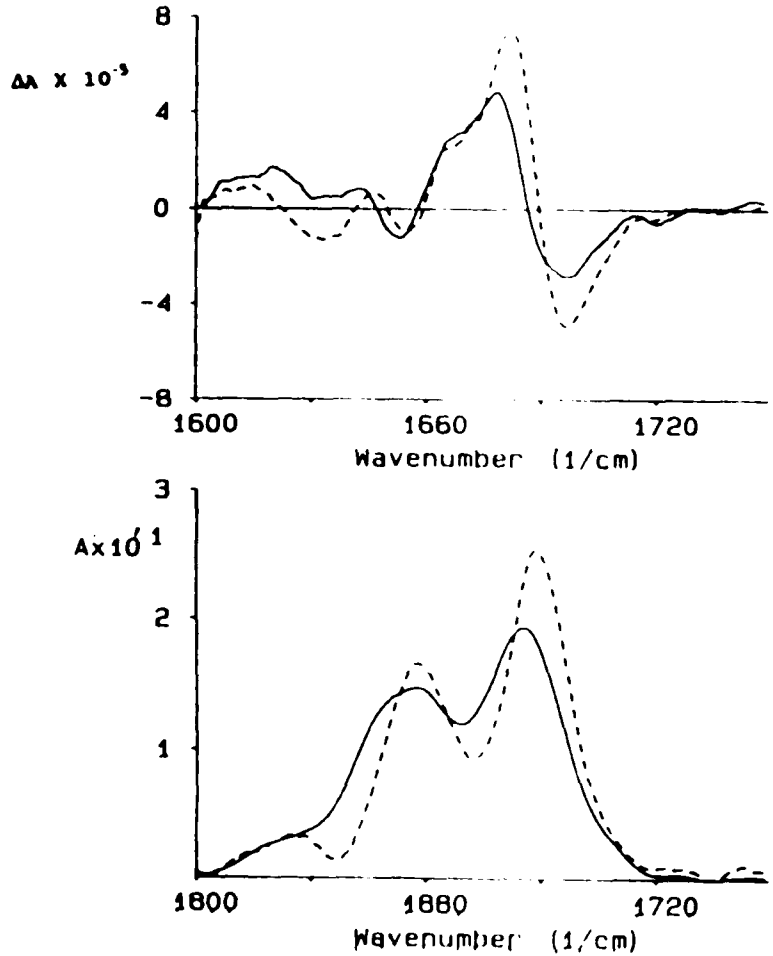

geometries are basically the same.

Other techniques also indicate that the helical structure of poly(dG-dC) is almost the same as that of poly(dG-me^{5}dC). X-ray diffraction studies show that the methylation of the 5 position carbon of the cytosine base has little effect on the orientation of the bases. The electronic CD spectra of the two oligomers is the same.[53]

The spectral characteristics of poly(dG)poly(dC), the three types of spectra seen for poly(dG-dC), pd(CG)$_5$, and poly(dG-me^{5}dC) are given in Table II.

Table I: Relationship between dipole geometry and dipole and rotational strength.
$\theta \equiv$ angle dipole vector makes with the Z-axis in the YZ-plane
$\varphi \equiv$ angle dipole vector makes with the X-axis in the XY-plane

Di-mer	φ^a	φ^b	θ^a	θ^b	$V^{ab} \times 10^{15}$ ergs	$\pm\nu$ cm^{-1}	$D^2 \times 10^{37}$ esu^2cm^2	$R^2 \times 10^{42}$ esu^2cm^2
1	90	90	90	0	0.0	0.0	2.8 2.8	±23.2
2	90	90	90	15	2.2	±11.1	3.5 2.1	±22.4
3	90	90	90	75	8.3	±41.5	5.5 0.1	± 6.0
4	90	90	90	135	6.0	±30.4	4.8 0.8	±16.5
5	0	90	90	0	0.0	0.0	2.8 2.8	0.0
6	15	90	90	15	0.6	± 2.9	3.0 2.6	± 5.8
7	15	90	90	75	2.8	±14.3	3.7 1.9	± 1.6
8	135	90	90	75	6.8	±34.4	5.0 0.6	±13.3
9	15	15	90	90	-16.3	±81.9	5.6 0.0	0.0
10	15	45	90	75	-17.1	±86.0	5.3 0.3	± 1.6
11	135	45	90	75	3.2	±16.0	5.6 0.0	±13.3

Table II: Infrared Absorbance and VCD Spectral Characteristics

sample	conditions	ir absorbance peaks cm^{-1}	VCD peaks cm^{-1}
poly(dG). poly(dC)	B-form adj. to VCII	1690, 1651, 1620	-1702 x1692 +1679 +1652
poly(dG-dC)	B-form type I ---------- type II ---------- type III	1686, 1658, 1622 ---------- 1686, 1650, 1626 ---------- 1687, 1649, 1623	-1700 x1686 +1678 +1667 ---------- -1698 x1689 +1677 x1655 -(1655 - 1609)
pd$(CG)_5$	B-form	1682, 1648, 1626	-1705 (sh) -1695 x1686 +1675 x1658 -1637
poly(dG-me^{5}dC)	B-form	1689, 1658, 1625	-1697 x1690 +1682 +1666 x1654 -1633

Rotational strength is measured as $R_L - R_R$. + indicates $R_L > R_R$, similarly - indicates $R_R > R_L$, x indicates $R_L = R_R$, (sh) means shoulder All wavenumber values are +/-3 cm^{-1}. All spectra are scaled for VCII.

Appendix 1: Proper Wavefunctions

To be proper wavefunctions, Φ_1^A and Φ_1^B must be normalized, orthogonal, eigenfunctions of H and must be stationary. The quantum mechanical definitions of these conditions are respectively:

$$\langle \Phi_1^A | \Phi_1^A \rangle = 1 \; ; \; \langle \Phi_1^B | \Phi_1^B \rangle = 1 \qquad (1)$$

$$\langle \Phi_1^B | \Phi_1^A \rangle = 0 \qquad (2)$$

$$\langle \Phi_1^A | H | \Phi_1^A \rangle = E ; \; \langle \Phi_1^B | H | \Phi_1^B \rangle = E \; , \text{ where } E \in \{\text{integers}\} \qquad (3)$$

$$\langle \Phi_1^A | H | \Phi_1^B \rangle = 0 \qquad (4)$$

IV. Left-Handed Conformations:

A: Experimental Results and Discussion:

At the poly(dG-dC) concentrations used in this study, a left-handed or Z-conformation could only be induced by NaCl or $MgCl_2$. Studies of the structure of poly(dG-dC) in the presence of $CoCl_2$, $NiCl_2$, and $[Co(NH_3)_6]Cl_3$ were also performed and conformations of poly(dG-dC) in the presence of these salts are discussed in chapter V.

The B-form near UV CD spectrum of poly(dG-dC) is characterized by a negative peak at 253 nm and a positive peak at 275 nm. In the vacuum UV region, the B-form spectrum is characterized by a very intense positive peak between 185 and 190 nm.[54] Like the near UV CD spectrum, the B-form VCD spectrum of poly(dG-dC) is also characterized by a negative/positive couplet. This couplet occurs at approximately 1700 and 1680 cm^{-1} respectively. In all three spectral regions, the transformation to a left-handed form is accompanied by an inversion of the CD peaks. The near UV CD spectrum of poly(dG-dC) in 3 M NaCl shows a positive peak at 265 nm and a negative peak at 292 nm. In the vacuum UV region, there is a negative peak at ca. 200 nm which is several times less intense than its B-form counterpart (Fig. 1).[54] In the infrared region, the VCD spectrum of poly(dG-dC) in 3 M NaCl shows a positive peak at 1690 cm^{-1} and a negative peak at 1661 cm^{-1} (Fig. 2).

Fig. 1: Electronic UV CD Spectra for the B- and Z-forms of Poly(dG-dC): Solid line - B-form spectrum, low salt, dashed line - poly(dG-dC) in 3 M NaCl. Samples were prepared in pH 7.5 tris buffer. The Gray cell was used and the path length was 0.0012 cm. Inset shows an enlargement of the 230-330 nm near UV region

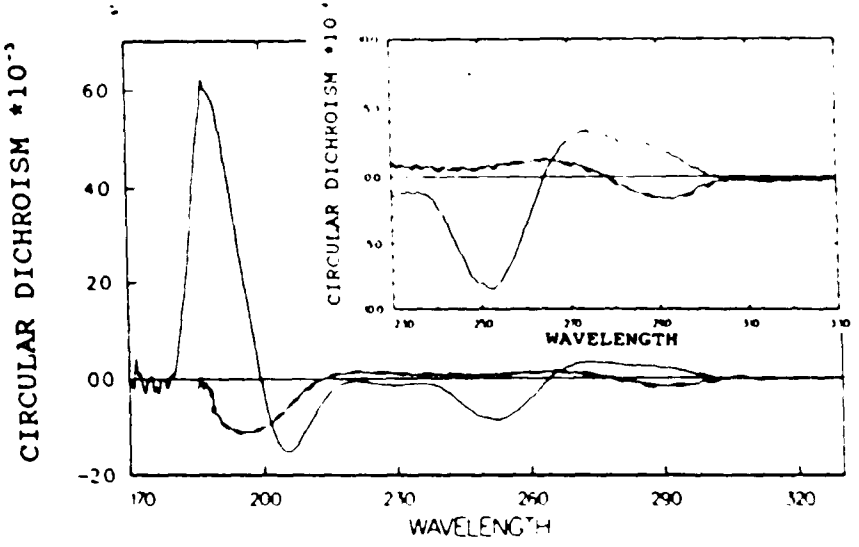

Fig. 2: Experimental IR Absorbance (bottom) and VCD (top) Spectra for the B- and Z-forms of poly(dG-dC) Solid line - poly(dG-dC) 19.8 mg/ml, 3 M NaCl, 10 mM cacodylate buffer pH 7, 0.0050 cm path. Dashed line - poly(dG-dC) 7.11 mg/ml, 50 mM NaCl, 10 mM cacodylate buffer pH 7, 0.01 cm path.

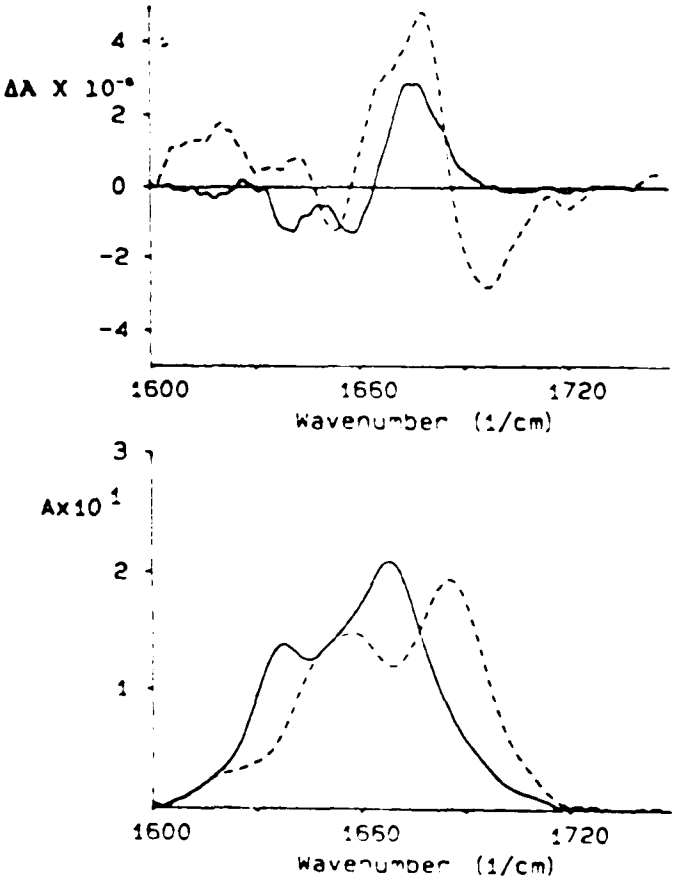

Methylation of the carbon atom in position 5 in cytosine greatly enhances Z-formation. Poly(dG-me^{5}dC) is in a right-handed conformation at low salt (chap. 3) but a left-handed conformation is induced by NaCl or $MgCl_2$ at less than half the amount of salt required to induce a Z-form in poly(dG-dC). The relative amounts of salt at the midpoint of a B-Z transition (monitored through UV absorbance) in poly(dG-dC) and poly(dG-me^{5}dC) are shown below:

TABLE I[53]

salt	poly(dG-dC)	poly(dG-me^{5}dC)
NaCl	2.5 M	0.7 M
$MgCl_2$	0.7 M	0.6 X 10^{-3} M

The electronic CD spectrum of the NaCl induced Z-form of poly(dG-dC) is the same as the spectrum for Z-form poly(dG-me^{5}dC).[53]

Poly(dG)poly(dC) does not form left-handed helices so no high-salt forms will be discussed. In the VCD spectra of both poly(dG-dC) and poly(dG-me^{5}dC), the transition from a B- to a Z-conformation is indicated by a change in the couplet orientation from the negative/positive couplet seen in the VCD spectrum of a B-form helix to a positive/negative couplet. In addition, the zero-crossing point of the Z-form spectrum is shifted to lower wavenumbers relative to the zero-crossing point of the B-form spectrum for both oligonucleotides. A

shift to lower wavenumbers is also seen in the ir absorbance spectra (Fig. 3).

The VCD spectrum of poly(dG-dC) in 3 M NaCl (Fig. 3 (LHS), dashed line; Fig. 4, solid line) shows a positive peak at 1676 cm^{-1} followed by a overlapping negative peaks with frequencies 1658 and 1642 cm^{-1} respectively. The zero-crossing point is shifted relative to ir absorbance maximum by approximately 3 cm^{-1} and occurs at 1665 cm^{-1}. The infrared absorbance peaks occur at 1668 and 1638 cm^{-1} respectively and the 1668 cm^{-1} peak is 1.5 times more intense than the 1638 cm^{-1} peak. The VCD spectrum for poly(dG-me^{5}dC) in a Z-conformation is composed of a positive peak at 1681 cm^{-1} and a negative peak composed of overlapping peaks at 1667 and 1659 cm^{-1} (Fig. 3 (RHS), dashed line; Fig. 4, dashed line). In addition, there is a broad negative region above 1700 cm^{-1} which does not exist in the poly(dG-dC) spectrum. The zero-crossing point in the VCD spectrum occurs at 1674 cm^{-1} again shifted relative to the highest frequency ir absorbance peak. The infrared absorbance spectrum shows three distinct peaks at 1676, 1646, and 1624 cm^{-1} respectively.

The shape of the VCD spectral peaks for the Z-forms of poly(dG-dC) and poly(dG-me^{5}dC) are similar. A general definition of Z-form DNA from the VCD spectrum in the carbonyl stretching region can be defined as follows: the spectrum shows a positively biased positive/negative couplet with a single positive peak and two negative peaks. However, the

Fig.. 3: Comparison of the IR Absorbance (bottom) and the VCD (top) Spectra of Poly(dG-dC) (LHS) and Poly(dG-me^{5}dC) (RHS). LHS: solid line - poly(dG-dC) 2.11 mg/ml, 50 mM NaCl, 0.01 cm path, dashed line - poly(dG-dC) 19.8 mg/ml, 3 M NaCl, 0.005 cm path. RHS: solid line - poly(dG-me^{5}dC) 12.5 mg/ml, 50 mM NaCl, 0.005 cm path, dashed line - poly(dG-me^{5}dC) 12.5 mg/ml, 2.1 M NaCl, 0.005 cm path. All samples were prepared in 10 mM pH 7 sodium cacodulate buffer.

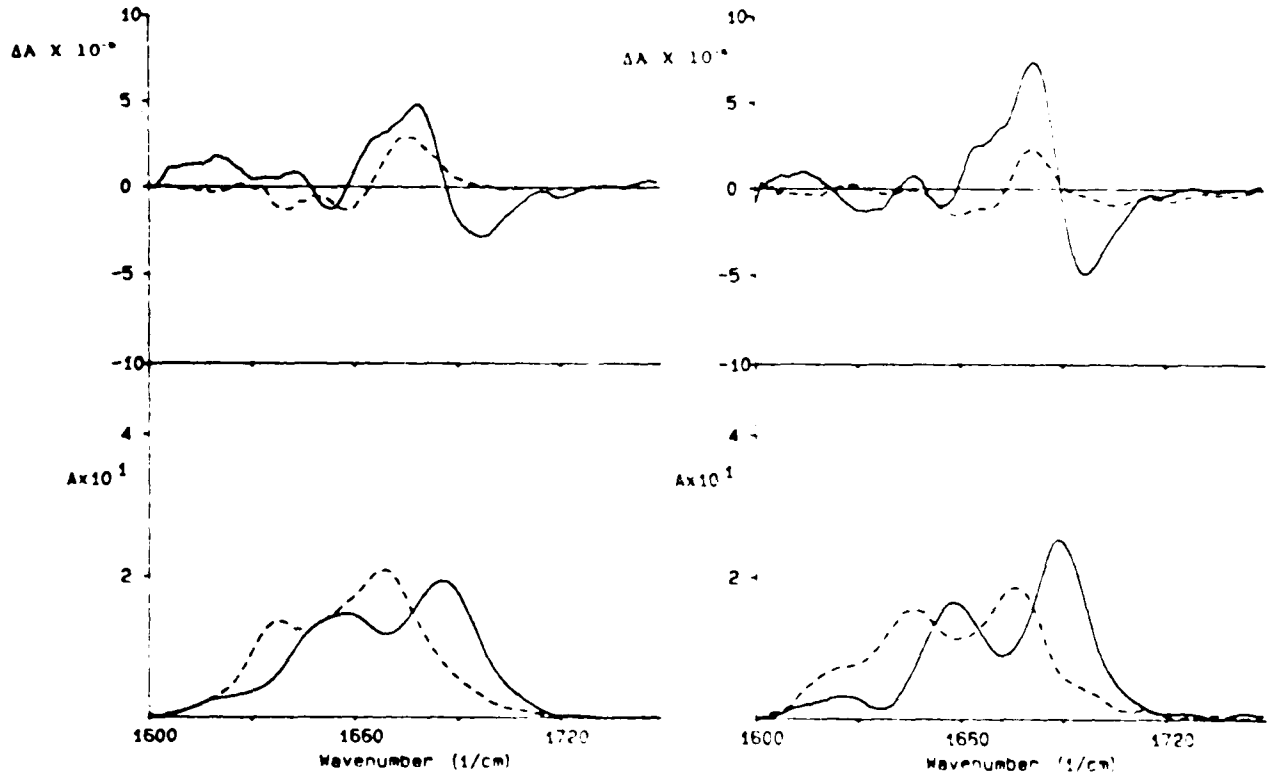

Fig. 4: Comparison of the IR Absorbance (bottom) and the VCD (top) Spectra of Poly(dG-dC) (solid line) and **Poly(dG-me^{5}dC) (dashed line)** in High Salt Solution. Solid line - poly(dG-dC) 19.8 mg/ml, 3 M NaCl, 0.005 cm path. Dashed line - poly(dG-me^{5}dC) 12.5 mg/ml, 2.1 M NaCl, 0.005 cm path. All samples were prepared in 10 mM pH 7 sodium cacodulate buffer.

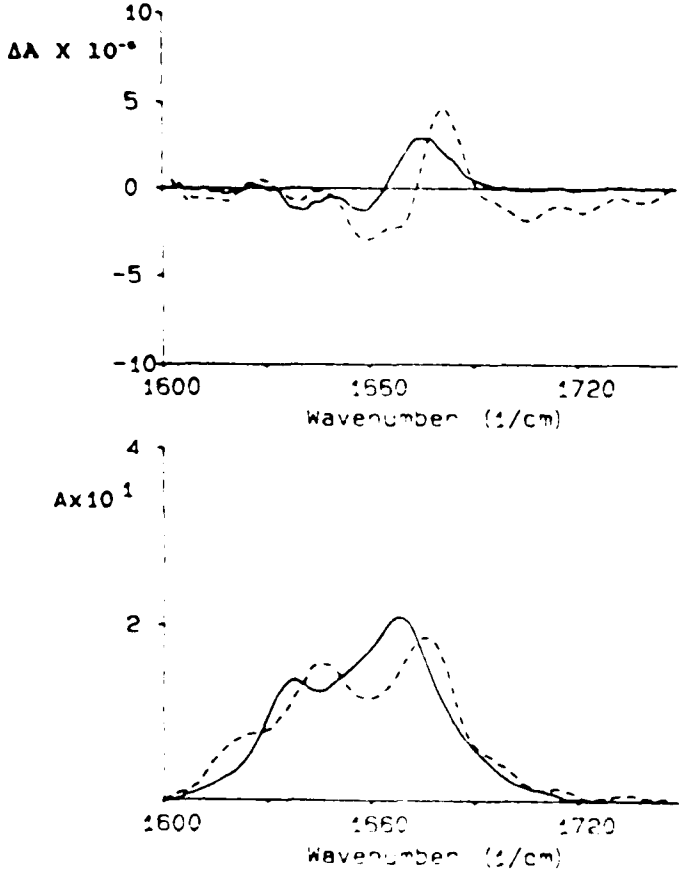

frequencies at which these peaks occur and the splitting between them is not consistent between the two oligonucleotide spectra. There is a 10 cm^{-1} difference between the zero-crossing points of the VCD spectra of the Z-form of poly(dG-dC) and poly(dG-me^5dC). In addition, the peaks of the poly(dG-dC) spectrum are broader and less intense than those of the poly(dG-me^5dC) spectrum. At 3 M NaCl, the poly(dG-dC) spectrum shows the positive peak 18 cm^{-1} from the closest of the two negative peaks. The two negative peaks are split by 16 cm^{-1}. In the Z-form VCD spectrum of poly(dG-me^5dC), the positive peak is only 14 cm^{-1} from the first negative peak and the splitting between the two negative peaks is 8 cm^{-1}. The similarity in the shape of the peaks in the VCD spectra of poly(dG-dC) and poly(dG-me^5dC) indicate that relative positions of the carbonyls is similar for both of these oligonucleotides. This result is consistent with what has been determined by x-ray crystallography.[55] However, the differences in the frequency of the transitions indicates that the presence of the methyl group on the cytosine ring does interfere with the carbonyl stretching vibrations. There is considerable evidence that the methyl group affects the hydrogen bonding between the bases. However, x-ray diffraction studies indicate that there is little difference between the two oligonucleotides. These results indicate that methylation alters the vibrational transitions of the carbonyl groups by altering the hydrogen bonding thereby affecting the

rotational strengths and splitting.

In addition to the differences in the VCD spectra of the two oligonucleotides, their ir absorbance spectra are different. None of the three peaks seen in the ir absorbance spectrum of poly(dG-me^{5}dC) lie at the same frequency as either of the peaks in the poly(dG-dC) spectrum. However, for both oligonucleotides, the highest frequency peak occurs at a frequency very near to the zero-crossing frequency of the corresponding VCD spectrum indicating that the transition associated with this peak is mainly responsible for the optical activity observed. It should be noted that Gaussian curve fitting of the ir absorbance spectrum of poly(dG-dC) indicates it is likely that there is at least one more transition at a frequency somewhere between the two observed peaks, accounting for the difference in the number of ir absorbance peaks seen in the two spectra. However, the closeness of the peaks in the poly(dG-dC) spectrum indicates that there is less splitting and therefore less of an interaction energy than there is for the methylated oligomer. This supports the notion discussed above that the methyl group alters the interaction of the base carbonyls.

Fig. 5 shows the ir absorbance and VCD spectra of poly(dG-dC) titrated with NaCl. The figure indicates that a B-form conformation exists for poly(dG-dC) in 50 mM (solid line) and 2.2 M NaCl (dashed line). The VCD spectra are nearly identical and have the same zero-crossing point at 1686

Fig. 5: IR absorbance (bottom) and VCD (top) spectra of Poly(dG-dC) Titrated with NaCl. Solid line - B-form spectra; poly(dG-dC) 7.11 mg/ml, 50 mM NaCl, 10 mM cacodylate buffer pH 7, 0.01 cm path. The rest of the samples all contained poly(dG-dC) 14.35 mg/ml and were prepared in 11.6 mM cacodylate buffer pH 7. The path length for these samples was 0.005 cm. Dashed line - 2.2 M NaCl, Dash-dot-dash line - 3.2 M NaCl, Dotted line - 4.2 M NaCl.

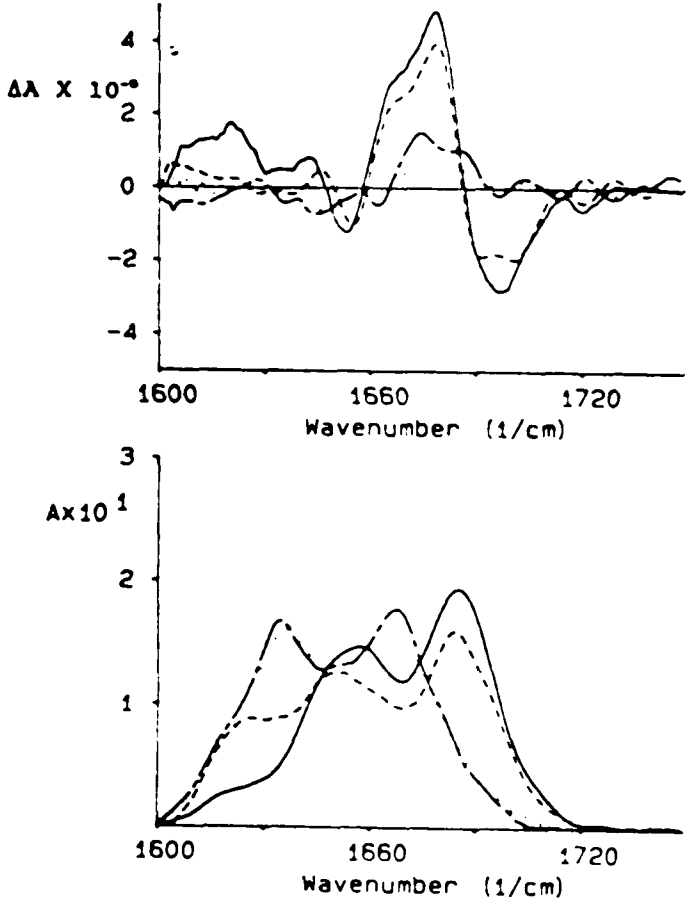

± 1 cm^{-1}. The ir absorbance spectra are consistent with the B-form ir absorbance spectra discussed in chapter III. The dash-dot-dash (3.2 M NaCl) and the dotted line (4.2 M) VCD both show a positive/negative couplet which is consistent with Z-form spectra. The intensity of the peaks in the NaCl induced Z-form VCD spectra are half as intense as the peaks seen in the B-form VCD spectrum. Although the VCD spectrum of the 4.2 M NaCl solution is very weak, there is a positive/negative couplet with peaks at 1679 and 1644 cm^{-1} respectively and a zero-crossing point at 1666 cm^{-1}. The 3.2 M NaCl solution has more resolvable features. The positive peak of the couplet is seen to be comprised of two overlapping peaks at 1686 and 1674 cm^{-1} respectively. The broad negative peak is also a combination of overlapping peaks which occur at 1662, 1644 and 1635 cm^{-1}. Inconsistencies between the shape of the Z-form peaks seen in this figure with the previous description of Z-form spectra are largely due to poor signal/noise in the later spectra. The ir absorbance spectra for these two poly(dG-dC) solutions are nearly identical and are comprised of two peaks at 1668 and 1636 cm^{-1} respectively. Here, the two ir absorbance peaks have almost the same intensity whereas their intensities are very different in the ir absorbance spectrum of the Z-form spectrum shown in Fig. 3 (RHS, dashed line). A closer examination of the two spectra shows that the difference is actually in the intensity of the 1636 cm^{-1} peak. We attribute this difference

to the coupling of N=C and C=C vibrations. The peaks of VCD spectra have the same frequencies and are of the same orientation indicating that this change in intensity does not effect the C=O transition.

The ir absorbance and VCD spectra of poly(dG-dC) with $MgCl_2$ are shown in Fig. 6 (dashed line and dash-dot-dash line). Unfortunately, during the time this study was performed, there were changes made in the production of poly(dG-dC) by the supplier. These alterations caused differences in the behavior of the poly(dG-dC) samples used in the beginning of the study and those used later on. The reasons for this are not clear at this time. The Z-form spectrum of poly(dG-dC) in $MgCl_2$ drawn in the dashed trace cannot be reproduced with the current samples commercially available. However, this spectrum shows the same general features as the current poly(dG-dC) Z-form spectrum drawn in a dash-dot-dashed trace. For clarity, the dashed line Z-form spectra will be designated as the original $MgCl_2$ induced Z-form infrared spectra. In both cases, the VCD spectrum of poly(dG-dC) in $MgCl_2$ resembles the NaCl induced Z-form spectrum in both frequency and shape. The ir absorbance spectrum for the original $MgCl_2$ induced Z-form (dashed line) shows two peaks which are separated by 26 cm^{-1} compared to the 30 cm^{-1} separation of the NaCl induced Z-form (solid line). However, there is no shift in the peaks to lower wavenumber in the $MgCl_2$ spectrum. The highest frequency peak is seen at

Fig. 6: Comparison of the IR Absorbance (bottom) and VCD (top) Spectra of Poly(dG-dC) in Z-conformations Induced by NaCl (solid line) or $MgCl_2$ (dashed line and dash-dot-dashed line). Solid line - poly(dG-dC) 19.8 mg/ml, 3 M NaCl, 0.005 cm path; Dashed line - poly(dG-dC) ca. 20 mg/ml, 1.5 M $MgCl_2$, 0.0025 cm path; Dash-dot dash line - poly(dG-dC) 7 mg/ml, 1.2 M $MgCl_2$, 0.01 cm path. All samples were prepared in 10 mM pH 7 cacodylate buffer. Dashed line spectra are the original $MgCl_2$ induced Z-form poly(dG-dC) spectra.

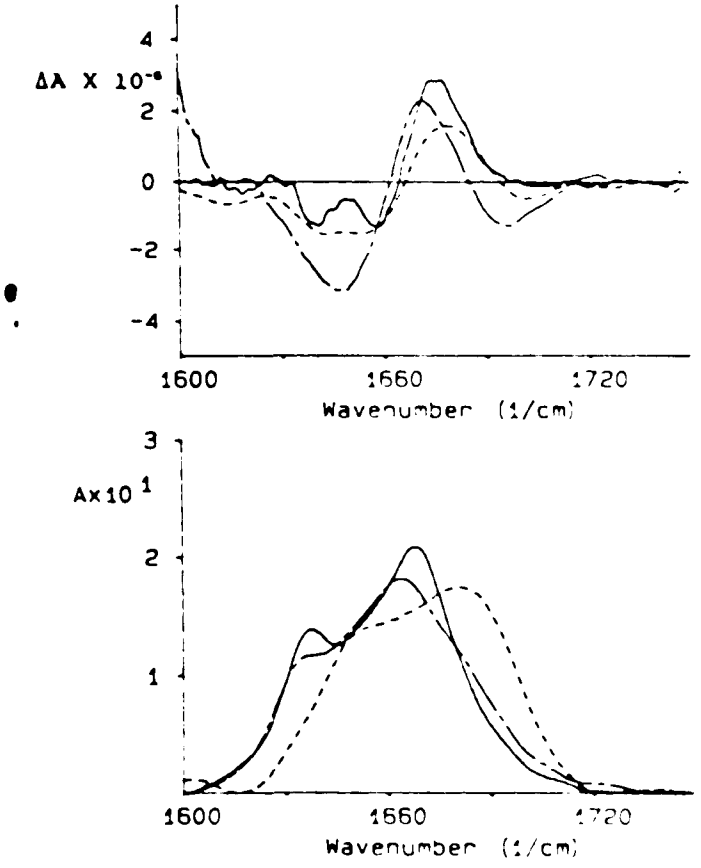

1681 cm^{-1} which is almost the same frequency as the corresponding peak of the B-form spectrum. The original VCD spectrum for poly(dG-dC) in $MgCl_2$ has a positive/negative couplet with the zero-crossing point at 1666 cm^{-1}. The negative peak is clearly comprised of two overlapping negative peaks at 1653 and 1643 cm^{-1} respectively. In addition, there is a small negative peak at ca. 1700 cm^{-1}. With the exception of the small negative peak which is not seen in the spectrum of poly(dG-dC) in NaCl, the spectrum of poly(dG-dC) in $MgCl_2$ is in good agreement with the NaCl Z-form spectrum. The ir absorbance spectrum for the $MgCl_2$ Z-form of poly(dG-dC) (Fig. 6, dash-dot-dash line) shows the same red-shift that is seen in the NaCl induced Z-form spectrum. However, there is a third peak seen at 1681 cm^{-1} which is the same frequency as the high frequency ir absorbance peak of the original poly(dG-dC)/ $MgCl_2$ spectrum. The VCD spectrum for poly(dG-dC) in $MgCl_2$ has the same positive/negative couplet and a smaller negative peak at 1695 cm^{-1}. The negative peaks are more pronounced than those seen in the corresponding original $MgCl_2$ Z-form poly(dG-dC) spectrum and the positive peak has been shifted towards a slightly lower frequency.

Figs. 7 and 8 show titrations of poly(dG-me^5dC) with NaCl and $MgCl_2$. The VCD and the ir absorbance spectra of poly(dG-me^5dC) in 52 mM (solid line, Fig. 7) and in 500 mM NaCl (dashed line, Fig. 7) are both indicative of a B-conformation. The VCD spectra are nearly identical

Fig. 7: Experimental IR Absorbance (bottom) and VCD (top) Spectra of Poly(dG-me^{5}dC) Titrated with NaCl. All samples contained 12.5 mg/ml poly(dG-me^{5}dC) in 11.6 mM pH7 cacodylate buffer. The path length used was 0.005 cm. Solid line - 52 mM NaCl; Dashed line - 500 mM NaCl; Dash-dot-dash line - 1.5 M NaCl; Dotted line - 4.2 M NaCl.

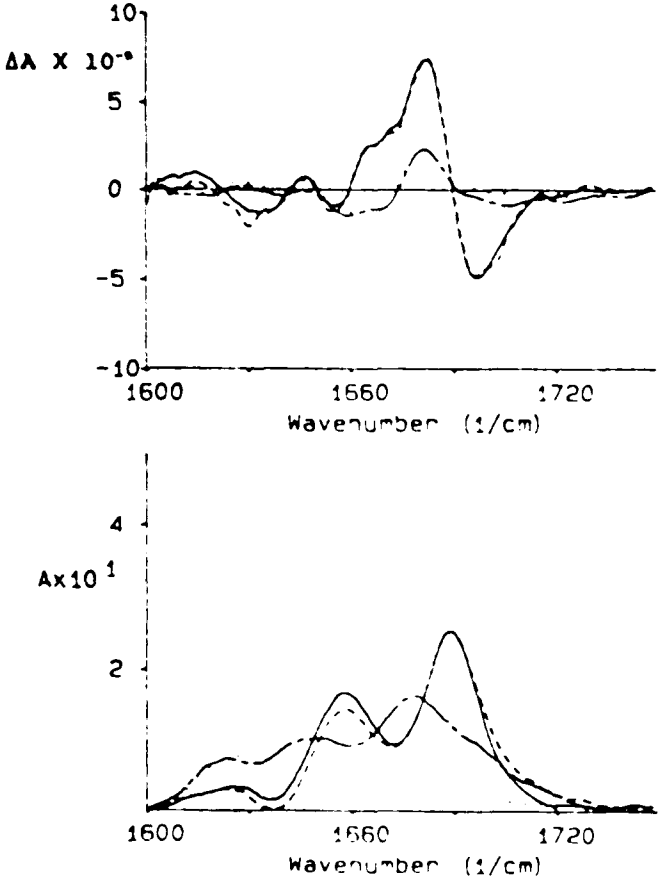

Fig. 8: Experimental IR Absorbance (bottom) and VCD (top) Spectra of Poly(dG-me^{5}dC) Titrated with $MgCl_2$. All samples contained 12.5 mg/ml poly(dG-me^{5}dC) and were prepared in 10 mM cacodylate pH 7. Path length was 0.005 cm. Solid line - without $MgCl_2$; Dashed line - 1.0 mM $MgCl_2$; Dash-dot -dash line - 2.6 mM $MgCl_2$. Dotted line - 57 mM $MgCl_2$.

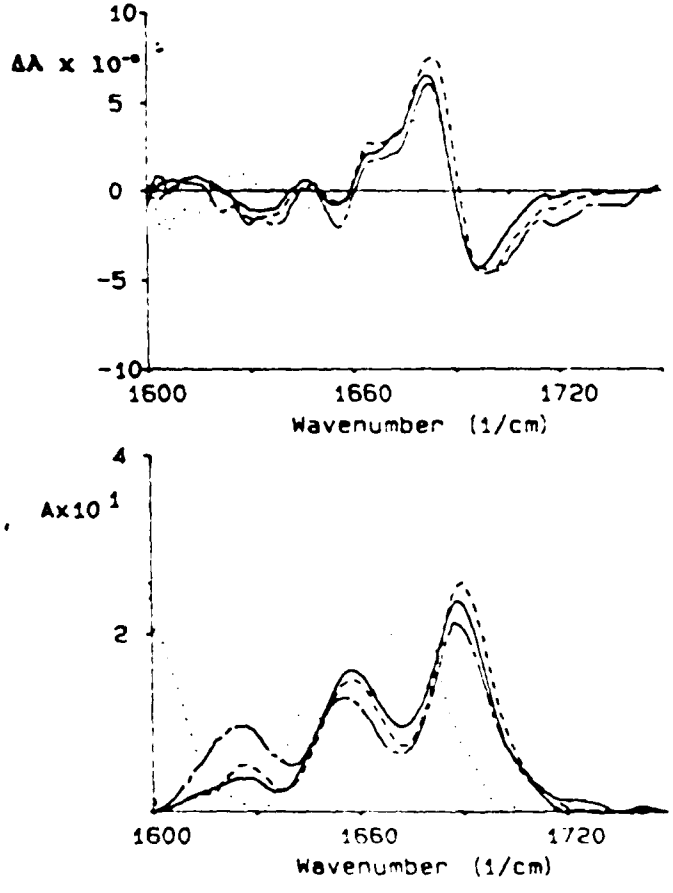

indicating than the extra NaCl has made no detectable difference in the handedness of the conformation of the poly(dG-me^{5}dC). The 1690 cm^{-1} peak seen in the spectrum of the 52 mM sample has the same intensity and nearly the same rotational strength as the corresponding peak in the 500 mM solution. The ir absorbance spectrum of poly(dG-me^{5}dC) in 1.5 M NaCl (Fig. 7, dash-dot-dash line) has peaks at 1678, 1649, and 1624 cm^{-1} respectively. At 2.1 M NaCl, the ir absorbance spectrum shows a slight shift to lower wavenumbers in the 1678 and 1649 cm^{-1} peaks to 1676 and 1646 cm^{-1} respectively. However, the VCD spectrum of these two samples are similar, both have positive peaks at 1681 cm^{-1}, negative peaks at 1668 cm^{-1}, and the zero-crossing point occurs at 1674 cm^{-1}. There is a small difference between the negative peaks of the VCD spectra of the 1.5 M NaCl and that of the 2.1 M NaCl sample. The negative peak of the VCD spectrum of the 1.5 M NaCl solution is composed of two overlapping peaks, the second at 1659 cm^{-1} which is not seen in the spectrum of the 2.1 M NaCl sample. In Fig. 8, the ir absorbance and VCD spectra of poly(dG-me^{5}dC) in 50 mM NaCl and 0, 1 mM and 2.6 mM $MgCl_2$ are all indicative of a B-form sample. At 57 mM $MgCl_2$, both the ir absorbance and the VCD spectra are radically altered and the peaks in the VCD spectrum are "flipped" from a negative/positive couplet to a positive/negative couplet indicating that the poly(dG-me^{5}dC) is in a Z-conformation. In the ir absorbance spectrum, the 1689 cm^{-1} has been shifted to

1676 cm^{-1} and the 1656 cm^{-1} peak to 1646 cm^{-1}. The peak seen at 1626 cm^{-1} in the B-form ir absorbance spectrum and seen at 1624 cm^{-1} in the ir absorbance spectrum of poly(dG-me^{5}dC) in 2.1 M NaCl is not seen in the ir absorbance spectrum of the 57 mM $MgCl_2$ sample. However, the shift of the other two ir absorbance peaks is the same as that seen in the spectrum of poly(dG-me^{5}dC) in 2.1 M NaCl. The major difference between the ir absorbance spectra of poly(dG-me^{5}dC) in 2.1 M NaCl versus in 57 mM $MgCl_2$ is the relative intensity of the 1676 and 1646 cm^{-1} peaks. For the ir absorbance spectrum in 2.1 M NaCl, A_{1676}/A_{1646} = 1.20. For the ir absorbance spectrum in 57 mM $MgCl_2$, A_{1676}/A_{1646} = 1.41. The VCD spectrum of poly(dG-me^{5}dC) in $MgCl_2$ has a positive peak at 1682 cm^{-1} followed by a negative peak at 1665 cm^{-1}. The zero-crossing point is 1673 cm^{-1}. These are the same frequencies as seen in the 2.1 M NaCl VCD spectrum. However, the intensities are about twice as great for the peaks in the VCD spectrum of poly(dG-me^{5}dC) in 57 mM $MgCl_2$ solution than they are in the 2.1 M $MgCl_2$ solution. However, this difference is not seen in the electronic UV CD spectra (data not shown).

B. Application of the DECO Model to Z-form Helices:

The coordinates for the Z-form helices used for the DECO calculations were obtained from Z-form helices generated by Macromodel[47] in the same way that the coordinates were obtained for the B-form helices (chap. III). Macromodel bases its Z-form structures on data from Wang et al.[6] In the Z-form

geometry of an alternating GC-oligonucleotide, alternating bases are in the syn- and anti-conformations respectively. The cytosine bases are all in anti-conformations relative to the sugar and the guanines are all in syn-conformations. In addition, the sugar pucker of the deoxyguanosines in a Z-form helix is C3'-endo while that of the deoxycytosines is C2'-endo. The sugar pucker for both deoxyguanosines and deoxycytosines is C2'-endo in B-form helices. Z-form helices are twisted tighter than B-form helices; 12 bases/turn versus 10.5 for a B-form helix. The DECO calculated and the experimental ir absorbance and VCD spectra for $d(CG)_{10}$ (Macromodel) and poly(dG-dC) (experimental) in the high salt Z-forms are shown in Fig. 9. Neither the calculated ir absorbance nor the calculated VCD spectrum are in agreement with the observed spectra. The experimental ir absorbance spectrum shows two peaks at 1668 and 1638 cm^{-1} respectively. The calculated ir absorbance spectrum also shows two peaks but their frequencies are 1690 and 1656 cm^{-1}. Both the calculated and the experimental VCD spectra have a zero-crossing point at 1660 ± 3 cm^{-1}. However, the experimental VCD spectrum shows a positively biased positive/negative couplet while the calculated VCD spectrum shows a conservative negative/positive couplet. In addition, the negative peak of the experimental VCD spectrum is comprised of two peaks at 1658 and 1642 cm^{-1} respectively, whereas the peaks in the calculated VCD spectrum do not show any splitting. Unfortunately, the

Fig. 9: Experimental and DECO Calculated IR Absorbance (bottom) and VCD Spectra (top) of Z-form Poly(dG-dC).
Solid line - experimental spectra, poly(dG-dC) 19.8 mg/ml, 3 M NaCl, 10 mM cacodylate buffer pH 7, 0.005 cm path
Dashed line - DECO calculated spectra of d(CG)10

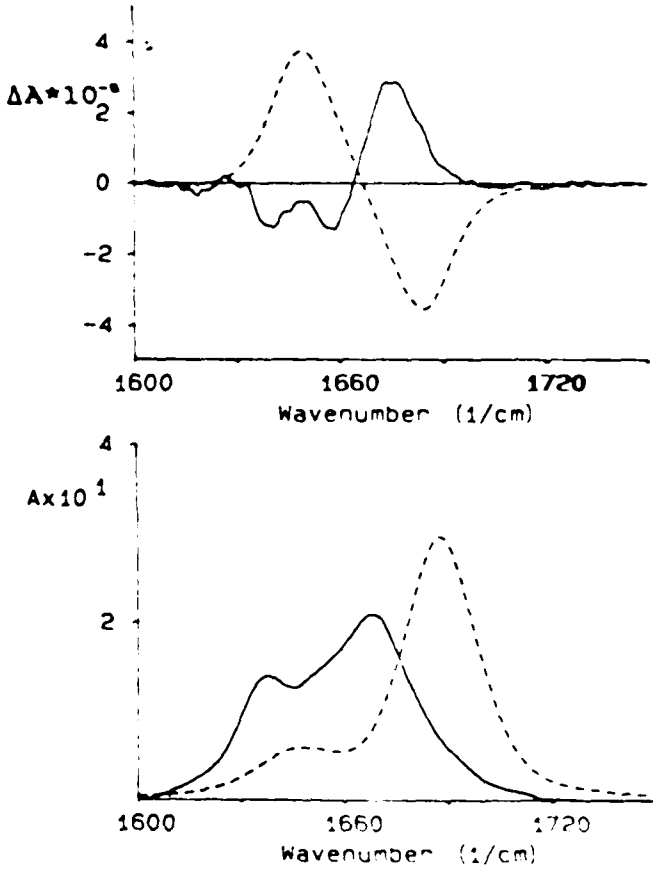

negative/positive couplet seen in the calculated VCD spectrum is suggestive of a B-form helical conformation, and not a Z-form conformation.

There are two possible causes for the inconsistent results. The first is that the helix generated by Macromodel is not the same as the solution state helical conformation of poly(dG-dC) in high salt solution. The second is that the degenerate extended oscillator (DECO) model needs to be modified for predicting Z-form VCD spectra.

It is difficult to determine which coordinates should be used for the DECO calculations. Other crystal based structures were obtained from the Protein Data Bank [Protein data bank, Brookhaven National Laboratory, New York, USA] but these were of tetramers and hexamers which are too short to be considered good geometric models of the polymer. Calculations based on these small molecules did not yield the positive/negative couplet expected for the VCD spectrum of a Z-form helix (spectra not shown). However, one geometric modification was tried. In a Z-form helix of alternating purine and pyrimidine bases, the angle between the base and the sugar, χ, alternates between syn- and anti-conformations. The x-ray diffraction studies have all indicated that it is the guanine bases that take on a syn-conformation while the cytosine bases are all in conformations which are anti- relative to the sugar. Energy calculations of Z-form helices indicate that having the purine bases in a syn-conformation relative to the sugar and

the pyrimidine bases in an anti-conformation is energetically favorable to having a Z-form helix where the purines are in an anti- and the pyrimidines are syn-conformation. NMR data indicates that there are two sugar/base conformations but the association of the purine bases with the syn-conformation is assumed from the x-ray results and has not been determined directly from the NMR spectra. The calculated ir absorbance and VCD spectra for a " irregular" Z-form GC-helix where the guanines take on anti-conformations relative to the sugar ring and the cytosine bases take on syn-conformations is shown in Fig. 10. The peaks in the calculated spectrum are at much higher frequencies than those of the experimental spectrum. The most prominent peak in the calculated ir absorbance spectrum is at 1705 cm^{-1} which is more than 30 cm^{-1} greater than the high frequency peak of the experimental spectrum. The peaks of the calculated VCD spectrum are also at higher frequencies than the corresponding experimental VCD spectral peaks. However, the calculated VCD spectrum shows a positive/negative couplet which is consistent with the spectrum of a helix with Z-form geometry.

If the helix coordinate geometry is considered accurate, then the DECO model must be considered to be inadequate for describing Z-form helix geometries. Thus, the helix generated by Macromodel[47] was used as the geometric representation of the conformation of poly(dG-dC) in high salt solution. For the DECO calculations, it is assumed that the carbonyls on the

Fig. 10: DECO Calculation for a CG-helix with an Irregular Z-form Geometry. Infrared absorbance (bottom) and VCD (top) spectra for Z-form $(CG)_{10}$ where the anti- and syn- conformations of the bases is reversed and the experimental spectra for poly(dG-dC) in NaCl. Solid line - poly(dG-dC) 19.8 mg/ml, 3 M NaCl, 10 mM pH 7 cacodylate buffer, 0.005 cm path. Dashed line - calculated spectra for Z-form $(CG)_{10}$

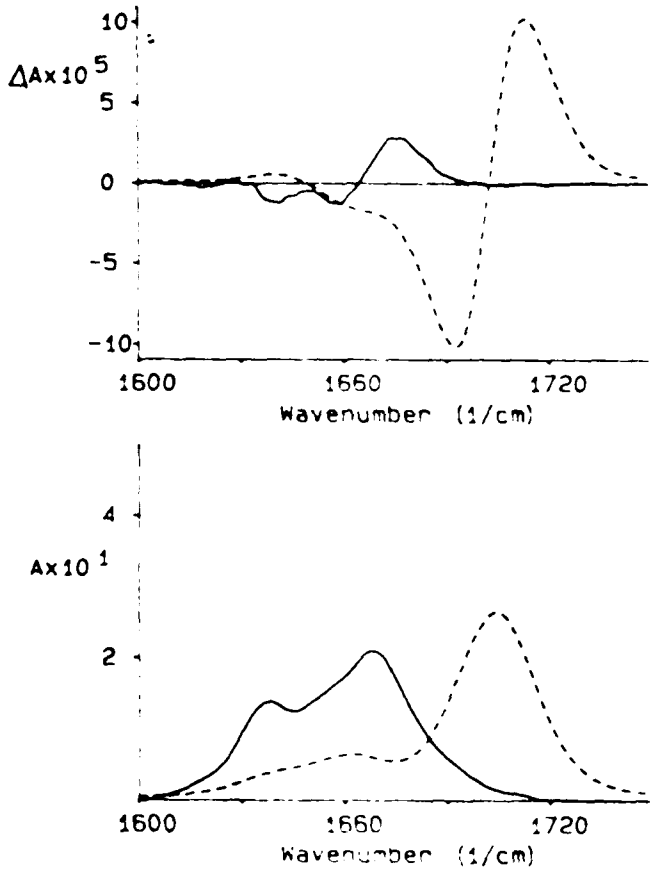

cytosine and guanine bases have identical stretching frequencies and extinction coefficients at this frequency (Fig. 9, dashed line). It is assumed that other base vibrations and interactions between the carbonyl groups and the sugar ring have no influence on the carbonyl stretching vibrations. In addition, the effects of hydrogen bonding on the charge distribution of the carbonyls and interactions between the oligonucleotide and the solvent are also not taken into account. In chapter three, we demonstrated that despite its simplicity, the DECO model could be used with great accuracy in the carbonyl stretching region in the interpretation of VCD spectra of deoxyoligonucleotides existing in right-handed conformations. We claimed that the differences below 1650 cm^{-1} in the experimental and calculated VCD spectra could be attributed to the omission of the N=C and C=C stretching vibrations. Recently Xiang and coworkers have confirmed this.[56] However, it is unlikely that the omission of the N=C and C=C vibrations affects the handedness of the spectra.

Comparison between the carbonyl positions for a B-form versus a Z-form helix suggest that the carbonyls are less likely to all be equivalent in the Z-form helix than in the B-form helix. For a single-stranded B-form and Z-form helix, the length of each carbonyl vector and the angle between the vector and the x-axis are given in Table II. For the B-form helix, each successive step down the helix (z-axis value

decreases) is accompanied by a clockwise movement in the xy-plane. For the Z-form helix the steps alternate between clockwise ($\Delta\theta < 0$) and counterclockwise ($\Delta\theta > 0$). However, if the cytosine carbonyls are considered separately from the guanine carbonyls, then a counterclockwise pattern is mapped out for each (Table III). In addition, the cytosine carbonyls of a Z-form helix all point into the center of the helix and are completely surrounded by the guanine carbonyls which lie on the outer surface of the helix (Fig. 11). In the B-form helix, the guanine and cytosine carbonyls are intermixed throughout the helix. In an attempt to obtain a better fit between the DECO calculated Z-form spectra and the experimentally observed spectra, some of the carbonyl interactions were reduced. Fig. 12 shows the calculated ir absorbance and VCD spectra of a Z-form helix where some of the possible carbonyl interactions have been reduced as follows: each cytosine carbonyl was allowed to interact with other cytosine bases in the same strand and with the guanine base that it was paired with. Cross-strand cytosine-cytosine interactions and same strand cytosine-guanine interactions were forbidden. Guanine base interactions were treated the same way. The calculated spectra are in surprisingly good agreement with the experimental spectra. One argument in support of these restrictions is that since the cytosine carbonyls face into the center of the helix while the guanine carbonyls face outward or are imbedded in the helix surface,

Fig. 11: Diagram of the Carbonyl Coordinates in Z-form $d(CG)_{12}$. Guanine carbonyls are designated by a single straigt line connecting the carbonyl carbon and oxygen while cytosine carbonyls are designated by three lines originating from the carbonyl carbon and connecting it to: the carbonyl oxygen, the N1 nitrogen, and the N3 nitrogen.

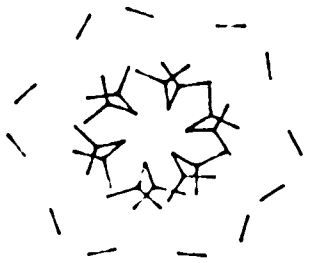

Fig. 12 : Modified DECO Calculations for a Z-form CG-helix. IR absorbance spectrum (bottom) and VCD spectrum (top). Solid line - poly(dG-dC) 19.8 mg/ml, 3 M NaCl, 10 mM cacodylate buffer pH 7, 0.015 cm path. Dashed line - calculated spectra for $(CG)_{10}$. In the calculation, only same bases within a strand and base pairs interacted

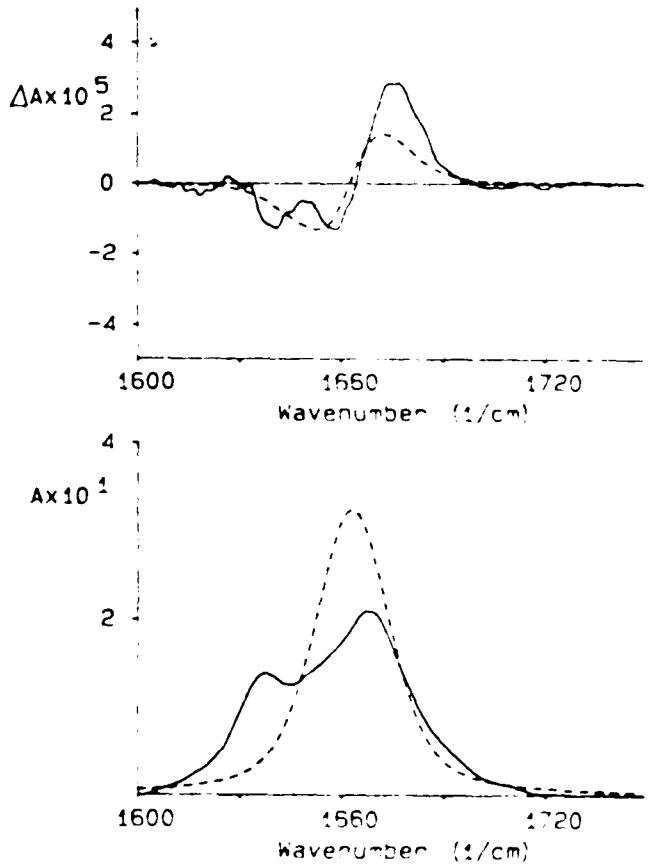

the environment of the cytosine carbonyls is not the same as that around the guanine carbonyls. The result of this difference would be that the two types of carbonyls are no longer degenerate and do not interact in the same fashion. The non-degeneracy of the cytosine and guanine carbonyls within a helix has been proposed through Raman studies.[57] However, the non-degeneracy is thought to occur for both B-form and Z-form helices and this is contradictory to our VCD evidence (chap. III). For completeness, we developed a program based on Faulkner's theory of the non-degenerate coupled oscillator.[58] Faulkner's model leads to a different perturbation term for the Hamiltonian; however, the non-degenerate carbonyls weakly interact. Results from this modified DECO program were no better at generating Z-form spectra and the effort was abandoned. In addition, it is unlikely that in a solution of 3 M NaCl, there is any difference in the environment inside and outside the helix which would have to be the case in order to justify the complete removal of same strand C-G interactions. The sodium ions are small and flow through the helix easily. As of this date, we have found no experimental or theoretical evidence that supports the restrictions.

C. Summary:

The results presented here illustrate that both poly(dG-dC) and poly(dG-me^{5}dC) undergo cooperative B-Z transition with increased divalent or monovalent salt concentrations.

Infrared absorbance and VCD spectra indicate that the Z-form induced by NaCl is not the same as that induced by $MgCl_2$ and that the Z-forms of poly(dG-dC) are not the same as those of poly(dG-me^{5}dC).

DECO calculations performed on Z-form helices did not generate spectra which resembled the experimental spectrum of Z-form poly(dG-dC). Modifications made to the DECO model produced a much better correlation between experimental and calculated spectra but the scientific validity of the modifications has yet to be proven.

TABLE II: Screwsense
θ is the angle that the base carbonyl makes with the positive x-axis in the xy-plane. Table includes only strand I carbonyls. The view is from the 5'-end to the 3'-end.

carbonyl position read 5'-3'	B-form base	θ	Z-form base	θ	Z-form irregular base	θ
1	cyt	300	cyt	301	gua 105	0
3	gua	131	gua	116	cyt	288
5	cyt	48	cyt	58	gua	168
7	gua	238	gua	180	cyt	40
9	cyt	156	cyt	97	gua	244
11	gua	346	gua	206	cyt	109
13	cyt	264	cyt	161	gua	326
15	gua	305	gua	322	cyt	174
17	cyt	192	cyt	314	gua	83
19	gua	22	gua	74	cyt	201

TABLE III: Screwsense of the Cytosine and Guanine Bases Table includes only strand I carbonys.

cytosine bases positon	θ	guanine bases position	θ
1	301	3	116
5	58	7	180
9	97	11	206
13	161	15	322
17	316	19	79

TABLE IV: Infrared Absorbance and VCD Spectral Characteristics

sample	conditions	ir absorbance peaks in cm^{-1}	VCD peaks in cm^{-1}
poly(dG-dC)	3 M NaCl	1668, 1638	+1675 x1664 -1659, -1641
	1.0 M $MgCl_2$ 1.0 M NaCl	1687, 1664, 1633	-1699 (broad) x1688 +1673 x1663 -1649 -1635
poly(dG-me^5dC)	2.0 M NaCl	1676, 1646, 1624	+1681 x1674 -1667
	0.930 M $MgCl_2$	1676, 1646	+1682 x1673 -1665

Rotational strength is measured as R_L - R_R. + indicates R_L > R_R, similarly - indicates R_R > R_L, x indicates R_L=R_R, (sh) means shoulder All wavenumber values are +/-3 cm^{-1}.

V. Conformations with other salts:

The "alternate", L-conformation (now called Z) of DNA proposed by Pohl and Jovin in 1972 had far reaching biological implications. Pohl and Jovin suggested that the conformational transition between the R- and L-forms of DNA may play a role in regulation phenomena like transcription and differentiation. In addition, the "alternate" conformation could be important in tertiary structure determination.[21] Unfortunately, the conditions used to induce the transition were too harsh to be considered possible for in vivo systems.

Changes in temperature, solvent, and metal salts or combinations of metal salts have all been used in an attempt to find more biologically relevant (salts in millimolar concentrations) way of causing what is now called the B- to Z-structural transition in oligonucleotides.[59,60,61]

This study focused on the changes in secondary structure due to changes in the metal cation of the inducing salt. Z-conformations induced by NaCl and $MgCl_2$ were discussed in chap. 4. In this chapter, the effects of adding $NiCl_2$, $CoCl_2$ and $[Co(NH_3)_6]Cl_3$ to poly(dG-dC) are discussed.

A. $NiCl_2$ and $CoCl_2$:

Like $MgCl_2$, both $NiCl_2$ and $CoCl_2$ contain divalent cations. However, the behavior of poly(dG-dC) in the presence of $CoCl_2$ or $NiCl_2$ is very different from that of $MgCl_2$. The B-Z transition induced through $MgCl_2$ is monophasic, but the transition induced by $CoCl_2$ or $NiCl_2$ is biphasic suggesting

that a there is another conformation between the B- and Z-form when $CoCl_2$ or $NiCl_2$ are used to induce the B-Z transition.

In 1982, van de Sande and coworkers reported that a B-Z transition could be induced using $NiCl_2$, $CoCl_2$ or $MnCl_2$ at concentrations which were 1000-2000 times less than what was required to induce the transition with $MgCl_2$.[61] The transition to a Z-form was monitored by examining the A_{295}/A_{260} ratio of the UV absorbance spectrum. For a B-form, this ratio is approximately 0.12 while for a Z-form, the ratio is increased by approximately 3.2 times.[61] The CD spectrum of poly(dG-dC) (80 ±μM) in 0.6 mM $CoCl_2$ that was shown in the paper does not closely resemble the Z-form spectrum of poly(dG-dC) in 3 M NaCl. Zacharias and coworkers also found that the CD spectrum of poly(dG-dC) in the presence of $CoCl_2$ did not closely resemble the Z-form spectrum of poly(dG-dC) in 3 M NaCl. Since the electronic CD spectrum of the $NiCl_2$ induced Z-form was not shown in Jovin's paper, we performed an electronic CD experiment using their conditions. The resulting CD spectrum was completely anomalous, not clearly representative of a B- or Z-form conformation (Fig. 1, bold line and bold solid line). The conditions were altered slightly to check for problems due to aggregation or $Ni(OH)_2$ precipitation but the CD spectra were all qualitatively the same (Figure not shown) and we were unable to make a determination of the handedness of poly(dG-dC) in the presence of $NiCl_2$ using the electronic CD spectrum taken in the 230-330 nm region.

Fig. 1: UV CD Spectrum of Poly(dG-dC) & $NiCl_2$: All samples were prepared in distilled water. Dashed line - without $NiCl_2$; bold solid line - 4.9 mM $NiCl_2$; solid line - 10.5 mM $NiCl_2$.

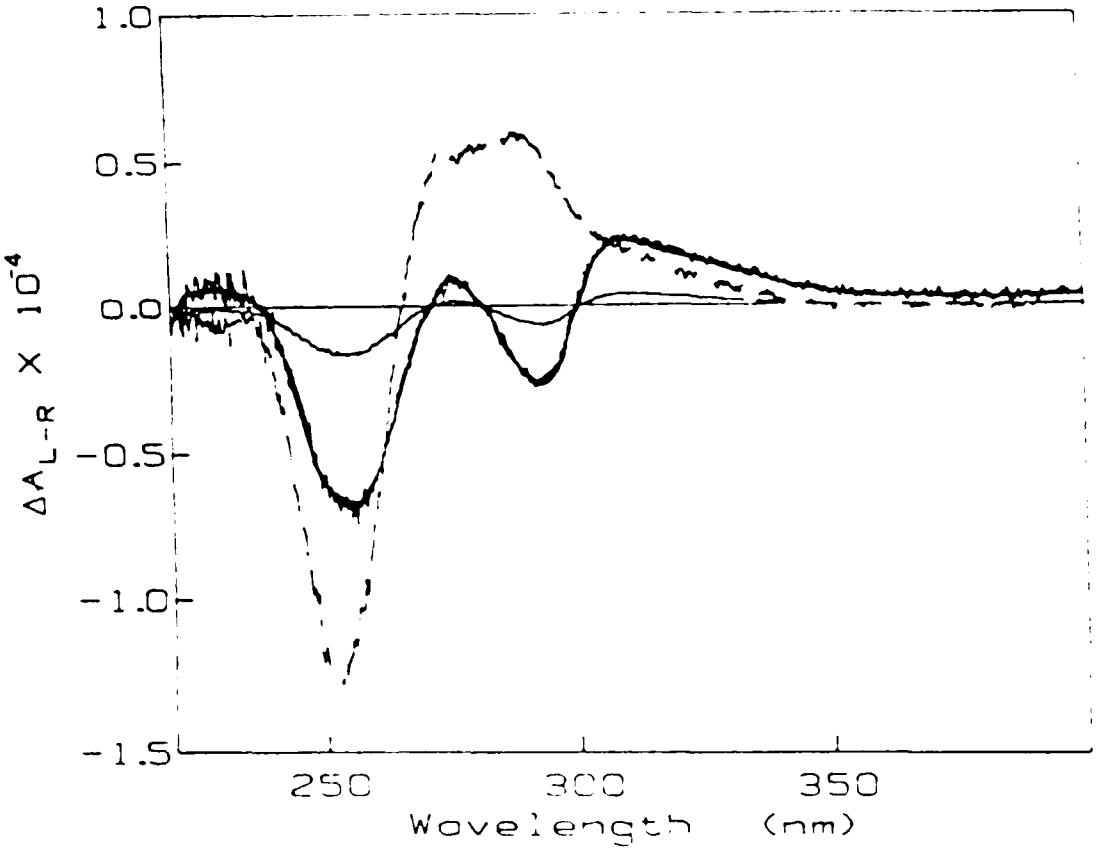

Previous infrared spectra taken on films of poly(dG-dC) in the presence of $NiCl_2$ showed that a Z-formation was induced only when the humidity was 75%. At a relative humidity of 32%, the ir absorbance spectrum showed that the conformation was a modified B-form.[62] However, the question of whether or not the solution conformation of poly(dG-dC) in the presence of $NiCl_2$ was left-handed in orientation still remained.

Infrared (Vibrational) circular dichroism presented a viable means of solving this question. In order to perform an ir CD (VCD) experiment, the concentration of poly(dG-dC) had to be increased from 0.05-0.1 mg/ml used in the UV CD samples to between 12-17 mg/ml. The resulting VCD spectrum was clearly still characteristic of a B-form. The corresponding ir absorbance spectrum showed a shift in the lowest frequency peak from 1586 cm^{-1} when no $NiCl_2$ was added to 1591 cm^{-1} for the 0.55 mM $NiCl_2$ sample (Fig. 2 RHS, solid line) to 1603 cm^{-1} for the 9.2 mM $NiCl_2$ sample (Fig. 2 RHS, dashed line). When $CoCl_2$ was used in place of the $NiCl_2$, that peak was seen at 1602 cm^{-1} even when only 0.5 mM $CoCl_2$ has been added (Fig. 2 LHS, dashed line). In addition, there was an almost 2-fold increase in the intensity of this peak with increased divalent salt concentration. The higher frequency peaks (associated with the carbonyl stretching vibrations) decreased in intensity but their frequencies remained almost the same. An ir absorbance peak in the 1580-1590 cm^{-1} region is seen in the spectrum of 5'GMP but not in the spectrum of 5'CMP (data not shown).

Fig. 2: Infrared Absorbance (bottom) & VCD (top) Spectra of poly(dG-dC) in the Presence of $CoCl_2$ (LHS) or $NiCl_2$ (RHS): All samples were prepared in 10 mM pH 6 cacodylate buffer with between 10 and 30 mM NaCl except where indicated. **LHS:** solid line - without any divalent salt; dashed line - 0.5 mM $CoCl_2$, 10 mM NaCl; dash-dot-dash line - 15 mM $CoCl_2$. **RHS:** solid line - 0.5 mM $NiCl_2$; dashed line - 9.2 mM $NiCl_2$.

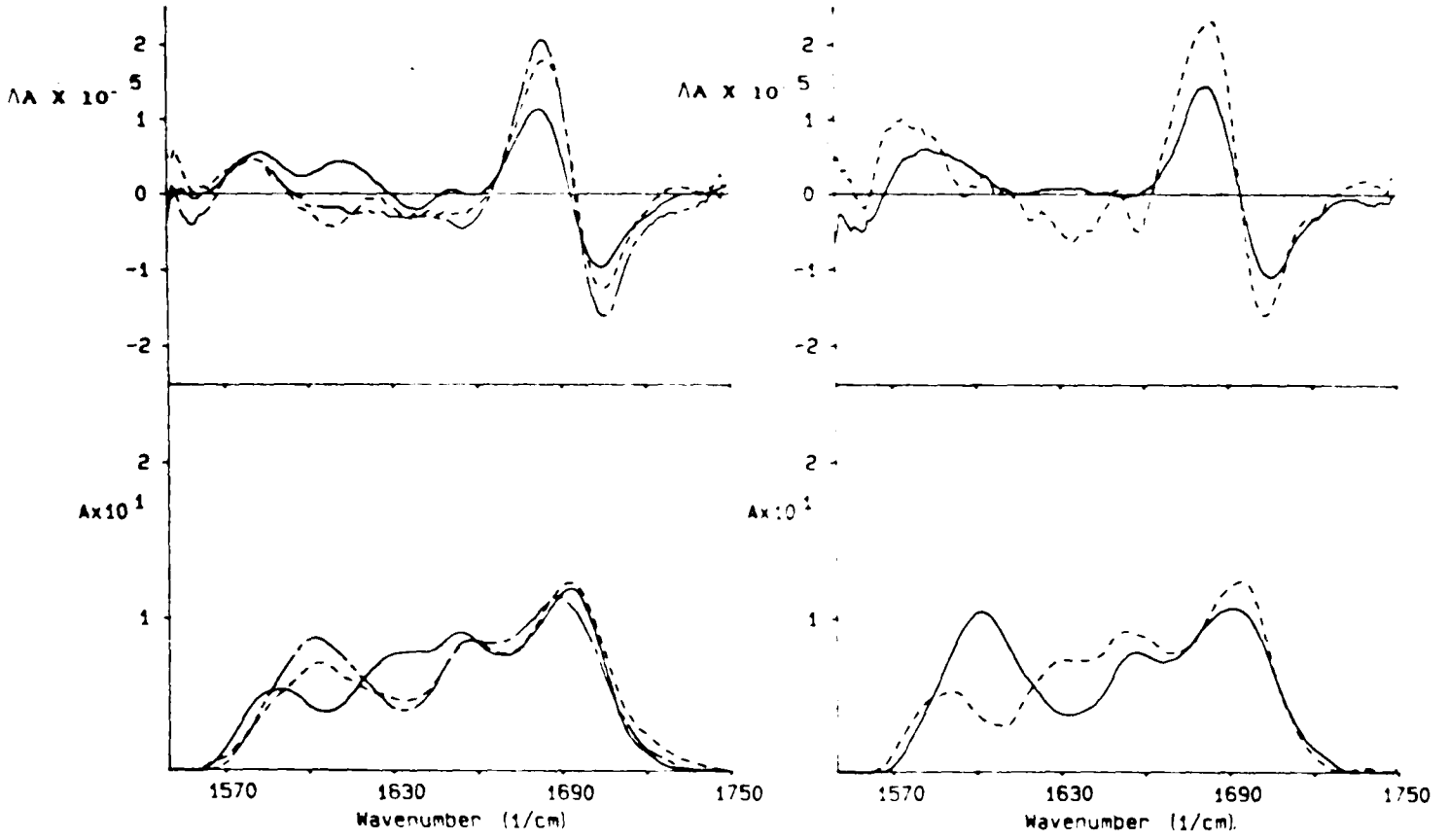

Tsuboi assigned the 1580 cm^{-1} peak seen in the ir absorbance spectrum of d(G) to the C=C and C=N stretching vibrations of the guanine base.[51] Pilet assigns this peak to the guanine ring breathing vibration (chap. 1, table I).[63] Taillandier explains that the changes seen in the ir spectrum of poly(dG-dC) upon the addition of $NiCl_2$ are a result of the $NiCl_2$ binding to the N7 position on the guanine base.[62] We concluded that although the $NiCl_2$ altered the B-form poly(dG-dC) helix, it did not induce a left-handed conformation.

To further prove this conclusion, several samples of the poly(dG-dC) in $NiCl_2$ were prepared and run in the vacuum UV CD region (220-180 nm). The conditions were similar to those used for the infrared samples. The vacuum UV CD spectrum was taken from 300-185 nm. In the 230-320 nm region, the CD spectrum was similar to the spectra shown in Fig. 1. However, the spectrum of the below 200 nm region indicated that the poly(dG-dC) was still in a right-handed conformation (figure not shown); thereby confirming the VCD result.

The electronic CD spectrum of poly(dG-dC) in 1.4 M NaCl and 88 mM $NiCl_2$ is shown in Figure 3. This spectrum has the same characteristics as the CD spectrum of poly(dG-dC) in 3 M NaCl. It is very unusual for the addition of NaCl to aid a multivalent cation in inducing a Z-conformation. In most instances, the presence of NaCl competes with the multivalent salt ions and can cause a shift in the B-Z equilibrium back to

Fig. 3: UV CD Spectrum of Poly(dG-dC) with 1.4 M NaCl & $NiCl_2$: Samples were prepared in distilled water. Dashed line - poly(dG-dC) in its low salt B-form; solid line with dots - poly(dG-dC) in 1.4 M NaCl; solid lines without dots - poly(dG-dC) in 1.4 M NaCl and 88 mM or 170 mM $NiCl_2$ (spectra are almost identical).

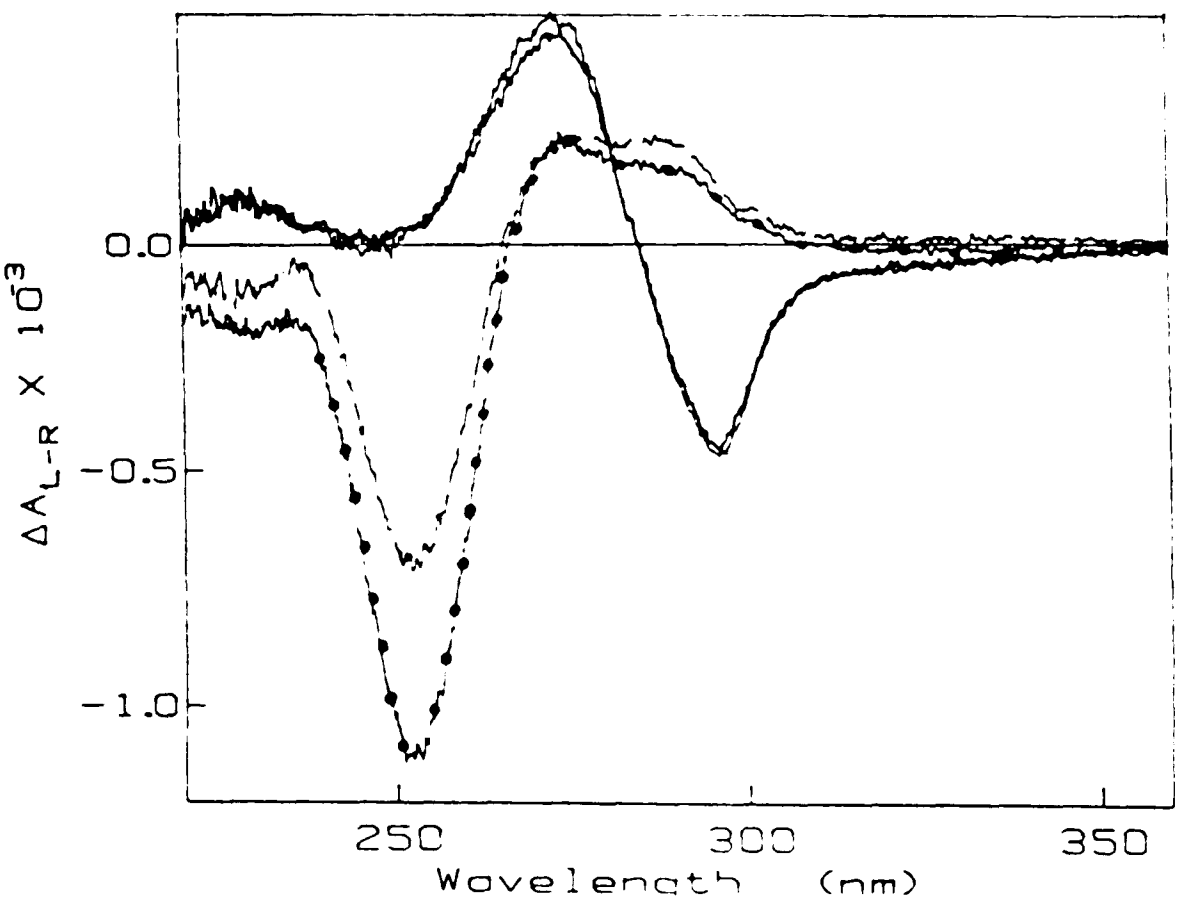

the B-form.[53,61] Unfortunately, it was impossible to prepare a concentrated poly(dG-dC) solution at this salt concentration because precipitation occurred.

Conformations of poly(dG-dC) in $[Co(NH3)_6]Cl_3$:

$[Co(NH_3)_6]Cl_3$ is the only trivalent metal salt used in this study. Divalent cations like $MgCl_2$ offer a 2-fold reduction in the amount of salt required to induce a B-Z transition but trivalent cations offer a 10^5-fold reduction in the amount of salt required. In a solution of poly(dG-dC) and only 23 μM $[Co(NH_3)_6]Cl_3$ the electronic CD spectrum indicates that the oligomer is in a Z-form.[53] Z-form crystals have also been obtained for a CG-hexamer in 23 μM $[Co(NH_3)_6]Cl_3$.[64] Crystal structure analysis indicates that the left-handed form is similar to that seen in $MgCl_2$.

It was very difficult to keep $[Co(NH_3)_6]Cl_3$ in solution with poly(dG-dC) in the concentrations needed to run VCD spectra, 17 mg/ml or 0.026 M (in nucleotide base). $[Co(NH_3)_6]Cl_3$ is capable of inducing the condensation of native DNA into a more compact form which leads to aggregation.[53,65] We found that in many cases, the poly(dG-dC) precipitated out of the solution. However, even in solutions of up to 1.1 mM $[Co(NH_3)_6]Cl_3$ the VCD and ir absorbance spectra indicated that a right-handed helix remained (Fig. 4). This result was confirmed by vacuum UV CD results taken at Brookhaven National Laboratory (Fig. 5).

The implication of this result is that at high concen-

Fig. 4: Ir Absorbance (bottom) and VCD (top) Spectra of Poly(dG-dC) in the Presence of [Co(NH3)6]Cl3: Solid line - 50 mM NaCl and 0.0245 mM [Co(NH3)6]Cl3; dash-dot-dash line - 252 mM NaCl and 0.165 mM [Co(NH3)6]Cl3.

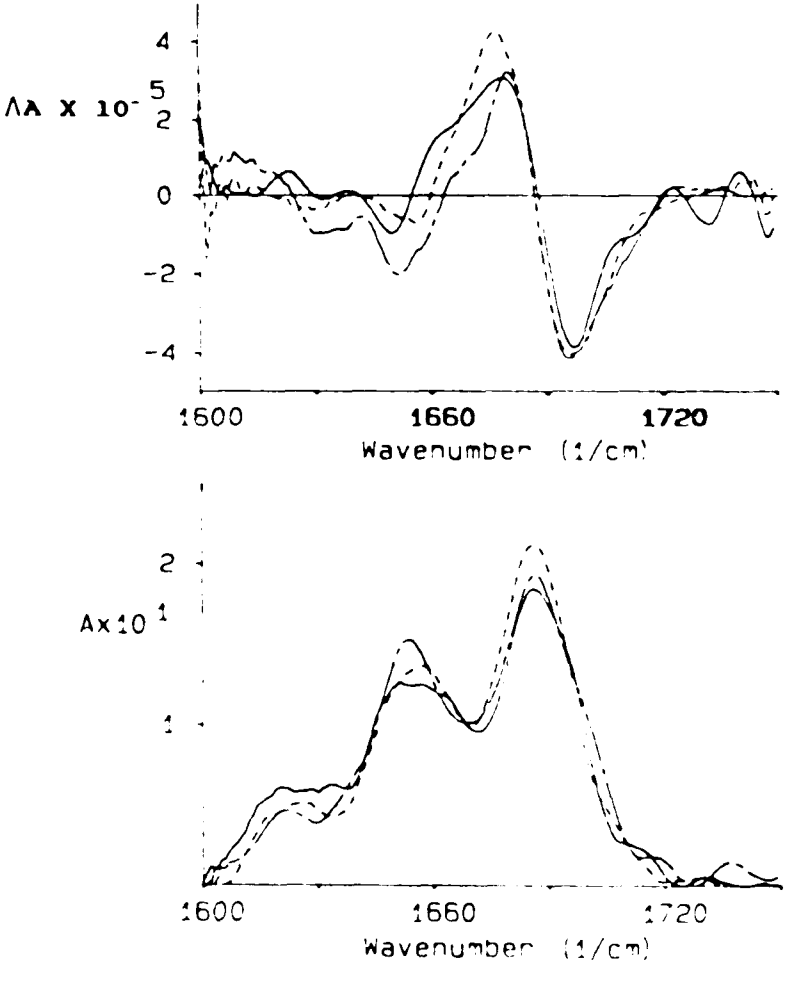

Fig. 5: Vacuum UV CD Spectra of Poly(dG-dC) with and without $[Co(NH_3)_6]Cl_3$: Solid line - poly(dG-dC), 10 mM pH 7 sodium phosphate buffer; solid line with dots - poly(dG-dC), 10 mM NaCl, 0.023 mM $[Co(NH_3)_6]Cl_3$, 20 mM pH 7 tris buffer. The sample cell had a 0.1 cm path length.

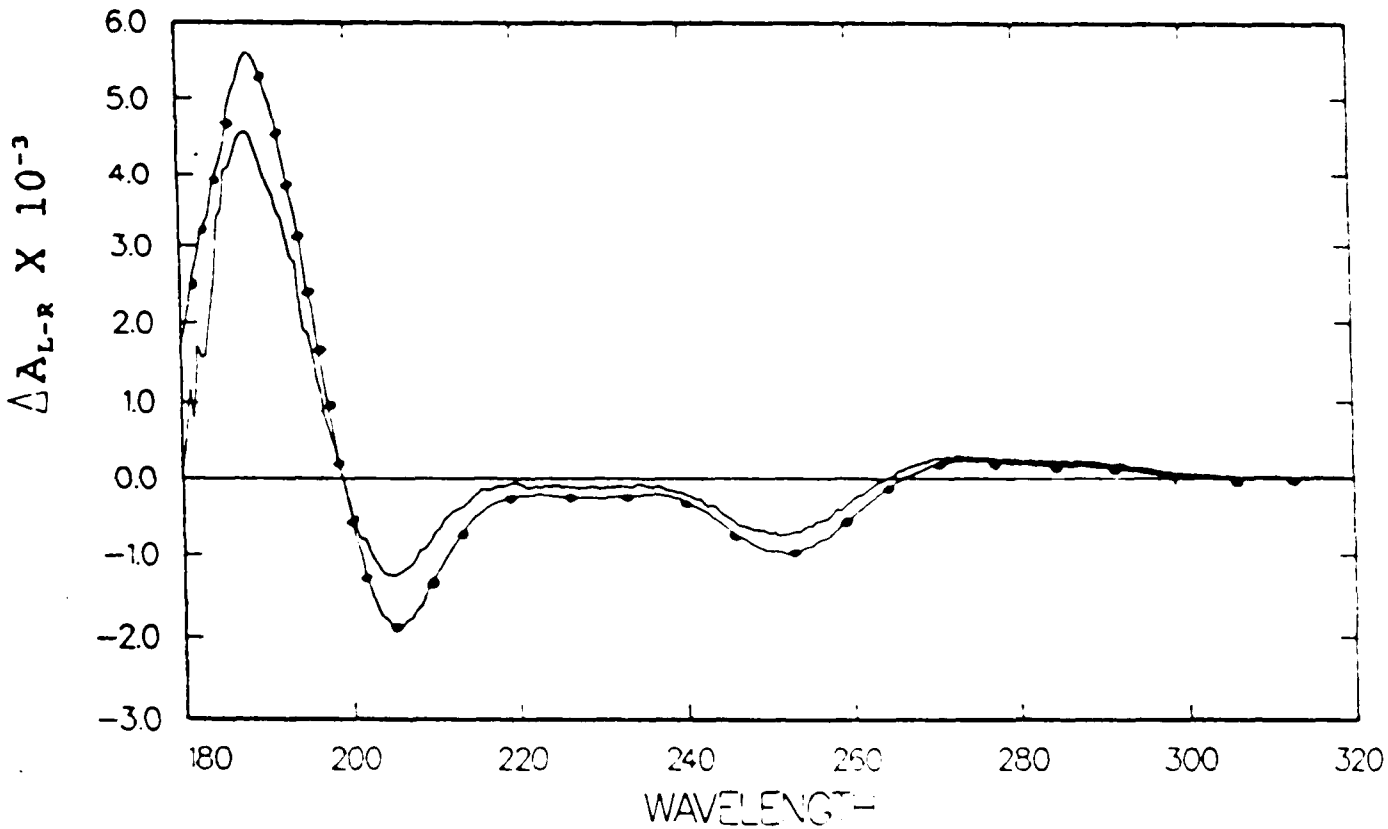

trations of DNA, the energy barrier between the B-form and the Z*-form, the left-handed aggregate form of poly(dG-dC), is lower than the B-Z transition barrier. This is consistent with what is known about Z*-DNA. The aggregated conformation is much more commonly seen when poly(dG-dC) rather than poly(dG-me^{5}dC) is used for a DNA analog but a Z*-conformation may be induced from a solution of poly(dG-me^{5}dC) in the Z-form if additional multivalent cation salt is added.[53]

In high concentrations of oligonucleotide, $NiCl_2$, $CoCl_2$, and $[Co(NH_3)_6]Cl_3$ could not be used to induce a solution state B-Z transition. Although the A_{295}/A_{260} ratio of the UV absorbance increases upon the addition of multivalent salts, this is an unreliable indicator of a B-Z transition. The handedness of the oligonucleotide could not be determined from the CD spectrum in the 230-330 nm range; however, the vacuum UV region still proved to be an accurate indicator of a right- or left-handed conformation. The VCD spectrum of the oligonucleotide in the presence of these salts also gave reliable information about handedness.

VI. Summary

In this thesis we have demonstrated that infrared (vibrational) circular dichroism (VCD) is a viable technique for examining the secondary structure of deoxyoligonucleotides. In these studies spectra were taken in the 1550-1750 cm^{-1} carbonyl stretching region. In this region, VCD peaks may be attributed to C=O, N=C and C=C stretching vibrations of the bases and to interactions between these vibrational transitions of neighboring bases. The B-form VCD spectrum of a CG-deoxyoligonucleotide is characterized by a negative/positive couplet. The negative peak occurs at approximately 1700 cm^{-1} and the positive peak occurs at approximately 1680 cm^{-1}. The couplet is attributed to interactions between the carbonyl groups of the bases. In addition, the low salt spectrum of poly(dG)poly(dC) shows an additional positive shoulder at 1652 cm^{-1}. A positive shoulder is also often seen in the low salt B-form spectra of poly(dG-dC)poly(dG-dC) and poly(dG-me^5dC)poly(dG-me^5dC); however, it occurs at 1667 cm^{-1}. There is no shoulder seen in the VCD spectrum of pd$(CG)_5$. The shoulder is most likely also due to carbonyl coupling. The shoulder seen in the observed poly(dG)poly(dC) spectrum is also seen in the DECO calculated spectrum and therefore may be attributed to carbonyl coupling. The peak is not always visible in the B-form poly(dG-dC)poly(dG-dC) spectra which suggests that its intensity is enhanced in some forms and not others. Enhancement is most

likely due to coupling with other vibrational transitions in this infrared region; possibly from the solvent.

We have characterized three types of B-form ir absorbance and VCD spectra for poly(dG-dC)poly(dG-dC). Although the negative/positive couplet of the VCD spectrum remains virtually the same for all three, there are differences in the low wavenumber region of the VCD spectra and in the ir absorbance spectra. The differences can be attributed to changes in the coupling between the carbonyls and the C=C and C=N vibrations of the bases. In addition, the lengths of the polymers and the amount of single stranded ends may vary between samples. Treatment with S1 nuclease will ensure that there are no single stranded ends. The single stranded ends are most likely not in the same conformation as the double stranded region.

The VCD spectra of poly(dG-dC)poly(dG-dC) and poly(dG-me^{5}dC)poly(dG-me^{5}dC) in high salt solution varies depending on which salt was used to induce the transition. Left-handed conformations are characterized by a positive/negative couplet. For poly(dG-dC)poly(dG-dC), the positive peak occurs at 1675 cm^{-1}. The negative peak is comprised of two negative peaks which occur at 1659 and 1641 cm^{-1} when NaCl is used to induce the Z-conformation and at 1649 and 1635 cm^{-1} when $MgCl_2$ is the Z-inducer. For poly(dG-me^{5}dC)poly(dG-me^{5}dC), the positive peak occurs at 1681 cm^{-1} and the negative peak at 1665 cm^{-1}.

The Degenerate Extended Coupled Oscillator (DECO) model was purposed as a means of interpreting the VCD experimental data. The model uses the cartesian coordinates of the carbonyl groups to determine the interaction energy between these groups as well as the effect of the interactions on the dipole and rotational strengths. From the output of the model, calculated spectra can be generated. We have demonstrated that the DECO model is able to account for the B-form VCD spectra but the model is unable to account for the Z-form spectra. We have attributed the problems with the Z-form calculations to interactions between the oligonucleotide and the salt solution which are not currently taken into account. Modifications of the model suggest that the cytosine and guanine carbonyls are not degenerate for the Z-form helix. One possible reason for this is that since the cytosine carbonyls lie on the inner surface of the helix while the guanine carbonyls lie more towards the outside surface, there may be a difference in the environment of the guanine and cytosine carbonyls. If the difference in the environment affects the dipole moment of the vibrational transitions, the two types of carbonyl groups will be non degenerate.

BIBLIOGRAPHY

(1) Curtis, H. Biology; Worth: New York, 1983.

(2) Stryer Biochemistry; 1988.

(3) Lehninger, A. L. Biochemistry; Worth : New York, 1970.

(4) Watson, J. D. The Double Helix; Atbeneum: New York, 1968.

(5) Rich, A.; Nordheim, A.; Wang, A. H.-J. Ann. Rev. Biochem. 1984, 53, 791-846.

(6) Crawford, J. L.; Kolpak, F. J.; Wang, A. H.-J.; Quigley, G. J.; van Bloom, J. H.; Van der Marel, G.; Rich, A. Proc. Natl. Acad. Sci. USA 1980, 77, 4016-4020.

(7) Dickerson, R.; Drew, H. J. Mol. Biol. 1981, 149, 761-786.

(8) Wang, A. H.-J.; Quigley, G. J.; Kolpak, F. J.; Crawford, J. L.; van Boom, J. H.; van der Marel, G.; Rich, A. Nature 1979, 282, 680-86.

(9) Gessner, R. V.; Frederick, C. A.; Quigley, G. J.; Rich, A.; Wang, A. H.-J. J. Biol. Chem. 1989, 264, 7921-7935.

(10) Dickerson, R. E. in Usual and Unusual DNA Structures: A Summing Up; Wells, R. D. Harvey, S. C.; Springer-Verlag, New York, 1988; pp 287-306.

(11) Saenger, W. Principles of Nucleic Acid Structure; Cantor, C. R.; Springer-Verlag: New York, 1984.

(12) Cantor, C. R.; Schimmel, P. R. Biophysical Chemistry Part I: The Conformation of Biological Molecules; W.H. Freeman and Co.: New York, 1980.

(13) Wells, R. D.; Larson, J. E.; Grant, R. C.; Shortle, B. E.; Cantor, C. R. J. Mol. Biol. 1970, 54, 465-497.

(14) Dickerson, R. E. J. Biomolec. Struc. and Func. 1989, 6, 627-635.

(15) Webster, G.; Merriam, C., Webster's New 20th Century Dictionary, Unabridged; William Collins Pub., Inc.: New York, 1979; 843, 1750.

(16) Zimmerman, S. B. Ann. Rev. Biochem. 1982, 51, 395-427.

(17) Patel, D. J.; Kozlowski, S. A.; Nordheim, A.; Rich, A. Proc. Natl. Acad. Sci. USA 1982, 79, 1413-1417.

(18) Sheth, A.; Ravikumar, M.; Hosur, R. V.; Govil, G. Biopolymers 1987, 26, 1301-1313.

(19) Chen, C.; Cohen, J. S.; Behe, M. Biochem. 1983, 22, 2136-2142.

(20) Benevides, J. M.; Thomas, G. J., Jr. Nuc. Ac. Res. 1983, 11, 5747-5761.

(21) Pohl, F. M.; Jovin, T. M. J. Mol. Biol. 1972, 67, 375-396.

(22) Sutherland, J. C. BioScience 1981, 31, 587-592.

(23) March, J. Advanced Organic Chemistry; John Wiley & Sons: New York, 1985; pp 82-109 .

(24) Cantor, C. R.; Schimmel, P. R. Biophysical Chemistry Part II: Techniques for the Study of Biological Structure and Function; W.H. Freeman and Co.: New York, 1980.

(25) Tomasz, M.; Barton, J. K.; Magliozzo, C. C.; Tucker, D.; Lafer, E. M.; Stollar, B. D. Proc. Natl. Acad. Sci. USA 1983, 80, 2874-2878.

(26) Stinson, S. C. C&EN 1985, 21-32.

(27) Polavarapu, P. L. 1984, 38, 26-28.

(28) Lal, B. B.; Diem, M.; Polavarapu, P. L.; Oboodi, M.; Freedman, T. B.; Nafie, L. A. J. Am. Chem. Soc. 1982, 104, 3336-3342.

(29) Nafie, L. A.; Keiderling, T. A.; Stephens, P. J. J. Amer. Chem. Soc. 1976, 98, 2715-2723.

(30) Nafie, L. A.; Oboodi, R. M.; Freedman, T. B. J. Am. Chem. Soc. 1983, 105, 7449-7450.

(31) Paterlini, M. G.; Freedman, T. B.; Nafie, L. A. Biopolymers 1986, 25, 1751-1765.

(32) Pancoska, P.; Yasui, S. C.; Keiderling, T. A. Biochem. 1989, 28, 5917-5923.

(33) Pancoska, P.; Keiderling, T. A. Biochem. 1991, 30, 6885-6895.

(34) Annamalai, A.; Keiderling, T. A. J. Am. Chem. Soc. 1987, 109, 3125-3132.

(35) Gulotta, M.; Goss, D. J.; Diem, M. Biopolymers 1989, 28, 2047-2058.

(36) Zhong, W.; Gulotta, M.; Goss, D. J.; Diem, M. Biochem. 1990, 29, 7485-7491.

(37) van Steenbergen, A. Nucl. Instrum. Meth. 1980, 172, 25.

(38) Gray, D. M.; Lang, D.; Kuner, E.; Vaughan, M.; Sutherland, J. C. Anal. Biochem. 1984, 136, 247-250.

(39) Diem, M.; Roberts, G. M.; Lee, O. Appl. Spec. 1988, 42, 20.

(40) Lee, O.; Diem, M. Anal. Inst. 1992, 20, 23.

(41) Lee, O., Ph.D. Dissertation, C.U.N.Y., 1992.

(42) Diem, M. in Application of Infrard CD to the Analysis of the Solution Conformation of Biological Molecules; Purdie, A.; 1992.

(43) Votavova, H.; Diem, M. 1993, in preparation.

(44) Davydov, A.S. Exp. Theor. Phy. 1948, 18, 210.

(45) Moffit, W. J. Chem. Phys. 1956, 25, 467-478.

(46) Tinoco, I., Jr. Rad. Res. 1963, 20, 133-139.

(47) Stodola, R.K.; Manion, F.J.; Berman, H.M.; Wood, W.P. DOCK v.5D 1987, Fox Case Cancer Center, Philadelphia.

(48) Still, C. Macormodel v.1.5 1986, Columbia Univ., New York.

(49) Arnott, S.; Cambell Smith, P. J.; Chandrasekara, R. in ch. 2; Fasman, G. D.; 1976; pp 412.

(50) Tsuboi, M.; Takahashi, S.; Harada, I. Duchesne, J.; 1973; pp 91.

(51) Tsuboi, M. in Detailed Structure of DNA Duplex in Solution as Revealed by its Vibrational Spectrum; Alix, A. J. P.; Bernard, L. Manfait, M.; John Wiley & Sons Ltd., Great Britain, 1985; pp 101-107.

(52) Birke, S.; Moses, M.; Diem, M. Biochem. 1992, in preparation.

(53) Behe, M.; Felsenfeld, G. Proc. Natl. Acad. Sci. USA 1981, 78, 1619-1623.

(54) Sutherland, J. C.; Griffen, P. K.; Keck, P. C.; Takacs, P. Z. Proc. Natl. Acad. Sci. USA 1981, 78, 4801-4804.

(55) Fujii, S.; Wang, A. H.-J.; van der Marel, G.; van Boom, J. H.; Rich, A. NAR 1982, 10, 7879-92.

(56) Xiang, T.; Diem, M.; Goss, D. J. 1993, in preparation.

(57) Howard, F. B.; Frazier, J.; Miles, H. T. Proc. Natl. Acad. Sci. 1969, 64, 451-458.

(58) Faulkner, T.R., Ph.D. Dissertation, Univ. Minn, 1976.

(59) Pohl, F. M.; Jovin, T. M. Nature (London) 1976, 260, 365.

(60) Zacharias, W.; Larson, J. E.; Klysik, J.; Stirdivant, S. M.; Wells, R. D. J. Biol. Chem. 1982, 257, 2775-2782.

(61) van de Sande, J. H.; McIntosh, L. P.; Jovin, T. M. EMBO 1982, 1, 777-782.

(62) Taboury, J. A.; Bourtayre, P.; Liquier, L.; Taillandier, E. Nuc. Ac. Res. 1984, 12, 4427-4258.

(63) Pilet, J.; Brahams, J. Biopolymers 1973, 12, 387-403.

(64) Gessner, R. V.; Quigley, G. J.; Wang, A. H.-J.; van der Marel, G. A.; van Bloom, J. H.; Rich, A. Biochem. 1985, 24, 237-240.

(65) Widom, J.; Baldwin, R. L. J. Mol. Biol. 1980, 144, 431-453.